Cranfield University

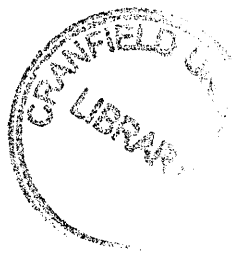

James Jarrett

Design and Development of a Diamond Fly Cutting System

School of Industrial and Manufacturing Science

MRes

Cranfield University

School of Industrial and Manufacturing Science

MRes THESIS

2005

James Jarrett

Design of and Development a Diamond Fly-Cutting System

Supervisor: Professor Paul Shore

Academic Year 2004 to 2005

This thesis is submitted in partial fulfilment of the requirements for the degree of MRes Innovative Manufacturing

ABSTRACT
This thesis presents a conceptual design, for a single point diamond fly-cutting system. This design is based on the performance of an existing, diamond facing lathe. The design requirements for a precision machine tool have been considered, and a deterministic design philosophy has been adopted. The error motions within the diamond facing lathe are considered as effects, generated by defined causes. These causes include geometric, kinematic and dynamic sources. Diamond turning and fly-cutting processes have been compared and consideration has been given to the process influences, including variations in; diamond tool geometries, cutting forces, rotational error motions and the process characteristics required for an optimal surface finish.

A single point diamond facing lathe has been refurbished and the dynamic error motions of this machine tool have been analysed, using different techniques. The stiffness properties have also been investigated, which indicate how the performance of the machine tool has been affected over time and during the refurbishment process.

The dynamic error motions have been used to generate a set of technical specifications, governing the design of the fly-cutting system. A design concept has been presented and optimised. This includes a fly-cutting head, with a quick release tool holder based on a kinematically located side locking clamp. A design concept for a dynamic workpiece holder has also been presented, which monitors the error motions of the machine tool and orientates the workpiece accordingly. A three pair flexure system has been simulated to orientate the workpiece. Consideration has been given to mounting the workpiece, feedback transducers and the design of the control system.

This thesis has provided the initial steps in the design of a single point diamond fly-cutting system. A further stage of development work is required to complete a detailed design.

Keywords:
Precision, Machine, Analysis, Error, Flexure

ACKNOWLEDGEMENTS

I would like to thank my supervisor Prof. Paul Shore for his helpful advice and guidance throughout this project. I would also like to thank Prof. John Corbett for his lectures on precision engineering and Mr Graham Fuller for his encouragement.

I would like to thank David Domingos for his contributions and support during the initial stages of the research. David's support included help with the refurbishment and analysis of the machine tool.

Technical staff; Mr Andrew Baldwin and Mr John Hedge have provided important help with the refurbishment process. Mr Alan Heume has contributed, through his assistance within the Ultra Precision Machining Laboratory. I am very grateful to these individuals, for giving me their time and help with this project.

I would like to express my gratitude to Rochelle Lobo for her continual encouragement, throughout the project.

TABLE OF CONTENTS

TABLE OF FIGURES

TABLE OF TABLES

TABLE OF EQUATIONS

NOTATION
(Order of application)

V ..... Vibration
F ..... Force
k_D ..... Dynamic stiffness
M ..... Mass coefficient
D ..... Damping coefficient
k ..... Stiffness coefficient
R_t ..... Optimal surface roughness
f ..... Feedrate
R_d ..... Diamond tool radius
R_c ..... Fly-cutter radius
k_{AXIAL} ..... Axial Stiffness
R_o ..... Outside radius of aerostatic thrust bearing
R_i ..... Internal radius of aerostatic thrust bearing
H_o ..... Air gap between aerostatic bearing surfaces
Ps ..... Supply Pressure
Pa ..... Ambient Pressure
W ..... Axial load capacity
Q ..... Gas flow rate
C_{Loop} ..... Static loop compliance
$C_{Spindle}$ ..... Spindle compliance
$C_{Slideway}$ ..... Slideway compliance
$C_{Z\text{-}Slide}$ ..... Z-Slide compliance
$C_{Tool\text{-}Holder}$ ..... Tool holder compliance
F_R ..... Radial force
D_R ..... Deflection
m ..... Mass
R_m ..... Radius of mass
ω ..... Angular velocity
W ..... Applied force
l ..... Length of flexure
E ..... Young's modulus
I ..... Second moment of area
B ..... Width of flexure
h ..... Thickness of flexure
r ..... Flexure radius
V_T ..... Vertical deflection in combined mode
k_T ..... Axial stiffness in combined mode
α ..... Tip angle (DOF 1)
β ..... Tilt angle (DOF 2)
Z ..... Axial displacement (DOF 3)
A ..... Actuator A displacement
B ..... Actuator B displacement
C ..... Actuator C displacement
a ..... Dimension a on flexure design
b ..... Dimension b on flexure design

1.0 INTRODUCTION

The scientific and technological advancements in precision optical engineering, are endlessly specifying higher precision components. In the field of optics, these components may be categorised by their surface quality and accuracy of their geometric shape. An example of this is the design of the new James Webb space telescope. The spectrometer optics specified, require a range of highly specified curved and flat surfaces (Figure 1-1). These surfaces may be produced by precision engineering techniques, including single point diamond turning and fly-cutting.

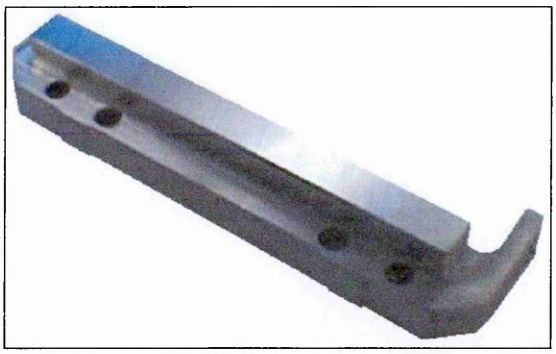

Figure 1-1: James Webb space telescope spectrometer optic

Secondary processing techniques such as polishing are very time consuming and if rushed will often distort the geometric profile of the component. High precision components are very expensive to produce; therefore selecting the correct process is very important.

1.1 Single Point Diamond Fly-Cutters

A single point diamond fly-cutter is capable of producing a very smooth surface, with a high form (flatness) accuracy. This process generates a higher accuracy surface finish by minimising the thermal distortions within the workpiece. This is attributable to an intermittent cutting contact between the tool and the component's surface. The removed material is sliced off the workpiece as it is traversed horizontally, through the rotating cutting path of a diamond tool. This operation principle is shown in Figure 1-2.

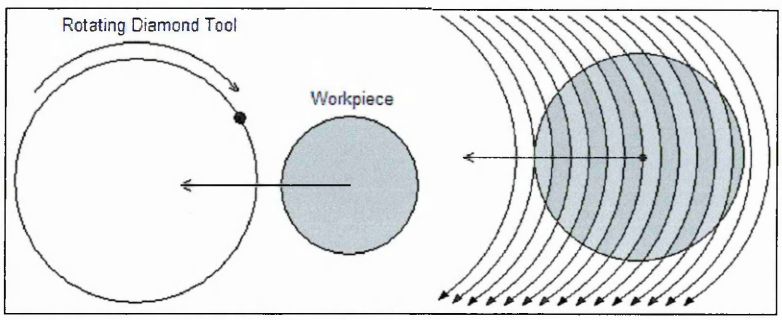

Figure 1-2: Operation principle of a diamond fly-cutter

During a diamond turning process, the machining operation is restricted to the first half of the component. Surface errors are therefore symmetrical about the centre of the component's rotation and produce an apex on the centre of the components surface. During a fly-cutting operation the whole of a static surface is cut by a rotating diamond tool. This technique removes the central apex from the machined surface and produces a flatter surface form. This comparison is shown in Figure 1-3.

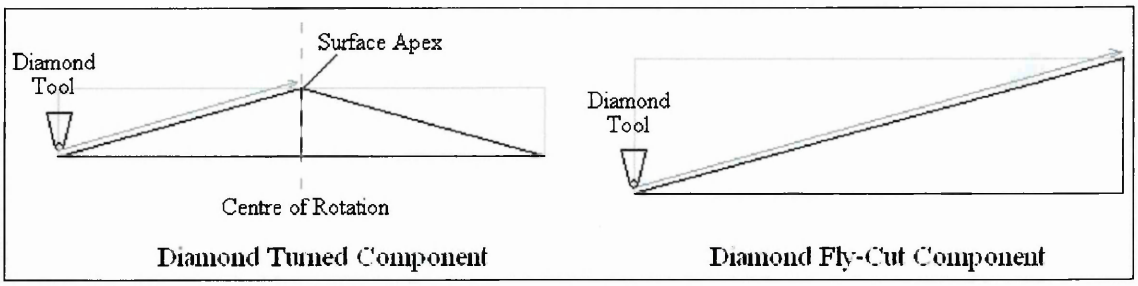

Figure 1-3: Surface comparison of diamond turning and fly-cutting

The distinctive cutting process of a fly-cutter also enables high quality micro-structured surfaces to be machined. By implementing a large cut radius, the orientation of the micro-structured surface is not limited about the rotational axis of the workpiece.

1.2 Thesis Aim

The aim of this Thesis is to design a single point diamond fly-cutting system, through the conversion of an existing diamond facing lathe (Figure 1-4). The dynamic error motions and stiffness values of the existing facing lathe should be investigated and evaluated within a feasibility study. Consideration should then be given to designing a fly-cutting system, capable of monitoring and reacting to these error motions. Detailed design of the final components should be included where possible. This Thesis will provide the initial stages of analysis and design, required to develop a complete fly-cutting system.

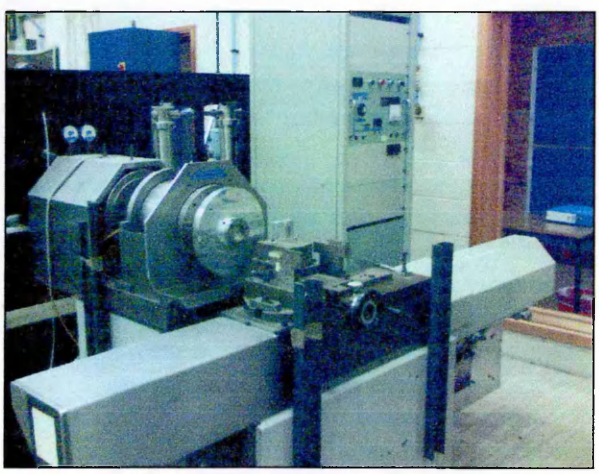

Figure 1-4: Diamond facing lathe

1.3 Thesis Objectives

Initially, the system is to be designed to produce flat surfaces with the specifications outlined below, but consideration is to be given to future development and research work. This work would include the generation of micro-structured surfaces on a range of part geometries and different materials.

1.3.1 Component Specifications

- Maximum Workpiece Diameter: 100mm
- Roughness: 50nm P-V (5nm RMS)
- Form Accuracy (Flatness): 200nm P-V

1.4 Task Identification

This Thesis follows the task structure outlined below:

1. Comprehensive literature review, including precision machine design, machining processes, commercial fly-cutting systems, errors in machine tools, aerostatic bearings and hydrostatic guideways.
2. Refurbishment of the current diamond facing lathe, including the aerostatic bearing and electronic control systems.
3. Analysis of the error motions generated by the spindle and slideway, according to documented standards and procedures.
4. Analysis of the dynamic and static stiffness properties of the machine tool.
5. Evaluation of these error motions in the form of an error budget and feasibility study.
6. Formation of a detailed specification, governing the performance and design of the fly-cutting system.
7. Design of a concept capable of fulfilling the design specification. This concept should be mathematically justified and simulated where feasible.
8. Detailed design of the design concept. This is to improve and analyse a range of plausible ideas for a design section, through a set methodology. The final design should be optimised and detailed.
9. Analysis and discussion of the designed components.
10. Future recommendations to continue the research covered by this Thesis.

2.0 LITERATURE REVIEW

2.1 Precision Engineering

2.1.1 Principles of Precision Engineering

Precision Engineering may be classified into three main disciplines; design for precision, metrology systems and precision manufacturing [1]. A successful machine tool should be capable of repeatably producing a high specification component. The tolerances of the specified component will affect the complexity of the machine design. By tightening the tolerances of this component and striving to produce a more refined machining process, the required number of processes may be decreased therefore increasing the production efficiency. Automated assembly machines and modular product designs [2] also require high tolerance components, if cost effective and efficient assembly processes are to be achieved. Figure 2-1 relates the reduction in tolerances, for normal, precision and ultra-precision engineering technologies over the past 50 years [2]. This figure demonstrates the current variations in the tolerance resolutions, for each engineering category. These trends follow the Tanaguchi prediction, regarding the technological developments in precision engineering.

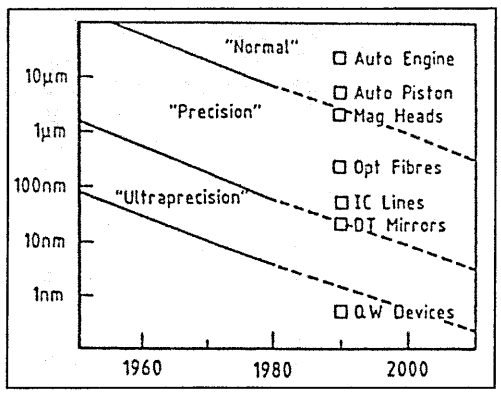

Figure 2-1: Recent trends in tolerance reduction [2]

Advancements in precision engineering evolve in parallel with advancements in technology. This is due to the rapidly increasing demand for higher accuracy instruments and consumer products [1]. Optical disk mastering systems used to record DVDs require precision components, as each one contributes to the overall accuracy. These errors are influenced by geometric (part size), kinematic (part location) and dynamic (response) sources [1]. Future technologies such as micro electrical mechanical systems (MEMS) and optical micro electrical mechanical systems (OMEMS) are reliant on these process advancements.

Precision engineering processes include single point diamond and Cubic Boron Nitride (CBN) cutting, multiple point diamond grinding, lapping and photo chemical machining [3]. These processes have benefited from advancements in precision actuator and transducer technology.

A greater understanding of the design requirements for a precision machine has led to "Eleven Principles and Techniques" [4], which have been defined by Professor P. McKeown of Cranfield University. These principles include kinematics, structure design, metrology systems, error budgeting, compensation techniques and actuator design.

2.1.2 Kinematics

A kinematic system is based on a deterministic design philosophy, which enables a designer to predict the performance of a component and therefore control its motions accordingly. A kinematic joint design is therefore capable of providing an accurate and repeatable constraint, between two bodies. In a kinematic design each of the component's degrees of freedom is only constrained by a single point contact. These degrees of freedom include the axes, through which the component is free to displace (Figure 2-2). According to Hertz contact theory, these single points only provide a low stiffness connection [5]. This is attributable to a low surface contact area between the two bodies.

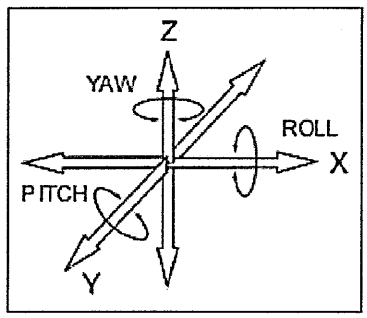

Figure 2-2: 6 Degrees of freedom [6]

Kinematic Constraints

Basic kinematic arrangements including the three-vee and the trihedral-vee-flat couplings are amongst the most frequently implemented designs in precision engineering. Slocum obtained a location repeatability of 0.36μm using a three-vee coupling, subject to a 75N cutting force and a 45kN preload [7]. Both of these designs, shown in Figure 2-3 (A and B), require a preload or uniform nesting force between the two bodies. The symmetrical design of the three-vee coupling allows a thermal expansion of the components around a central reference point. This is compared to the trihedral-vee-flat design, which allows a thermal expansion referenced to a single pivot point. The friction between and surface quality of the contacts, are the main causes of positioning non-repeatability [8].

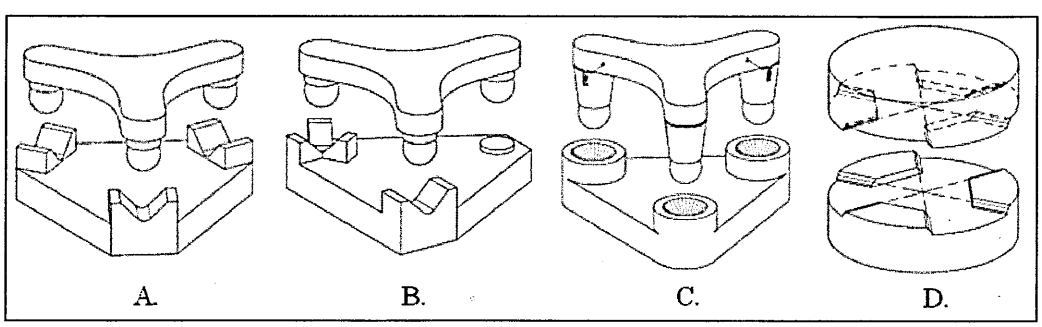

Figure 2-3: Kinematic couplings [9]

Two connection designs based on elastic averaging principles are also shown in Figure 2-3 (C and D). These designs are intended to increase the stiffness of the connection, through increasing the surface area of the contact. Equivalent to the three-vee arrangement, the three-sphere arrangement relies on accurately manufactured spheres and sockets. Tilting flexures are used to ensure a full surface contact between the spheres and sockets is achieved. Type D, shown in Figure 2-3, implements six diagonal flats on each component. Six contact regions are therefore used to constrain all degrees of freedom. The geometry and orientation of these flats will influence the axial and radial stiffnesses of the connection. High manufacturing tolerances are required to produce these large contact regions.

2.1.3 Metrology Systems

Artefact, global and parametric calibration techniques are designed to monitor and correct for error motions [10]. These are based on the ISO 230, test code standard for machine tools. In 1979 Bryan published an update to the Abbé measurement principle. The Abbé principle states that "The distance being measured should be a straight line extension of the scale" [4]. Bryan's revision of this principle, discusses the geometric limitations on a precision machine designer. According to Bryan, "The displacement must be free of angular motion" [11]. Bryan is combining a semi-kinematic framework around the metrology system, to constrain the measurement to a single degree of freedom. The structure of a high precision machine is generally based around a metrology frame. This frame is designed to separate the forces experienced during the process, from the location of the feedback transducers. Under the guidance of McKeown and Wills-Moren, Cranfield Precision implemented a metrology frame in a large off-axis grinding machine (OAGM-2500). Commissioned for Eastman Kodak, it was used to produce optics for Very Large Telescopes (VLTs) including Keck [12].

2.1.4 Thermal Errors

"The largest single source of error in a commercial machine tool is thermally-induced, from either the environment or internally generated heat." [13]

The design of a precision machine tool requires the reduction of the thermal expansions, of the machine components. Further compensation techniques are then required to remove any thermal instability [14]. Generally, the geometry of the critical components susceptible to thermal errors should be designed to be as small as possible. Thermal errors can be classified into uniform and non-uniform effects [14]. Uniform effects include predictable errors at set temperatures and material expansions. Although coefficients of thermal expansion may not be exactly known, the influence of thermal expansions can be reduced by measuring the expansion of machined components during a controlled temperature change [1]. Non-uniform errors are caused by changes in the immediate environment and from the machining process, such as spindle rotation and cutting forces [14]. Due to the varying time constants of thermal expansions for different machine components and the presence of non-uniform errors, Donaldson recommends removing the heat at the source [15, 1]. To simulate the realistic response behaviour of a machine tool, the thermal and elastic geometric deformations must be accounted for. The variation in the component geometry changes the contact pressure within the joint, therefore varying the heat transfer coefficient. This variation generates a non-linear thermal expansion [16].

2.1.5 Structure Design

Machine structures are generally assembled from many different components, the structure will therefore behave accordingly to the properties and interactions between these components [1]. Vibrations generated by a machine structure limit the accuracy of the machine tool. 'Tool Interference' documented by Cheung, is a vibration induced error in the surface of a component. During the machining process the diamond tool prematurely removes a chip of the material, resulting in a "non-perfect surface generation" [17]. Equation 2-1 relates the dynamic stiffness and forces (rotational moments) to these vibrations.

$$V = \frac{F}{k_D}$$

Equation 2-1: Dynamic vibrations

Where,

V : Vibration
F : Force
k_D : Dynamic stiffness

When considering rotational motions, the force in Equation 2-1 may be evaluated into two dynamic excitation forces categories. These are synchronous and asynchronous forces, which occur at repeatable and non-repeatable angular positions respectively. The most common radial synchronous excitation force is the imbalance of a spindle rotor [18]. A technique known as turning (changing) the natural frequency, will reduce the generated vibrations attributable to resonance [19]. This technique may be applied to a simple spring, mass and damper model, with a single degree of freedom. The expression of force within the model is shown in Equation 2-2.

$$F = M\ddot{x} + C\dot{x} + kx$$

Equation 2-2: Simple dynamic structures

Where,

M : Mass
D : Damping
K : Stiffness

Equation 2-2 may be represented on a vector diagram (Figure 2-4). Using this diagram the effects on the structure, from varying the mass or stiffness coefficients may be evaluated. When the structure is exposed to frequencies below its subsequent fundamental frequency (f_n), the force is dominated by the stiffness. As the vibrations increase towards this next fundamental frequency, the mass and stiffness coefficients cancel. The resulting displacement error motions are therefore controlled exclusively by the damping coefficient.

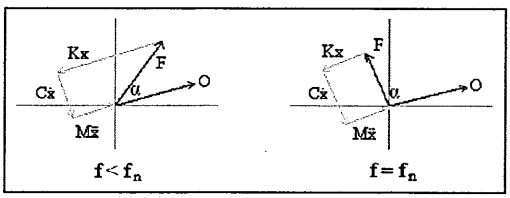

Figure 2-4: Vector representation of a dynamic structure

2.2 Single Point Diamond Fly-Cutters

Using a simple X, Y and rotational Z axis, a fly-cutter is capable of producing very high quality flat surfaces. Single point diamond tools can be implemented to produce similar surface finishes to a diamond turning process. The theory related to a diamond fly-cutting process may therefore be related to single point diamond turning.

2.2.1 Advantages of a Single Point Diamond Fly-Cutter

- When compared to diamond turning, fly-cutting is a more time efficient process for producing a precision flat surface on a non-circular workpiece.
- The linear speed remains constant for the duration of the cutting process, unlike diamond turning which varies according to the diameter of the component at the cutting location.
- The whole of a component's surface is machined, therefore a centre position does not have to be defined. This simplifies the control of the fly-cutter and increases the form accuracy of the component, as a central surface apex is not generated.
- The intermittent cutting action of a fly-cutter minimises the geometric thermal distortions of the workpiece.
- The surface quality of a fly-cut component is not affected by swelling tool marks, as exhibited in the surface of a diamond turned component. Cheung documents one possible cause for this error, which is the free flow of the material during the cutting process. "The thrust force in the infeed direction pushes aside the work material near the tool nose, causing it to flow to the free surface" [20].
- Micro-structured surfaces may be produced.

2.2.2 Disadvantages of a Single Point Diamond Fly-Cutter

- The feedrate for diamond fly-cutting remains the same as a diamond turning process. The component is machined from one side to another, therefore requiring twice the machining time compared to a turning process.
- The rotating diamond tool requires additional safety protection. Safety features are required to stop the operator handling the rotating tool and to contain the tool in the event that it propels outwards towards the operator.

2.2.3 Conventional Fly-Cutters

Conventional single point fly-cutting systems are used to produce delicate parts, where only the removal of a thin section of material is required (Figure 2-5). The single point of the tool may be adjusted to cover the workpiece so that only one pass of the cutter is necessary. This is compared to conventional milling processes where a number of passes may be required, to fully machine the part [21].

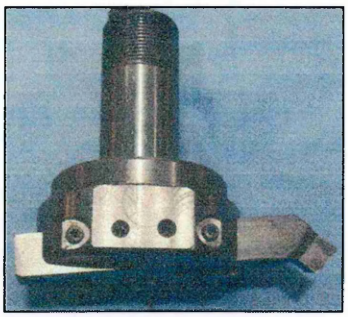

Figure 2-5: Conventional fly-cutting tool for a vertical milling machine

Depending on the style of the fly-cutter, a secondary cutting tool may be accommodated into the body of the cutting head (dual point fly cutter). This is to counterbalance the primary cutting tool, and in milling operations it may be used to produce an initial rough cut. A fly-cutter may therefore be used to produce two different cutting operations, in one pass of the workpiece [22].

Fly-cutters are implemented where there is a possibility of damaging the surface of a delicate component due to the amount of heat generated during machining. As fly-cutting is an intermittent process the material has the opportunity to cool between each cut cycle. This process is particularly advantageous when machining alloys of, Brass, Copper, Aluminium, Bronze, Phosphor Bronze, Carbon and Graphite. All of these materials generate heat quickly during a machining process [21].

Diamond fly-cutters are preferred over conventional processes where high quality surface finishes are required and polishing is not a possible option. An example of this is during the production of fine tooth gears, where polishing the workpiece often distorts the tooth flank profile [23].

2.3 Structured Surfaces

Precision engineered structured surfaces, are designed to provide a particular function. This function is often based on the surface geometry produced from a diamond machining process. Research into the development of micro-structured surfaces at IPT Aachen, has produced complex surface structures with sub-micron structure dimensions [24]. Research undertaken at the University of Bremen has generated structured surfaces from a fly cutting process. Figure 2-6 shows the geometry of a micro-structured surface which has been produced using a Nanotech 500 Freeform Generator with a fly-cutting head [25].

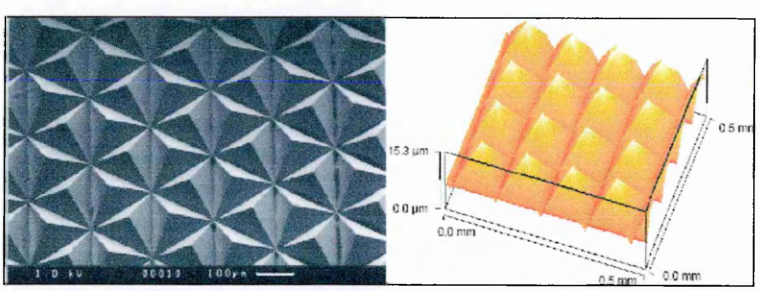

Figure 2-6: Micro-structured surface

Roger Appleton, a scientist from 3M has developed techniques to generate micro-structured surfaces on a range of products, including Fresnel lenses for projectors and Scotchlite™ reflective sheeting, used in road signs [26, 27]. The high aspect ratio of a structured surface compared to a good diamond turned surface provides the reflective optical capabilities. Fraunhofer ISE has implemented this theory and produced a 'broad band' anti-reflective coating. This surface structure is based on a period shorter than the illuminating wavelength [28].

2.4 Single Point Diamond Turing

High precision single point diamond turning is capable of producing very high quality surface finishes (roughness), down to 0.5nm RMS. For small parts of 50mm in diameter, the form accuracy of the machined surface is below 50nm peak to valley. These developments can be attributed to the level of detail and understanding in the machine design. The asynchronous error generated between the relative position of the tool point and workpiece can be held accountable for the resulting surface roughness errors.

Infrared materials such as Silicon and Germanium are very pure materials and have very high refractive indexes. Combining these materials with a diamond turning process, advanced hybrid optics may be produced. These optics are generally used in the aerospace industry and allow different wavelengths of light to be focused at a single point.

Single point diamond machining is capable of achieving a surface roughness of 1nm RMS. For pure materials this surface quality is limited by the asynchronous errors of the machine tool. Table 2-1 shows the form accuracies for commercially available diamond turning machines [29].

Diameter of Part (mm)	Form Accuracy (nm) (Peak to Valley)
50	50
100	100
250	200

Table 2-1: Diamond turning capabilities

Zhou demonstrated that the main influence on the form accuracy of a diamond turned component, with respect to the tool set up errors is the tool offset [30]. This is the horizontal position of the tool, when related to the axis of rotation. Setting the tool offset position is a time consuming procedure and often requires a tool setting station.

2.5 Single Point Diamond Tools

Monocrystalline diamonds are the hardest material available on the planet, this is attributable to their atomic grid structure. They are the preferred diamond type for the ductile machining of fine surfaces. Diamonds contain carbon, therefore due to the "affinity of carbon and iron, the machining of ferocious metals results in high wear rates" [31].

Three causes of wear in diamond tools [23]*:*

1) Hard inclusions (oxides) in the machined material.
2) Presence of carbides or hard metal chips (steel) in the material.
3) Emery grains and dust particles on the surface of the material.

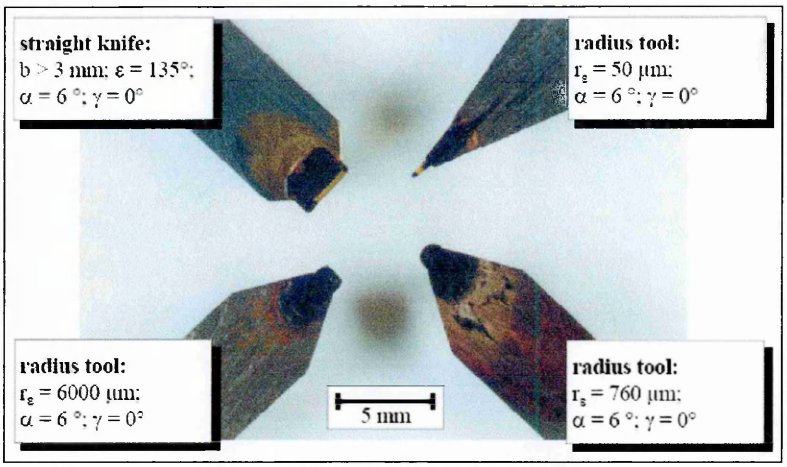

Figure 2-7: Diamond tool geometries

Figure 2-7 demonstrates the wide range of diamond tool geometries available. Section 2.6 describes the effects of various tool geometries and machining parameters on the cutting forces, experienced during a diamond turning process. Single point diamond fly-cutting tools have a large radius (for example 5mm), these are used to produce a smoother surface finish. Optimal surface finishes are described in section 2.8.

2.6 Cutting forces

The cutting forces for a single point diamond fly-cutting process are similar to a diamond turning process. Fly-cutting is an intermittent cutting process, where the diamond tool is only in contact with the workpiece for a short period of time per revolution of the cutting head. Shore, documents the tool wear, cutting forces and surface stress when diamond turning Germanium and Silicon material samples [29]. In each case the depth of cut was 3μm, with a 2μm/rev feedrate and a spindle speed of 1000rpm. The Germanium results show that after a linear cut distance of 12Km, there is 0% surface fracture and cutting force of 0.04N. After a linear cutting distance of 12.1Km the Silicon samples have 5% of surface fracture. They require a cutting force of 0.17N, a normal force of 0.77N.

2.6.1 Altering the Diamond Tool Geometry

Research documented by Byrne et al, at the University College Dublin highlights the relationship between the relative cutting force of a diamond turning process, with the diamonds geometry and process parameters [31].

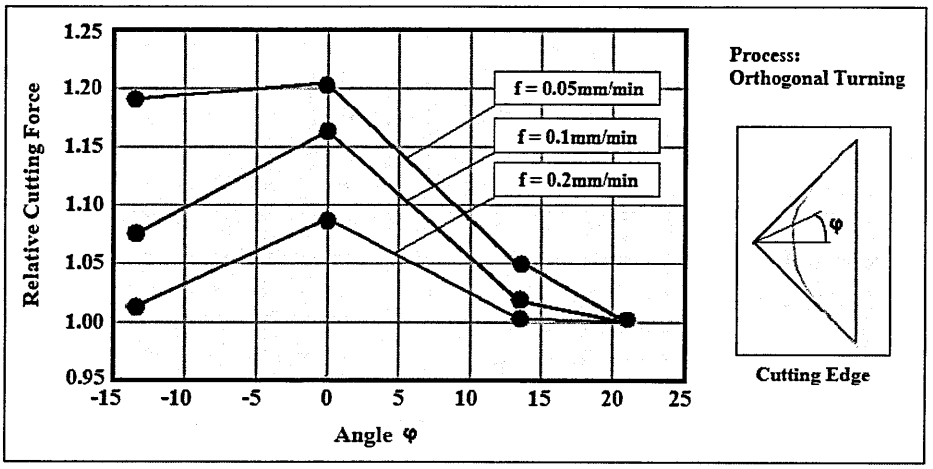

Figure 2-8: Cutting forces relative to tool geometry [31]

Byrne's results are summarised in Figure 2-8 and show that regardless of the process feedrate, an even chamfer geometry generates the highest cutting forces. Section 2.8 describes the optimal surfaces finishes, which may be improved upon by lowering the process feedrate. Byrne's results show an increase in the relative cutting forces, during these lower feedrates. These are generated by a greater influence of the cutting edge geometry on the surface finish. "The machining force can be reduced with an unevenly chamfered cutting edge" [31]. This approach will also increase the surface quality and the 'life' of the diamond tool.

2.7 Surface Finish

The optimal surface finish of a component does not include any spindle error motions. It demonstrates how the feedrate and diameter of the diamond tool will affect the surface finish of a machined component (Figure 2-9).

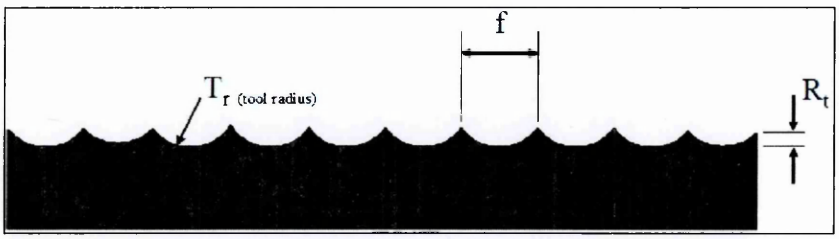

Figure 2-9: Optimal surface finish

For a diamond turning operation, the optimal surface finish may be calculated from Equation 2-3. A comparison of the optimal surface roughness with a range of feedrates and tool radii is shown in Figure 2-10.

Optimal Surface Quality [44]

$$R_t = \frac{f^2}{8 \times T_r}$$

Equation 2-3: Optimal surface quality

Where,

R_t : Optimal Surface Roughness
f : Feedrate (mm/min)
R_d : Diamond Tool Radius (mm)

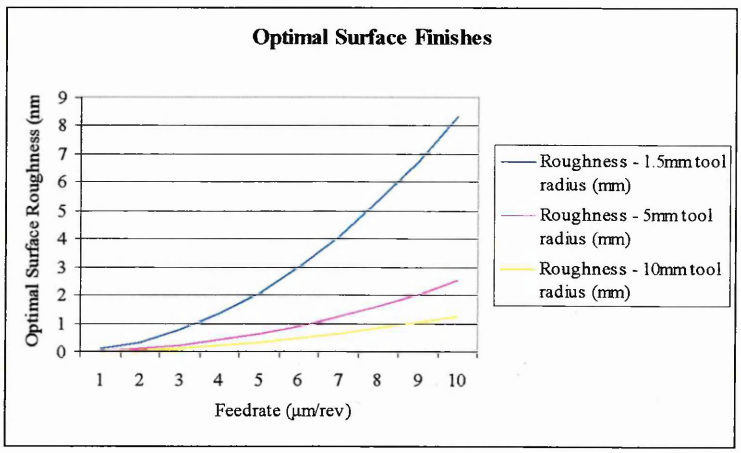

Figure 2-10: Tool radii and process feedrate effects on surface finish

During a single point diamond turning operation, the edge of the diamond tool remains in contact with the surface of the machined component. Professor Brinksmeier and his colleagues at the University of Bremen have determined that during a single point fly-cutting operation, small scallops of material are removed from the machined surface [25]. The alignment and orientation of these scallops may be seen in Figure 2-11.

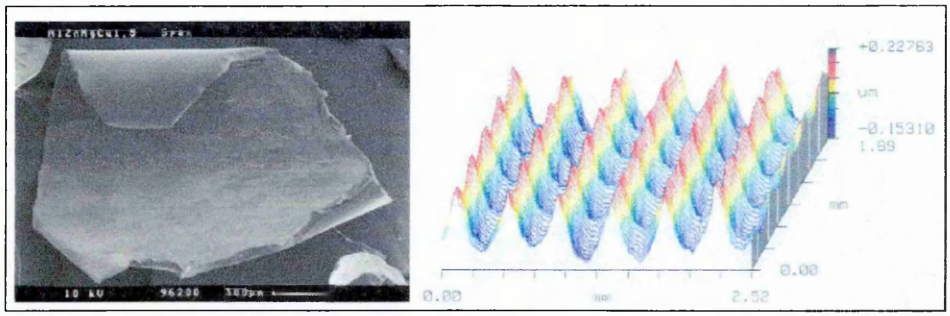

Figure 2-11: Fly-cut surface [25]

When considered in three dimensions, the roughness of an optimal machined surface is defined as a function of the depth of the scallop in both the cutting (D_c) and feed (D_f) direction. This principle is shown in Figure 2-12.

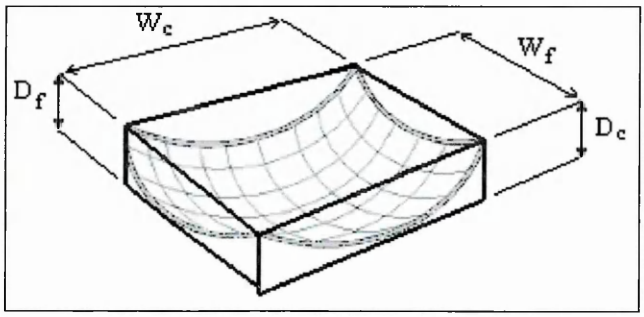

Figure 2-12: Fly-cut surface scallop

Equation 2-4 and Equation 2-5 relate the depth of the scallop to its width. These equations show that as the radius of the diamond tool and the radius cutting arc are increased, the roughness of the optimal surface finish decreases.

$$D_C = \frac{W_C^{\,2}}{(8 \times r_c)}$$

Equation 2-4: Scallop depth in cut direction [25]

Where,

r_c : Radius of fly-cutter

$$D_f = \frac{W_f^{\,2}}{(8 \times r_d)}$$

Equation 2-5: Scallop depth in feed direction [25]

Where,

r_d : Radius of diamond tool

From Equation 2-4 and Equation 2-5 it is possible to conclude that to obtain an optimal surface finish on a fly-cut component, the radius of the cutting arc and radius of the diamond tool should be as large as possible.

2.8 Rotational Error Motions

2.8.1 Synchronous Error Motions

Synchronous error motions are related to the angular position of a spindle. These error motions are repetitive over a period of time and can be used to determine the optimum form accuracy of a part.

2.8.2 Asynchronous Error Motions

Asynchronous error motions are not related to the angular position of a spindle and are related to the surface quality, of a machined component [32]. They can be generated by structural and floor vibrations, contaminated lubricants and manufacturing errors. Large asynchronous errors also result in premature tool wear [13]. The maximum asynchronous error motion may be used to predict the peak to valley surface roughness "for the machine under ideal cutting conditions" [44].

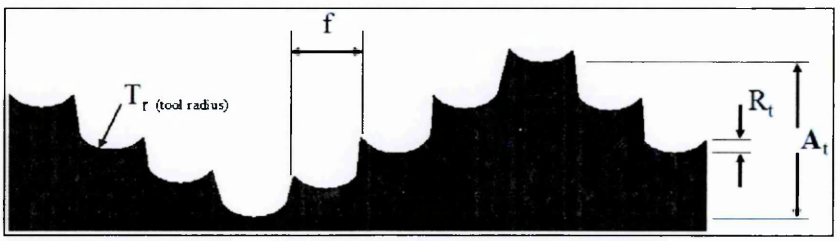

Figure 2-13: Asynchronous error motions

2.9 Machining Direction

Research undertaken at the University of Bremen highlights the importance of choosing the correct machining direction for a fly-cutting process [25]. Figure 2-14 documents their results, from a fly-cutting process. Three different materials have been machined with upwards and downwards cutting directions.

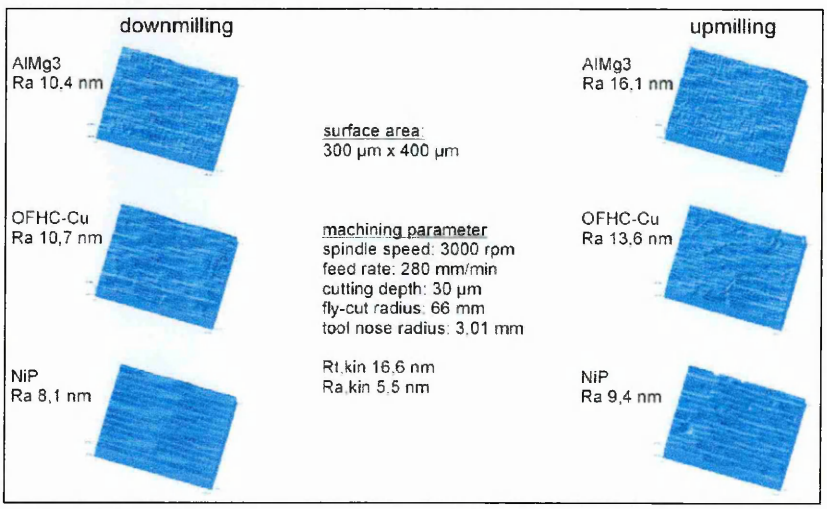

Figure 2-14: Down-milling and up-milling [25]

The average percentage improvement (according to the results in Figure 2-14) in surface roughness, by adopting a downwards cutting process is 32%. This is due to the removal of surface scratching, attributable to the machined chips being forced upwards towards the finished surface.

2.10 Commercial Machines

Kugler [33], LT Ultra [34] and Precitech [35], are all manufacturers of high performance fly-cutting systems. The standard specification for a precision fly-cut component from these manufacturers includes a surface roughness (Ra) from 1 to 2nm and a flatness of 100nm over a 100mm diameter part. Each of the systems machine vertically downwards, towards a workpiece which is mounted onto a horizontal slideway.

Kugler, a German machine tool manufacturer produces two high performance diamond fly-cutting systems. The F1000CNC system (Figure 2-15) implements a computer numerical control (CNC) system. This control system enables simultaneous interpolation of up to 8 individual axes, all with programmable acceleration and deceleration ramp inputs. This enables the user to machine different surfaces of a part, each having a different surface finish. Only 2 of these axes are required during a conventional fly-cutting operation.

Figure 2-15: KUGLER F1000CNC Fly-cutter [36]

The spindle rotation is generated by a brushless DC motor and driven through a precision air bearing. The spindle is capable of operating at cutting speeds of up to 3000rpm. The maximum workpiece height is 250mm and the depth of cut is applied vertically through a lead screw with roller bearing drive. The motions of this Z-Axis are monitored by interferometer with a 0.1μm resolution.

The horizontal slideway which traverses the workpiece across the face of the fly-cutting head has a maximum range of 1m. The slideway is driven by a linear motor and is mounted to a linear air bearing. The feedrate of the slideway is variable between 10 and 2000 mm/min.

Documentation supplied Precitech on their Planoform 650 fly-cutting system, provides a two dimensional (2D) profile of a machined surface. From this profile the asynchronous axial error motion of spindle can be seen to be approximately 7.5nm.

2.11 Gas Lubricated Bearings

Gas lubricated bearings can be classified into aerostatic and aerodynamic types. Aerostatic bearings require an external compressed air supply and are used in high precision diamond turning and measurement systems. These bearings create a platform for high precision, rotational (thrust bearing) and linear (journal bearing) motions. This is achieved by applying high pressure air, into a small clearance gap through a network of restrictor holes. These restrictors are located in one of two bearing plates. Aerodynamic bearings are capable of "generating their own pressure differentials" [37], "by the mechanism of viscous shearing" [38]. Porous ceramic restrictors can be used to create an averaging effect, with a smooth motion and a very high resolution [5].

Kammerling documents the application of aerostatic bearings to single point diamond fly-cutters, in the late 1960's. These machines replaced existing hand lapping equipment and were used to produce high specification metalography samples. An air bearing was chosen due to its low levels of vibration and low axial error motions [39].

Air bearings have low dynamic load capabilities when compared to hydrostatic bearings. This is because they have a very high stiffness and only exhibit low thermal distortion errors by exploiting the low viscosity of air [40]. This exploitation is related to a high stiffness to power efficiency ratio. Their low power requirements relative to a hydrostatic bearing, allow the geometry of an air bearing to be enlarged. This increases the first resonant frequency of the rotor [41]. Hydrostatic bearings generate higher operating temperatures, attributable to the greater forces required to sheer an oil film. Air bearings are very complex to design and require very high manufacturing tolerances [40].

Figure 2-16 shows a network of slot restrictors, mounted into a thrust bearing plate of annular design. This is the front thrust bearing taken from the small diamond facing lathe on which this thesis is based. Each of the 16 slot restrictors has an internal diameter of 180µm, and supplies an air pressure of 0.043N/mm2 when operated at 6 bar.

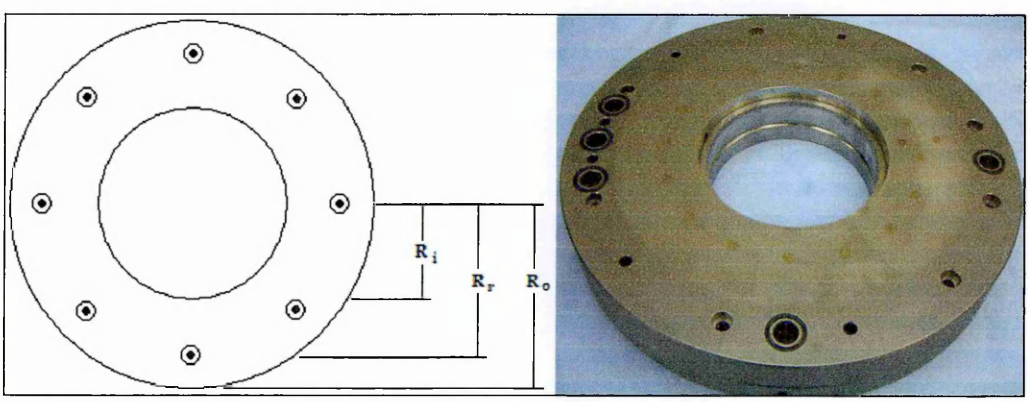

Figure 2-16: Aerostatic thrust bearing

2.12 Friction Drives

2.12.1 Operation Principles

A friction drive provides a linear motion from a rotary input (Figure 2-17). Due to elastic deformation between the drive roller and drive bar, this transmission technique has very low backlash and deadband transmission regions [42]. Friction drives are very sensitive to the drive bar cleanliness and have a low drive force and stiffness capabilities.

Figure 2-17: Friction drive and hydrodynamic slideway

A kinematic hydrodynamic slideway is used to support the drive bar. The averaging affect of the oil layer within hydrodynamic slideway provides a very smooth linear drive. The hydrodynamic slideway does however experience a range of error motions. The accuracy of a friction drive coupled to a hydrodynamic slideway provides a good linear transmission for ductile machining processes. The forces generated during this process must be lower than the drive force of the friction drive. In ductile machining applications where only a low linear velocity is required, the drive roller is often directly driven by the motor. This technique avoids "introducing transmission nonlinearities into the system" [42].

2.12.2 Hydrodynamic Slideway Error Motions

Kinematic slideway designs have five degrees of constraint and one degree of freedom. The important degrees of constraint in a fly-cutting system are, the tilt and straightness motions. These are shown in Figure 2-18, as Yaw and straightness in the Z direction. These are quasi-static mechanical errors and occur at frequencies far lower than the operational frequency of the machine. Quasi-static mechanical errors are caused by thermal expansions, external off centre loads and geometric errors. Hydrostatic bearings are insensitive to surface finish errors, as they are generally considerably less than the bearing clearance [43].

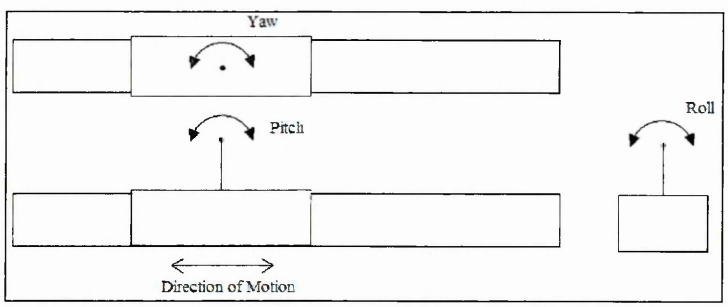

Figure 2-18: Hydrodynamic slideway error motions

3.0 DYNAMIC PERFORMANCE ANALYSIS

The design specifications of the fly-cutting system are based on the performance capabilities of a refurbished diamond facing lathe. These error motions are then combined into their corresponding degree of freedom. This process generates an understanding of the error motions attributable to a component machined on the diamond facing lathe. The surface characteristics of a machined sample can be compared to a set of measured results. A Lion Precision spindle error analyser is capable of calculating radial, axial and thermal errors using pre-positioned capacitance sensors. This technique is based on the conventional method for measuring spindle error motions, outlined in Appendix A of the ANSI/ASME B89.3.4M [44] standard.

3.1 Diamond Facing Lathe Refurbishment

The existing diamond facing lathe consists of two main components. A powered spindle used to rotate the workpiece and a slideway to traverse the diamond tool. This diamond facing lathe required a significant level of refurbishment work, before any development work could begin (Figure 1-4). The most recent documentation based on the diamond facing lathe was produced by P. D. Comley in 1990, for his MSc Thesis. His research includes a basic analysis of the error motions within the facing lathe and the design and analysis of a "Fast Tool Servomechanism for Single Point Diamond Turning" [45].

The rotation spindle is powered by a three phase AC induction motor connected through an air bearing. The spindle, requiring the highest level of refurbishment work was found to have a seized front thrust bearing. This refurbishment process is documented in section 3.1.1. Before the spindle could be tested a new variable frequency induction drive was installed. This drive is controlled by a new control panel, therefore the old electronic system could be removed. Additional panelling was attached to the control cabinet, to further improve the electrical safety of the system. The linear slideway is based on a friction drive and is mounted onto a hydrodynamic slideway. Once the unit was oiled and the old oil seal had been cracked, the slideway immediately became functional. The slideway is capable of traversing a diamond tool linearly across the face of the workpiece, at speeds between 1μm to 10m per minute. The venturi which creates a vacuum from a compressed air supply was replaced, as its internal components had perished. The vacuum generated is used to secure the workpiece onto the spindle. This venture is capable of producing a maximum vacuum of 80kPa, with a 600kPa compressed air supply. Figure 3-1 shows the refurbished diamond facing lathe.

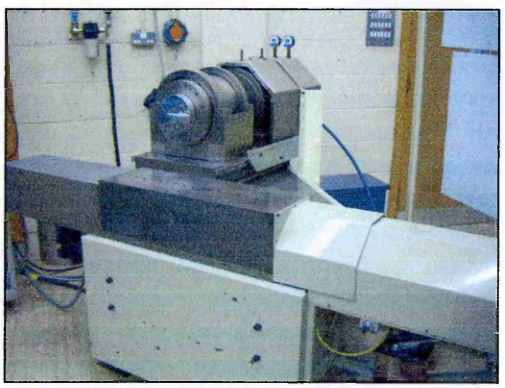

Figure 3-1: Refurbished diamond facing lathe

3.1.1 Thrust Bearing Refurbishment

The two bearing plates from the front thrust bearing on the aerostatic spindle, can be seen in Figure 3-2. The scratches on the insides of these two plates are responsible for seizing the air bearing. These have been formed by a small piece of contamination, which has gained access to the inside of the bearing.

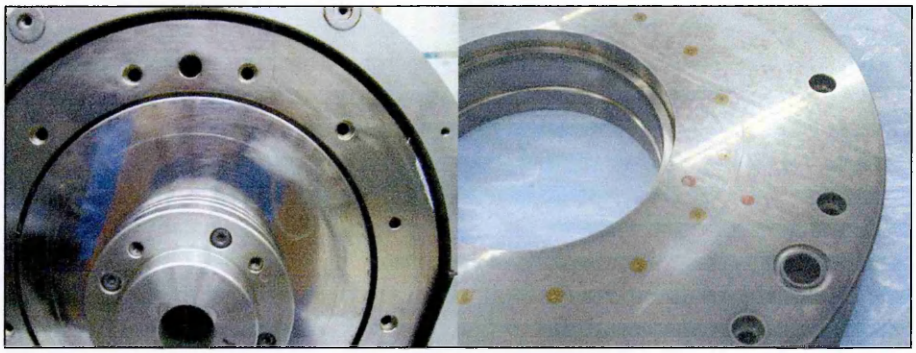

Figure 3-2: Seized thrust bearing

Figure 3-3 shows the Taylor Hobson Form Talysurf machine, analysing the surface quality of the interior surface of the air bearing.

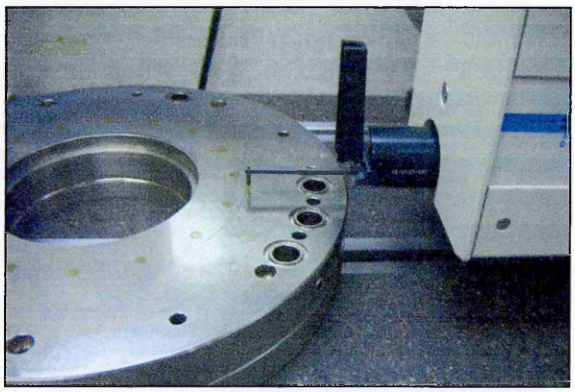

Figure 3-3: Scratch analysis of thrust bearing

The Talysurf results showed the air bearing to have a 14μm peak on its surface (Appendix 1). This peak blocked the 10μm air gap, which is pressurised with air during the operation of the bearing. The peaks of this scratch were removed using a fine smoothing stone and the restrictor holes inspected for debris. The refurbishment process has affected the stiffness and accuracy of rotation, exhibited by the aerostatic bearing.

3.2 Trial Cutting

Figure 3-4 shows the refurbished diamond facing lathe machining an aluminium specimen. This specimen (A) was being machined at 15mm/min, with a cut depth of 10μm from a 1.5mm radius diamond tool.

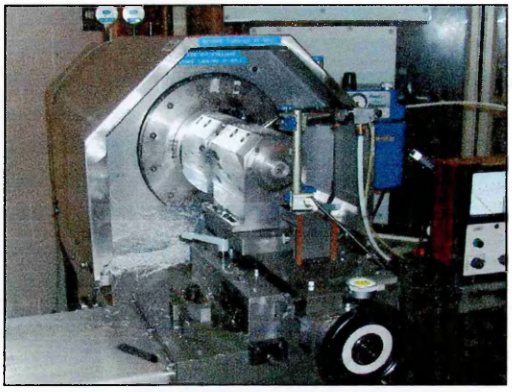

Figure 3-4: Diamond turning an aluminium sample

The surface quality and form accuracy of this specimen may then be analysed and the error motions highlighted. Two aluminium, one brass and one copper samples were machined (Figure 3-5).

Figure 3-5: Diamond turned samples

Each of the samples were individually analysed using the Wyko Typo metrology system, a three dimensional surface analyser. Figure 3-6 shows a three dimensional representation (3D) of a section of the surface, belonging to one of the aluminium samples. The tool cusps are clearly visible on the finished surface.

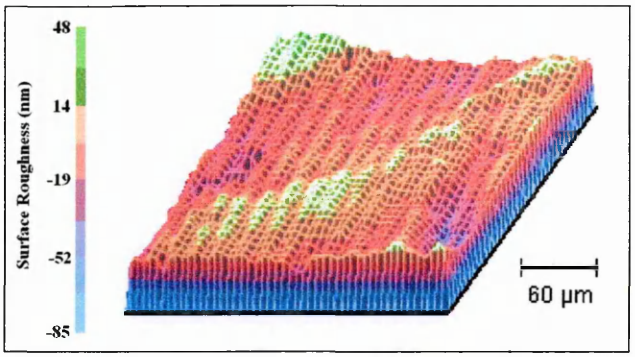

Figure 3-6: Turned aluminium surface

The asynchronous axial error motion may be found when the surface is viewed as a two dimensional slice through the sample (Figure 3-7).

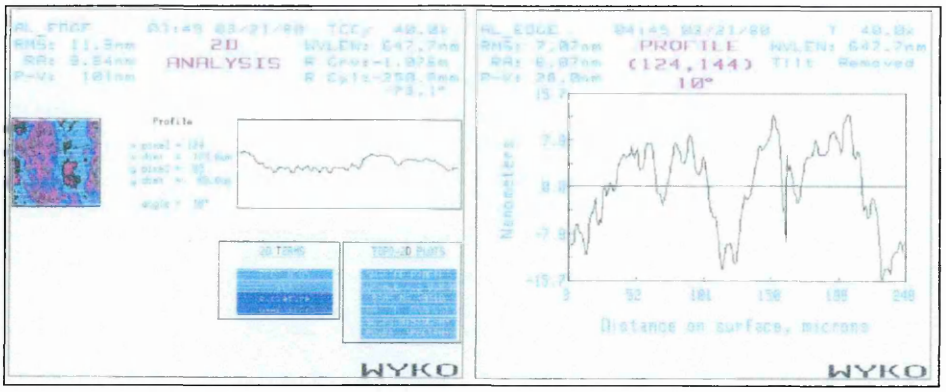

Figure 3-7: 2D results of aluminium surface

The two dimensional results from the Wyko Typo metrology system showed the asynchronous axial error motion of the aerostatic bearing to be 25nm. This was the maximum value of five different regional measurements, from aluminium specimen A. Adding the cusp height of 18.5nm (Equation 2-3) to the asynchronous error motion provides a total peak to valley roughness (R_t) of 43.5nm.

These results are confirmed in a map of the surface topology using the Taylor Hobson measurement probe (Appendix 2). The average roughness of the five largest peaks over a set distance (R_z) is 28nm and the total R_t of the surface is 54nm. The arithmetic roughness (R_a) of the machined sample is therefore 5.3nm.

3.3 Spindle Error Analyser

The Lion Precision Spindle Analyser is a sophisticated spindle error measurement system, capable of measuring radial, axial and thermal errors. The operating principle of the analyser is based on the monitoring of a perfectly spherical shaped target, rotating in the main spindle. Capacitance sensors are positioned around the target and record the errors. Using an analogue to digital acquisition board connected to a computer interface, eccentricity errors are used to calculate the speed of the spindle. Techniques such as the Donaldson Reversal Method exist, which subtract the geometric errors of the master target from the synchronous error motions [46].

3.3.1 Capacitance Probes

Capacitance is the capacity to build up charge in a non conducting material (dielectric), between two conductive plates. Using a constant dielectric (air), the total capacitance is proportional to the area of the plates and inversely proportional to the distance between them. The capacitance probes for the Lion Precision Spindle Analyser (Figure 3-8) have a maximum range of 375µm and a nanometre resolution.

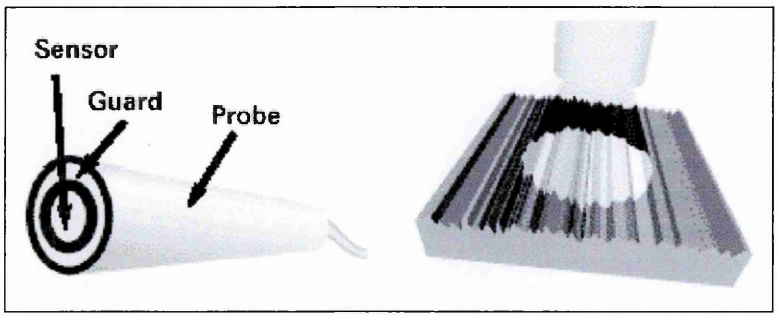

Figure 3-8: Capacitance probes [47]

Runout is defined as "the total displacement measured by an instrument sensing against a moving surface" [44]. Air-bearings have very linear stiffness therefore doubling the speed would have an effect of increasing the induced Runout by a factor of 4 [32] (neglecting damping).

3.3.2 Master Target Mount

A target mount was designed (Figure 3-9) to hold the master target for the analyser, in the centre of rotation of the spindle. This mounting block is very large due to the dimensions of the master target. Once attached onto the spindle face plate, the bearing was re-balanced. Any imbalance generated by the target mount increases the radial synchronous error motion. This does not affect the surface finish capability of the spindle. The imbalance is only noticeable on the synchronous error motions, as the angular position of the disturbance is constant [44].

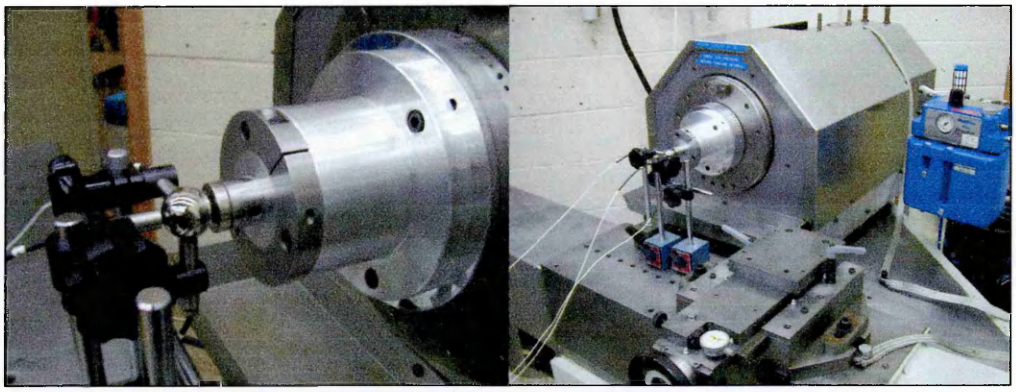

Figure 3-9: Spindle error analyser master target

3.3.3 Spindle Error Motions

To evaluate how the spindle error motions (Figure 3-10) will affect the surface characteristics of a fly-cut component, only a limited number of setups are required. The axial synchronous and asynchronous error motions will affect the form accuracy and surface quality of the component respectively. Although the diamond facing lathe is not located in a temperature controlled environment, the magnitude of the axial thermal error motion is also required.

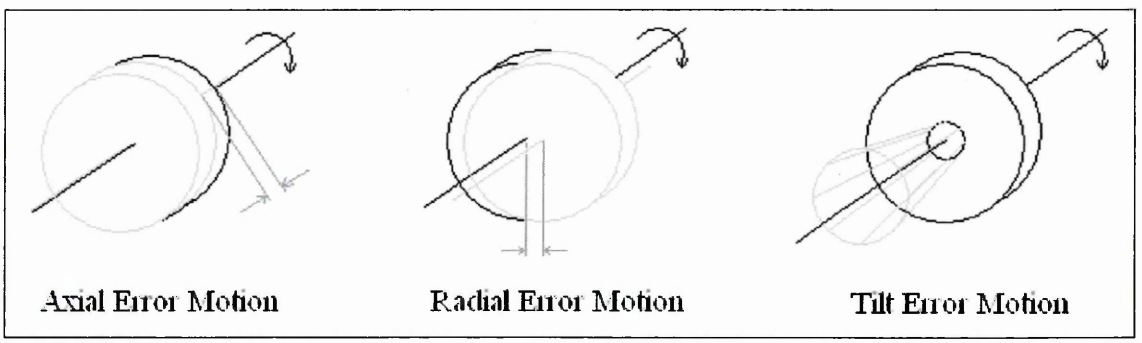

Figure 3-10: Spindle error motions

The limitations of the Lion Precision equipment setup include; a large degree of mains noise generated by the motor, low probe stiffness and the inaccurate placement of the capacitance probes. Each probe may be positioned independently, therefore an inaccuracy of the perpendicularity between each probe will exist. During the operation of the diamond facing lathe, vibrations generated by external equipment will influence the machine tool. Appendix 3 includes the potential errors generated by external vibrations during a worst case scenario. These vibrations are monitored on the top of the slideway, relative to the spindle face plate.

3.3.4 Probe Mount Stiffness

A good probe holder will oscillate with a small amplitude and a very high frequency (200 to 1500 Hz). In practice the natural frequency of the probe mount should be at least double the applied frequency. This frequency should be at least 5 times higher for precision measurements [32].

'Good Probe Mount Design' by Tim Sheridan [32]

- Short robust structures.
- Asymmetry design (symmetrical structures facilitate the generation of standing waves).
- Produced from a material with high internal damping.
- Have a good electrical conductivity (earth).
- Good joint design (high stiffness).

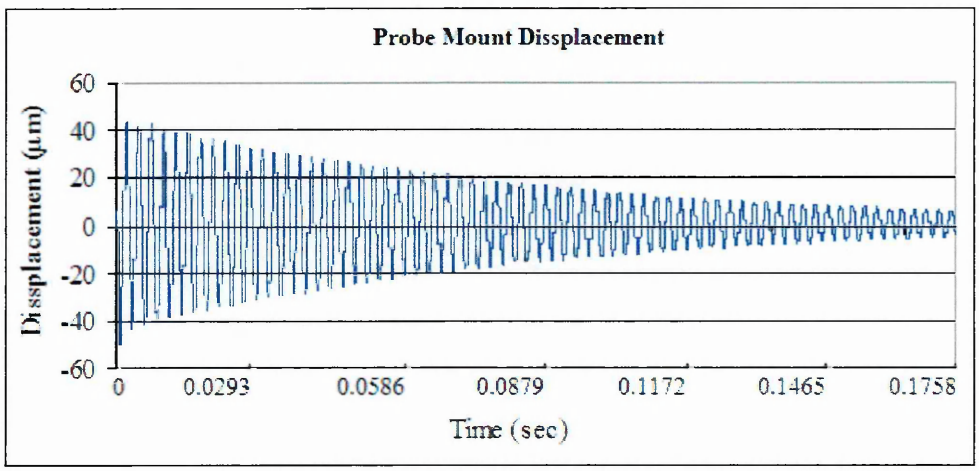

Figure 3-11: Displacement of a single probe mount

One of the errors introduced into the analysis equipment is the effect of the low stiffness of the probe mounts. Using a simple 'tuning fork' technique, the natural frequency of the probe mount may be estimated. Figure 3-11 shows the minimum and maximum amplitudes of this estimation, to be -50.1 µm and 43.4 µm respectively. The time taken to reach zero is 0.376seconds, therefore the oscillation time period is $2.5491x^{-3}$seconds. This gives a natural frequency of 392.3Hz. The spindle has a maximum frequency of 100Hz when spinning at 6000rpm. The stiffness of the probe holder is therefore acceptable.

3.3.5 Axial Error Motions

The asynchronous axial error motion plots, produced by the Lion Spindle Error Analyser are shown below. Figure 3-12 demonstrates the high levels of mains noise present in the motor. To counteract these noise levels, the spindle is earthed and the motor is switched off and allowed to freely rotate when the results are being obtained. Improvements to this system would include inserting a nylon washer between the master target and the spindle clamp.

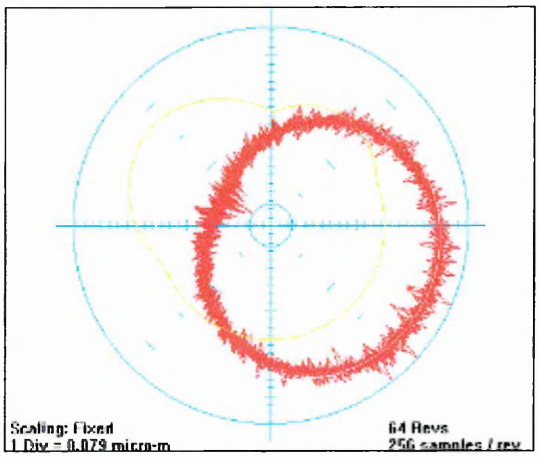

Figure 3-12: Axial error motion - motor on

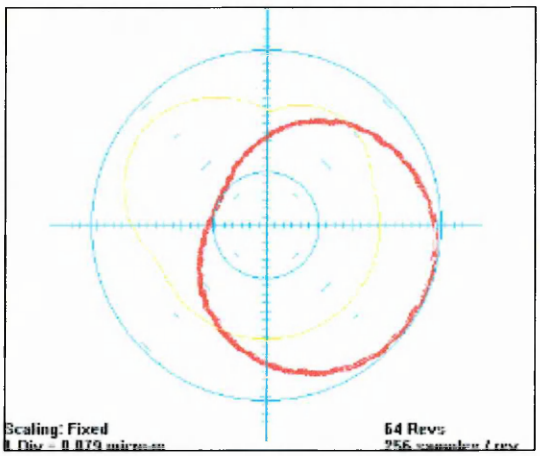

Figure 3-13: Axial error motion - motor off

Table 3-1 documents the axial error motions, collected by the lion precision equipment. The mean synchronous error motion has decreased from 13.4nm to 10.3nm, this is attributable to the reduction in electrical noise generated by the motor. The asynchronous error motion has also decreased to 53.7nm. The fundamental error is generated by the setup up of the equipment. It is related to the form accuracy of the master target and its respective position to the centre of rotation [13].

Axial Error Motions (1500 rpm) (nm)			
	Fundamental Error	**Asynchronous Error**	**Mean Synchronous Error**
Motor On	353 – 359	303.6	13.4
Motor Off	352 – 377	53.7	10.3

Table 3-1: Spindle axial error motions

3.3.6 Thermal Error Motions

Thermal error motions occur slowly and are caused by temperature and environmental fluctuations, both internally and externally to the machine. As different materials and geometrical parts exhibit different coefficients of thermal expansion, the overall thermal growth is not even. This difference generates distortions in the machine structure. Figure 3-14 shows an increase in the axial thermal growth of the spindle, when the rotational velocity of the spindle is increased. This is attributable to an increase in the level of viscous shearing within the aerostatic bearing's internal air gap.

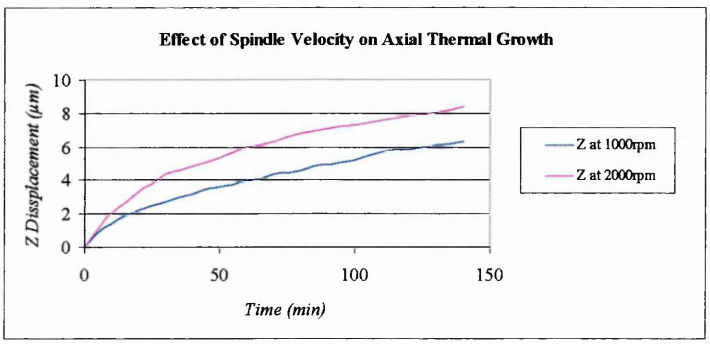

Figure 3-14: Effects of spindle velocity on axial thermal growth

Figure 3-15 demonstrates the relative axial thermal growth of a static and dynamic spindle under similar environmental conditions.

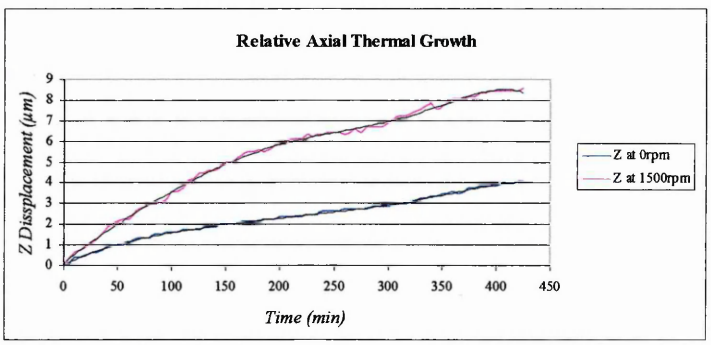

Figure 3-15: Relative axial thermal growth

As the spindle is not located in a temperature controlled environment, Figure 3-16 shows that a small 0.2°C temperature change in the environment will result in a dramatic displacement error.

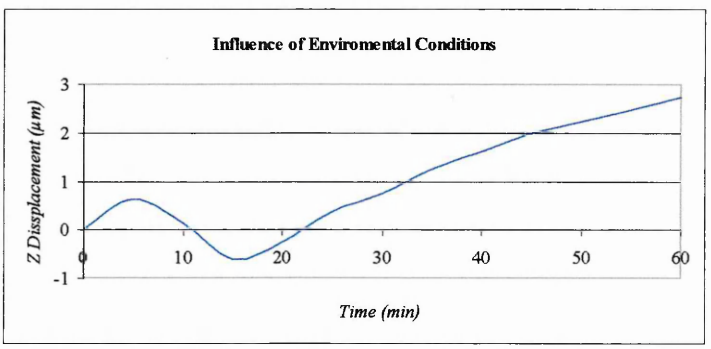

Figure 3-16: Influence of environmental conditions at 1500rpm

3.4 Slideway Analysis

A combination of the tilt and straightness error motions of the slideway were measured, using a precision straight edge and a single capacitance probe. The precision straight edge had a 300nm peak to valley flatness over a length of 150mm. Two different measurement locations were investigated. In the first location the straight edge is positioned onto the front of the spindle and the capacitance probe is mounted onto the slideway (Figure 3-17).

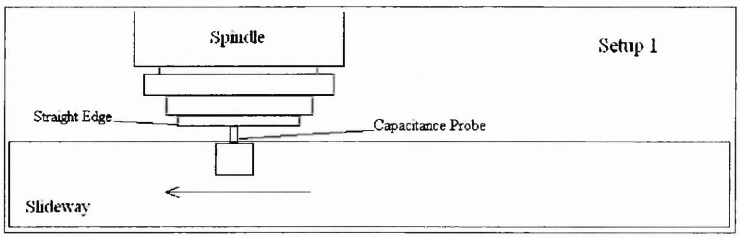

Figure 3-17: Slideway analysis - methodology 1

In the second location the capacitance probe is located on the front of the spindle, 75mm from the centre of rotation. The straight edge is positioned on the slideway (Figure 3-18).

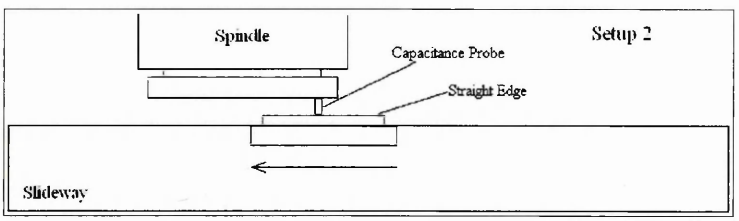

Figure 3-18: Slideway analysis - methodology 2

Figure 3-19 and Figure 3-20 show the tilt and straightness displacement errors of the hydrodynamic slideway. The maximum peak to valley error experienced with both locations is 0.7µm. The noise visible in Figure 3-20 may be attributed to the electrical noise present within the aerostatic bearing.

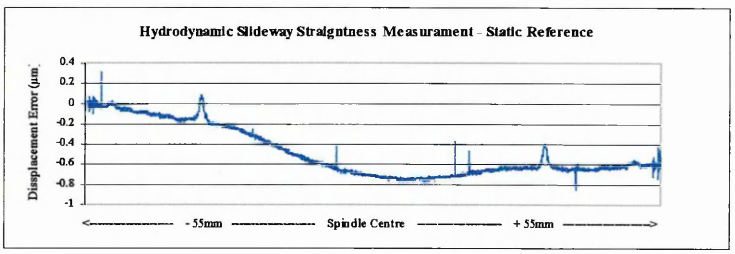

Figure 3-19: Slideway analysis results - methodology 1

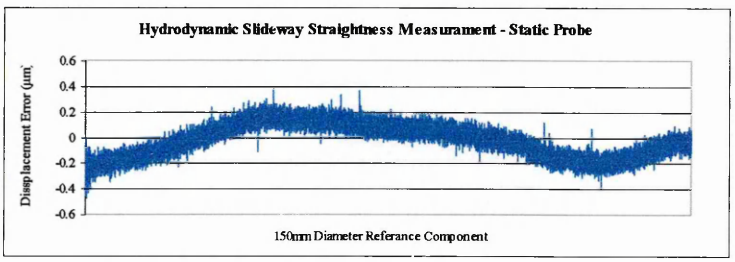

Figure 3-20: Slideway analysis results - methodology 2

4.0 STIFFNESS ANALYSIS

Static stiffness may be defined as, "A ratio between the force and the deformation induced by this force" [48]. Large static deflections of the machine tool components will result in lower achievable accuracies. The static loop stiffness of the machine tool, combines the stiffness for each joint through the load path of the cutting process. It is possible to increase a machine tool's static loop stiffness by implementing control software and feedback loops, with correctly positioned transducers and actuators. It is not possible to modify the dynamic stiffness of a precision machine tool, without modifying the geometry and physical characteristics of the structural components.

A static performance analysis can be used to analyse the refurbishment of the air bearing. This analysis will investigate how the theoretical stiffness values compare to the actual ones.

4.1 Theoretical Axial Stiffness

The stiffness of an aerostatic bearing is directly proportional to the internal pressure ratio. This ratio is a relation between the air gap between the plates and the air supply pressure.

As the axial load on the front of the bearing increases, the bearing's stiffness is also increased as the air gap is reduced. Equation 4-1 demonstrates the relationship between the bearings air gap and axial stiffness (k_{AXIAL}).

Axial Stiffness [40]

$$k_{AXIAL} = \frac{0.44\pi\left(R_o^{\,2} - R_i^{\,2}\right)\left(P_o - P_a\right)}{h_o}$$

$$k_{AXIAL} = 423.36N/\mu m$$

Equation 4-1: Axial stiffness of an annular type, aerostatic thrust bearing

Where,

- k_{AXIAL} : Axial Stiffness
- R_o : Outside radius (102.5mm)
- R_i : Internal radius (51mm)
- Ho : Air gap between bearing surfaces (15μm)
- Ps : Supply Pressure (0.6895N/mm^2)
- P_a : Ambient Pressure (0.10135 N/mm^2)

4.2 Design Layout

Aerostatic bearings are often arranged so that a journal bearing connects a pair of opposing thrust bearing. Different concepts of linking the thrust and journal bearings may be adopted during the bearing design. These concepts will affect the radial, axial and tilt stiffnesses, influence the assembly inaccuracies and vary the manufacturing complexity [49]. Figure 4-1 shows the two variations of a horizontal mounted aerostatic bearing. Table 4-1 shows a non-dimensional performance comparison of the two bearing designs, show in Figure 4-1.

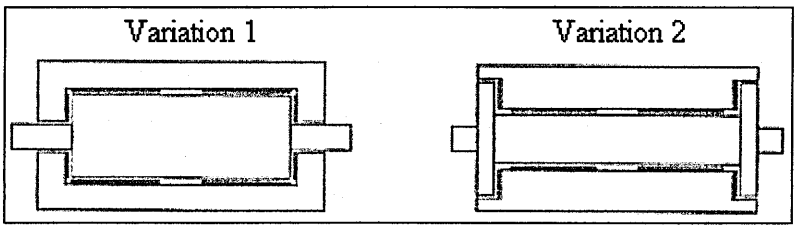

Figure 4-1: Aerostatic bearing design variations [49]

Variant	Stiffnesses			Combined Radial and Axial	Influence of preload	Easiness of manufacturing
No.	Radial (K_r)	Axial (K_a)	Tilt (K_t)	K_r x K_a		
1	0.54	0.50	0.42	0.27	no	normal
2	0.35	0.78	0.31	0.27	great	good

Table 4-1: Aerostatic bearing design comparison [49]

The bearing design within the diamond facing lathe is based on design variation 1. This design has a larger radial stiffness, generated by a larger journal diameter. The surface areas of the thrust bearings are smaller; therefore according to Equation 4-1 the axial stiffness is lower.

4.3 Load Capacity

The maximum axial and radial load capacities of an aerostatic bearing are limited by the maximum geometry and air supply pressure. The radial load capacity of the journal bearing within the diamond facing lathe may be determined experimentally, but there is no geometric information on its design available to calculate a theoretically value. The axial load capacity (W) of the front thrust bearing belonging to the diamond facing lathe is shown in Equation 4-2.

Axial Load Capacity [40]

$$W = 0.26\pi\left(R_o^{\,2} - R_i^{\,2}\right)\left(P_o - P_a\right)$$
$$W = 3752.44N$$

Equation 4-2: Axial load capacity of an annular type, aerostatic thrust bearing

Where,

W : Axial load capacity

The pair of opposing thrust bearings in the diamond facing lathe provides an axial loading capacity in two opposing directions. The resulting axial loading and stiffness attributes of the combined thrust bearings must be considered. Figure 4-2 shows the resultant loading in both directions for the thrust bearing arrangement. If the thrust bearings are assumed to be identical and the alignments of the bearings are geometrically perfect, the axial load capacity is increased by twenty five percent [50]. The bidirectional axial load capacity is therefore 4690.55N.

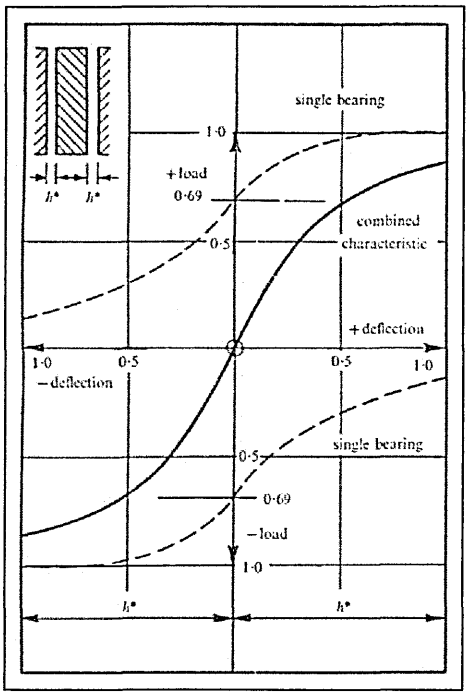

Figure 4-2: Load capacity of opposing thrust bearings [50]

4.4 Gas Flow Rate

The gas flow rate (Q) of an aerostatic bearing is an important economic factor in the bearing design. An excessive gas flow rate will render the bearing uneconomical [51]. The theoretical gas flow rate for the front thrust bearing, belonging to the small diamond facing lathe is shown in Equation 4-3.

Gas Flow Rate [40]

$$Q = \frac{0.27h_o^3\left(\frac{P_o}{P_a}\right)^2}{\left(3.42\times10^6\right)\times0.51\times\ln\left(\frac{R_o}{R_i}\right)}$$

$$Q = 0.0346m^3/\text{sec}$$

Equation 4-3: Gas flow rate for an annular type, aerostatic thrust bearing

Where,

Q : Gas flow rate

4.5 Experimental Axial Stiffness

The axial stiffness is measured using a load cell and a micrometer probe. The equipment setup may be seen in Figure 4-3. A displacement was applied to the front of the spindle and the axial force was measured by the load cell. The displacement is measured relative to the granite base of the aerostatic bearing.

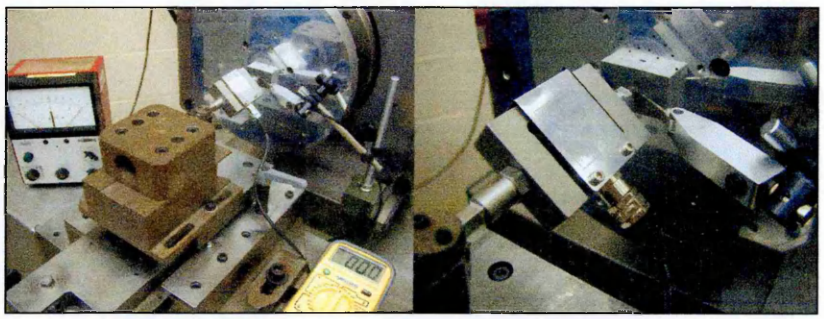

Figure 4-3: Air bearing axial stiffness component setup

Figure 4-4 shows the linear trend line of the spindle face plate displacement, with respect to an increasing force. The axial stiffness of the spindle is the gradient of the linear trend line. The axial stiffness of the aerostatic bearing is 33.759N/μm.

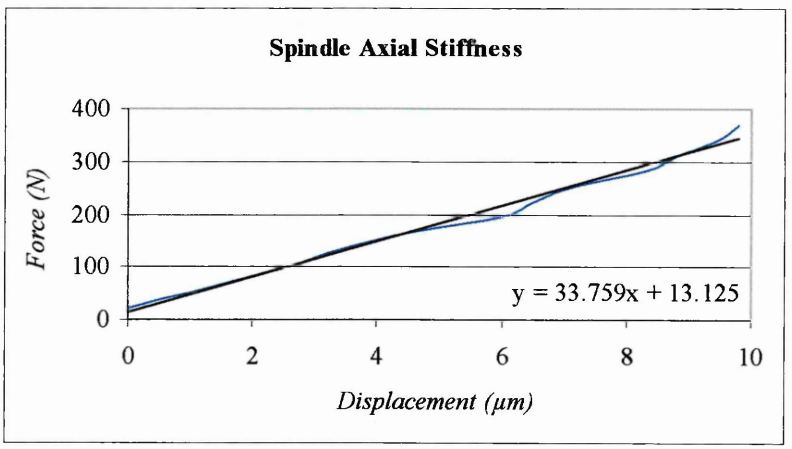

Figure 4-4: Air bearing axial stiffness

The original design specification for the axial stiffness of the spindle is 595N/μm [45].

4.6 Static Loop Stiffness

The static loop stiffness of the diamond facing lathe is a function of all of the different joints, within the load path. By inverting these stiffness values these joints are considered as compliances and the overall static loop compliance may be expressed as the sum of all the individual compliances.

$$C_{Loop} = C_{Spindle} + C_{Slideway} + C_{Z-Slide} + C_{Tool-Holder}$$

Equation 4-4: Static Loop Compliance

Where,

C_{Loop} : Static loop compliance
$C_{Spindle}$: Spindle compliance
$C_{Slideway}$: Slideway compliance
$C_{Z\text{-}Slide}$: Z-Slide compliance
$C_{Tool\text{-}Holder}$: Tool holder compliance

Figure 4-5 shows the equipment setup for the static loop stiffness test. The axial stiffness for the spindle has been determined in section 4.6. Assuming the epoxy base has an infinite stiffness, the slideway, Z-slide and tool holder joints remain. For each joint, the reference point remains constant and the location of the base of the micrometer probe is changed. The three location points are shown in Figure 4-5.

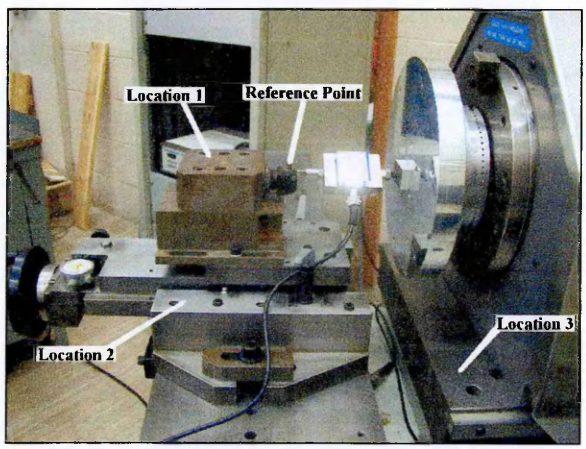

Figure 4-5: Static loop stiffness component setup

Equation 4-5 relates the location points which are shown in Figure 4-5, to each components individual compliance value.

$$C_{Location1} = C_{Tool-Holder}$$

$$C_{Location2} = C_{Z-Slide} + C_{Tool-Holder}$$

$$C_{Location3} = C_{Slideway} + C_{Z-Slide} + C_{Tool-Holder}$$

Equation 4-5: Component compliance values

The linear trend lines which represent the different location stiffness values are shown in Figure 4-6.

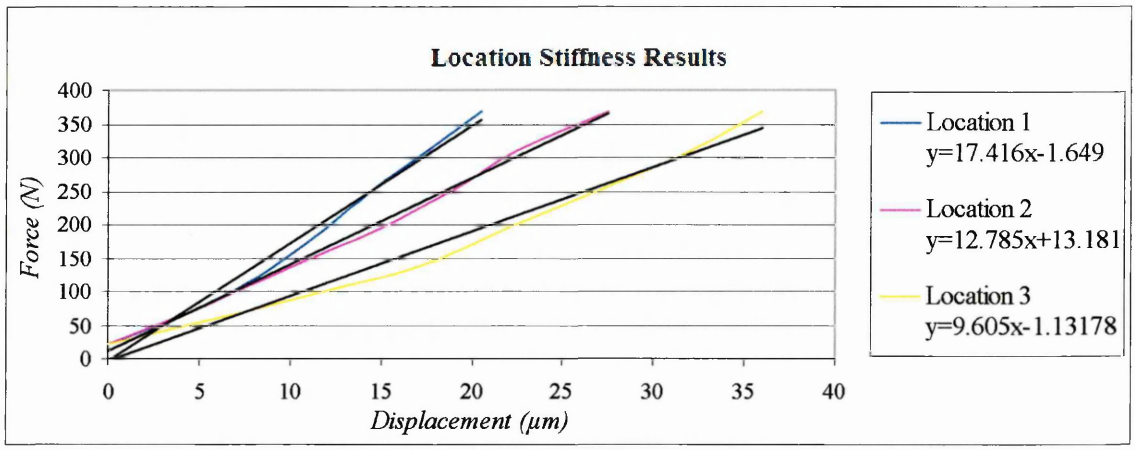

Figure 4-6: Location stiffness results

Table 4-2 contains the individual static stiffness values for each joint, within the load path of the diamond facing lathe. From these results the static loop stiffness may be calculated from the inverse of the static loop compliance, as shown in Equation 4-4.

Component	Compliance (µm/N)	Stiffness (N/µm)
Spindle	0.0296	33.759
Tool Holder	0.0574	17.416
Z-Slide	0.0208	48.03
Slideway	0.0259	38.59

Table 4-2: Static stiffness values

The static loop stiffness for the diamond facing lathe is 7.47N/µm.

4.7 Experimental Dynamic Radial Stiffness

The dynamic radial stiffness of the journal bearing may be estimated by applying a known load at the spindle's circumference (Figure 4-7). The difference in the radial error (D_R) when the spindle is operated at a known angular velocity (ω), can be related to the radial stiffness (Equation 4-6). The radial error can be measured using the Lion Precision Spindle Analyser.

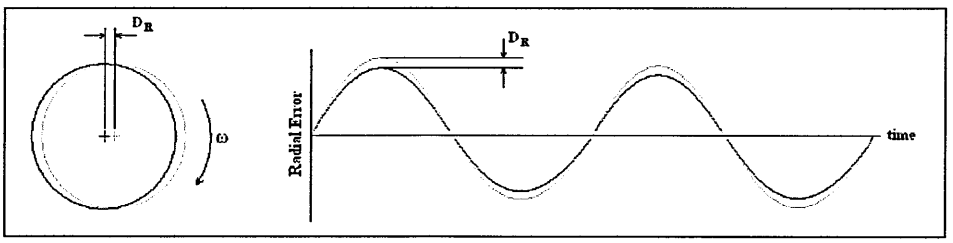

Figure 4-7: Dynamic radial stiffness

Stiffness Equation

$$k = \frac{F_R}{D_R}$$

Equation 4-6: Dynamic radial stiffness

Where,

k : Stiffness
F_R : Radial force
D_R : Deflection

Force Equation

$$F_R = m \times R_m \times \omega^2$$

Equation 4-7: Dynamic radial force

Where,

m : Mass
R_m : Radius of mass
ω : Angular velocity

From Equation 4-6 the dynamic radial stiffness of the spindle can be calculated. Two masses of 12 and 24 grams were used, with a constant radial velocity of 1500RPM.

Angular Force (N)	Deflection (µm)	Radial Stiffness (N/µm) 1500RPM
23.66	0.124024×10^{-6}	190.79
47.33	0.248048×10^{-6}	190.80

Table 4-3: Dynamic radial stiffness results

From Table 4-3, the dynamic radial stiffness of the aerostatic journal bearing is 190.8N/µm. The original radial stiffness specification according to Comley, was 183N/µm [45].

5.0 FEASIBILITY STUDY

This feasibility study will evaluate the influence of the error motions of the diamond facing lathe, against the design requirements of the fly-cutting system. The spindle and slideway errors motions are shown in section 5.1. The evaluation of these motions can then be used to produce a technical specification.

5.1 Error Budget

Spindle Errors	
Axial Synchronous Error:	10.3nm
Radial Synchronous Error:	n.a.
Static Axial stiffness:	33.759N/μm
Dynamic Radial stiffness:	190.790N/μm at 25Hz

X Axis Errors	
Straightness (X axis):	0.7μm P-V
Static Slideway Stiffness:	3.180N/μm
Static Z-Slide Stiffness:	4.631N/μm

Time Based Errors	
Thermal Drift in Spindle (0 rpm):	4.0μm
Thermal Drift in Spindle (1500 rpm):	8.5μm
Spindle Asynchronous Error:	53.7nm

Other Errors	
Floor Vibrations (Laboratory Conditions):	4.96nm P-V

5.2 Error Motion Evaluation

The maximum measured axial asynchronous error of the aerostatic spindle is 53.7nm. The acceptable surface roughness values will therefore be approximately 80nm P-V, including the cusp depth. This is greater than the initial specification of 50nm P-V, therefore the component specification must be altered to reflect the performance of the machine tool. An axial displacement of +/-10μm is required to compensate for the maximum straightness errors and thermal drift of the spindle. The angular displacement should therefore be 20arcsec. This is the angular displacement required for a 10μm axial displacement of a 100mm diameter component. The resolutions of these axial and radial motions should therefore be 10nm and 0.02arcsec respectively. These would enable the fly-cutter to generate the required component form-accuracies (200nm P-V). A closed loop control system is required to continuously monitor and adjust the relative positions of the diamond tool and the workpiece. This feedback system will require a minimum reference edge length of 100mm to compensate for the spindle drift. A 200mm reference length would enable the slideway motions to be monitored also. The fundamental frequency of all the machine components must be lower than the maximum frequency of the spindle (100Hz). The axial and radial stiffness must be as great as the current values, to limit their effects. The maximum unbalanced mass of the cutting head, should be equal to the maximum balancing moment at the circumference of the spindle face plate.

5.3 Technical Specifications

	Ideal Value	*Acceptable Value*
FLY-CUTTING HEAD		
Fundamental Frequency	160Hz	120Hz
Static Axial Stiffness	100N/μm	50N/μm
Radius of Diamond Tool Holder	80mm	65mm
Combined Mass	5kg	8kg
Maximum Diameter	275mm	320mm
Surface Reference for Error Compensation	200mm	100mm
Mass Imbalance	0.011.25kg	0.016.9kg
Diamond Tool Holder		
- CUPE Shank (6.35mm^2 x 20mm)		
- Quick Release Tool Change		
- Tool Replacement Repeatability Error	+/-5μm	+/-10μm
- Tool Setting Station		
- Tool to Holder Mass Ratio	1:3	1:4
Vacuum Chuck for Diamond Turning		
Combined Mass	5kg	8kg
Maximum Diameter	275mm	320mm
Surface Reference for Error Compensation	200mm	100mm
WORKPIECE HOLDER		
3 Degrees of Freedom (axial and two tilts)		
Component Diameter	130mm	100mm
Axial Displacement	+/-10μm	+/-8μm
Axial Displacement Resolution	10nm	30nm
Angular Displacement	20.0arcsec	16.5arcsec
Angular Displacement Resolution	0.02arcsec	0.05arcsec
Fundamental Frequency	160Hz	120Hz
Control System		
- Closed Loop Feedback		
- Sensor Resolution	10nm	30nm
- Sensor Range	1mm	0.5mm
GENERAL		
Single Phase Power Requirements		
Conform to ISO 14001 Standards		
Basic Maintenance Requirements Only		
Full Technical Documentation		
- Risk Assessment		
- Standard Operating Procedure		

6.0 CONCEPT DESIGN

This chapter identifies the components required for a diamond fly-cutting system. The design criteria and concept detail has been included on each component.

6.1 Concept Overview

The fly-cutting system requires a diamond tool mounted at a radius from the spindle's centre of rotation. This radius will be governed by the maximum part diameter specification. A dynamic workpiece holder containing a feedback loop, referenced to the relative error motions between the spindle and slideway is also required. Figure 6-1 demonstrates the locations of the identified components, relative to the existing diamond facing lathe. It can be seen that the workpiece holder is displaced horizontally across the front of the fly-cutting head. The cut depth is applied, by displacing the workpiece holder closer to the diamond tool. This is achieved manually by using the existing z-slide on the diamond facing lathe.

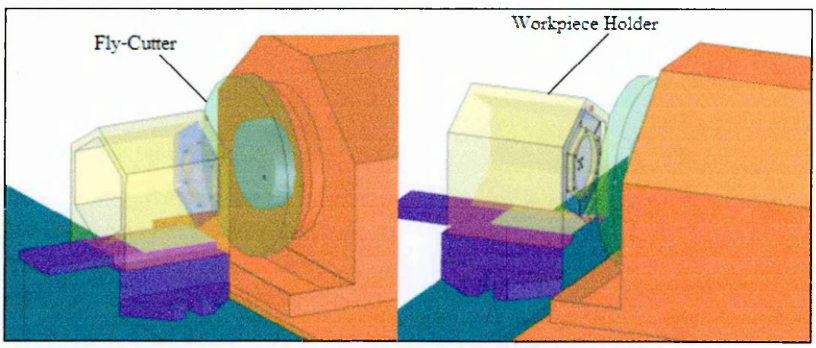

Figure 6-1: Fly-cutting system concept overview

6.2 Fly-Cutting Head

The fly-cutting head is secured to the spindle face plate and rotates the diamond tool around a 75mm radius. On completion of the machining operation a 25mm clearance gap is left around a 100mm diameter workpiece, as it remains stationary inside the cutting path. The diamond tool has a CUPE shank (6.35mm^2 x 20mm) and is held at a particular orientation within a quick release tool holder. The diamond tool is secured into the tool holder using a set of grub screws. This technique allows the diamond tool to be located into position using a microscope. The tool holder may then be repeatedly secured into position within the fly-cutting head, by using a quick release clamping mechanism.

The fly-cutting head is circular to decrease any synchronous radial excitation forces generated by an imbalance in the design. The large surface area of the cutting-head provides a reference datum for position sensors within the control system. These sensors are used to feedback the location of the cutting head to the control system. As this relative position changes according to the spindle and slideway error motions, the workpiece is orientated and positioned accordingly. This dynamic orientation of the workpiece is undertaken during the machining process.

Chapter 7 contains a detailed concept design and optimisation results, for the diamond fly-cutting head.

6.3 Dynamic Workpiece Holder

6.3.1 Workpiece Manipulation

A flexure is a frictionless displacement device, which relies on the elastic deformation of a material [52]. A three pair flexure design has been chosen to manipulate the workpiece. This arrangement is an improvement on a conventional three position flexure design, where only half of the number of flexures is used (Figure 6-2). The three pair configuration forms a symmetrical structure with twice the axial and rotational stiffness [53]. This design is capable of repeated and accurate positioning of the workpiece. However consideration must be given to ensure the mechanical properties of the materials chosen are not exceeded, as this could result in premature plastic deformation of the structure.

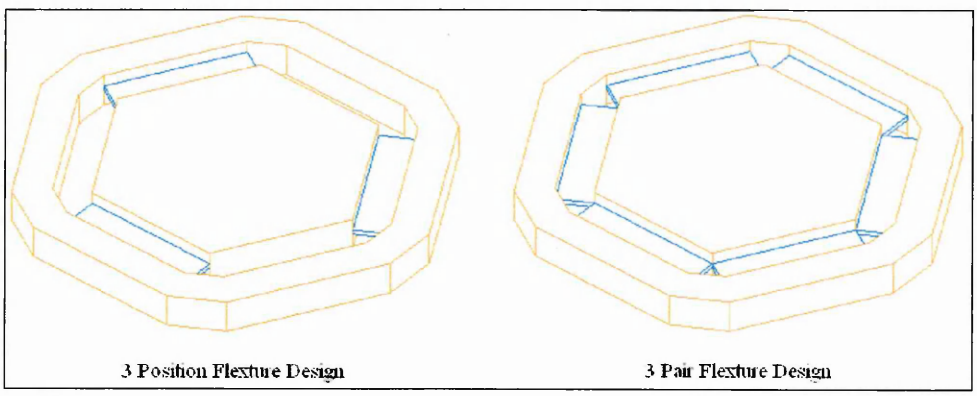

Figure 6-2: 3 Position and 3 pair flexure designs

By implementing this mechanical arrangement of flexures, this design is capable of orientating the workpiece through the Z axis and around the X and Y axes. These three degrees of freedom allow the workpiece to be orientated relative to the rotating diamond tool, to remove any thermal and geometric based errors in the machine tool. Each of the three degrees of freedom in the three pair flexure system requires an independent linear actuator. The independent positions of these actuators, generate the overall orientation of the workpiece holder. The feedback and control systems which are required, are discussed in section 6.3.4.

Linear Actuators

Plumbum (lead) Zirconate Titanate (PZT) based ceramic actuators, are capable of generating precision linear motions. They are able to generate high actuation forces and have an unlimited theoretical resolution. The resolution of a PZT actuator is not limited by friction or an operating threshold voltage, but by the mechanical design of its surrounding components and any electrical noise from the control amplifier. PZT actuators have a very fast response time and are not affected by electromagnetic fields [52]. A low voltage, preloaded PZT actuator (P-841.20 from PI) has been chosen for the manipulation of the workpiece. They include a closed loop positioning system with a maximum travel of 30µm and a nanometre resolution. Their internal preloading provides a forward actuation force of 1000N and a reverse force of 50N [52].

Flexure Design

The geometric design of a flexure is dependent on its stiffness. This stiffness governs the deflection of the flexure when a known force is applied. The geometric design of a pair of flexures is based on the bending moment of a single, simply supported beam. Further iterations of this model include the parallel bending mode of a single flexure and finally a model of a pair of flexures with opposing parallel moments. Each of these model iterations may be seen in Figure 6-3. The flexure design is based on the physical properties of generic isotropic mild steel.

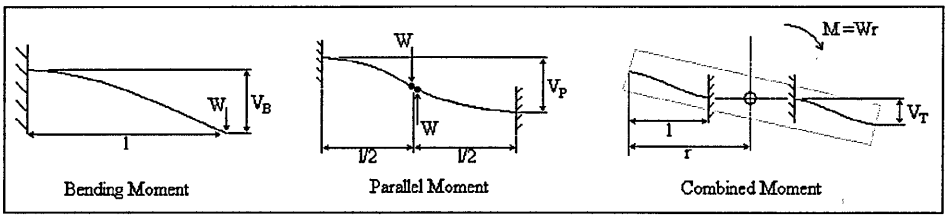

Figure 6-3: Parallel mode flexure design

Equations 13, 14 and15 govern the vertical deflection and axial stiffness for a pair of flexures [53]. These equations have been used to generate a look up table (Appendix 4), to aid the design of the three pair flexure system.

Second Moment of Inertia [53]

$$I = \frac{bh^3}{12}$$

Equation 6-1: Flexure design - second moment of inertia

Vertical Deflection [53]

$$V_T = \frac{Wl^3}{EI}\left(\frac{-r}{2(3l-6r)}\right)$$

Equation 6-2: Flexure design - vertical deflection

Axial Stiffness [53]

$$k_T = \frac{W}{V_T}$$

$$k_T = \frac{Ebh^3}{l^3}\left(\frac{1-2r}{-2r}\right)$$

Equation 6-3: Flexure design – axial stiffness

Where,

W	: Applied force
l	: Length of flexure
E	: Young's modulus
I	: Second moment of area
B	: Width of flexure
h	: Thickness of flexure
r	: Flexure radius
V_T	: Vertical deflection in combined mode
k_T	: Axial stiffness in combined mode

The exact flexure dimensions have not been calculated, because the stress relationship between the flexure pairs has not been considered. This relationship has been simulated using a finite element (FE) analysis package. A three dimensional mesh has been generated around the model and the underside of the outside mount has been fully constrained in all 6 degrees of freedom. The mesh and boundary condition set may be seen in Figure 6-4. The individual actuation forces have been applied in their corresponding locations at 120° intervals, with a pitch circle diameter of 40mm about the centre of the model.

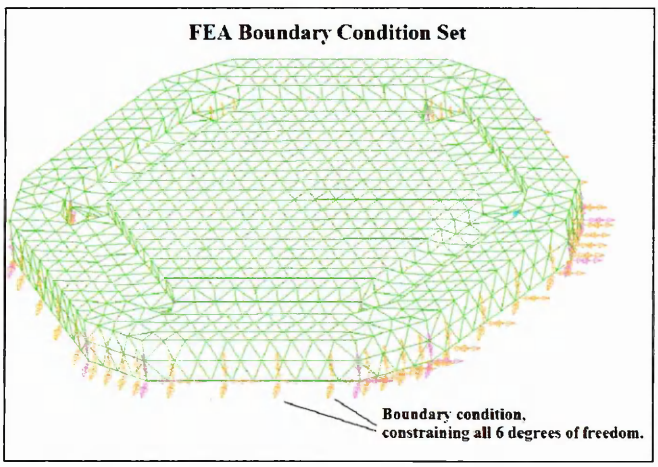

Figure 6-4: FEA Boundary Condition Set

Figure 6-5 shows the simulation of the axial motion of the flexures. The maximum axial displacement is 18.7µm with an input force of 1000N per flexure.

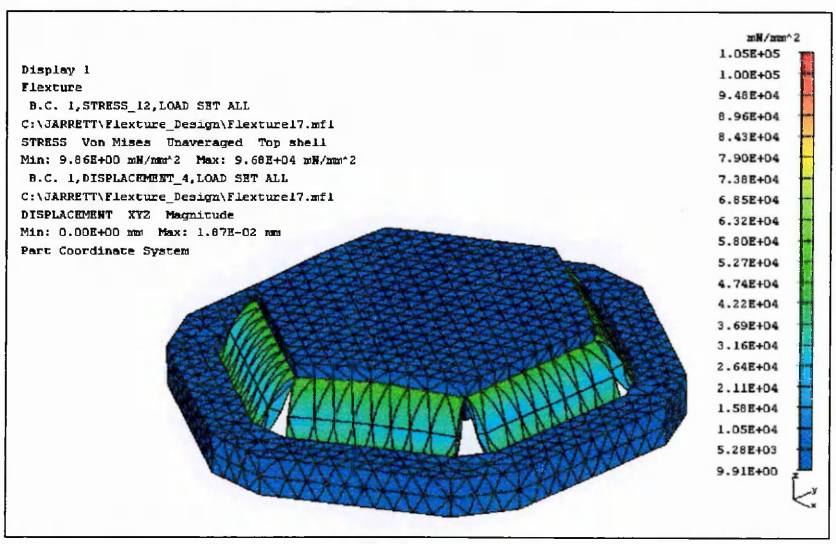

Figure 6-5: Flexure design simulation

Figure 6-6 shows the maximum orientations of the three pair flexure system, with each linear actuator individually activated. The maximum axial displacement for a single orientation is 12µm and a maximum orientation angle of 24.75arcsec.

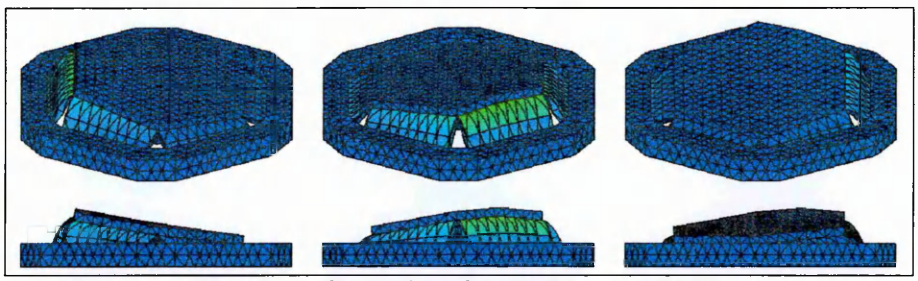

Figure 6-6: Simulation of workpiece orientations

The flexures in Figure 6-5 are 58mm wide, with a thickness of 2mm. The length of 15mm may be optimised to provide the correct maximum displacement. Table 6-1 shows the relationship between the length of the flexure and the maximum combined axial displacement.

Flexure Length (mm)	**Maximum Axial Displacement (μm)**
15.00	18.7
15.05	18.9
15.10	19.0
15.15	21.1
15.20	21.2

Table 6-1: Flexure geometry optimisation

The non-linear relationship between the flexure length and maximum axial displacement can be attributed to the inaccuracy of mesh, which surrounds the analysis model. This is caused by the modifications to the flexure geometry, during the analysis.

6.3.2 Workpiece Mounting

The design of the workpiece mount requires features to secure the axial and angular position of the component. This must be a repeatable position, implementing a clamping technique which does not influence the component's geometry. The mounting technique must not limit the geometry, or the maximum diameter of the workpiece.

The finite element analysis of the 3 pair flexure design employs a fixed point force, to represent a PTZ actuator. With these single point force boundary conditions, the geometry of the workpiece mount distorts (Figure 6-7). The distortion may be minimised by modifying the design of the workpiece mount and increasing the stiffness of the material used.

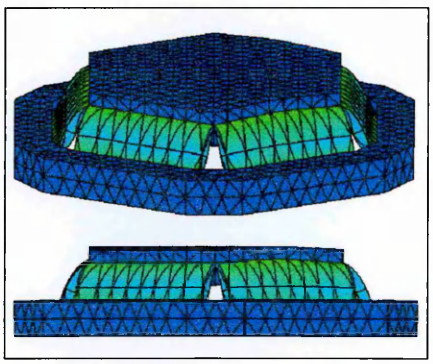

Figure 6-7: Simulation of workpiece mount distortions

As a result of the distortion generated by the PZT actuators, the workpiece mount is offset by 2mm, from the front of the flexure plate. This mount is secured to the flexure plate in three positions, at the opposing sides to the actuators. The plate includes a vacuum connection which is connected to the vacuum generator, through a hole in the centre of the flexure plate. The use of a vacuum provides a repeatable and non-influencing technique for securing the workpiece into its axial position. The angular position of the workpiece is set within the design of the mounting plate, which is bolted onto the front of the workpiece mount (Figure 6-8). This plate has a unique design for each different component and includes an array of restrictor holes for the vacuum supply.

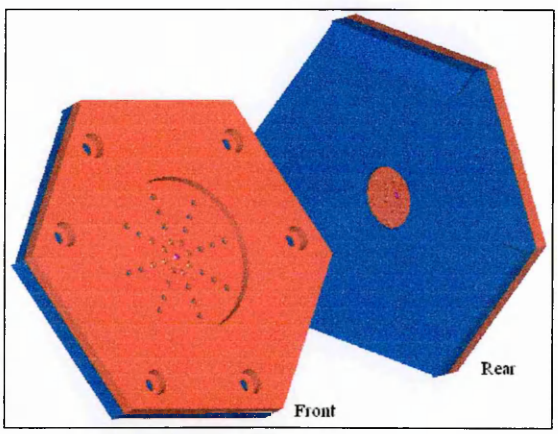

Figure 6-8: Workpiece mount

6.3.3 Probe Mounting

Four capacitance probes from Lion Precision (C6-D) are required to monitor the error motions within the machine tool. These capacitance probes have a resolution of 25nm, over a range of 125 to 625µm. This resolution is within the acceptable range of the technical specification. These probes are located at four corners of a square mount, around the outside of the workpiece holder. The location of these sensors enables a computer interface to calculate the relative X and Y rotations (Tip and Tilt) and Z displacement of the cutting path. The workpiece may then be orientated accordingly to counteract these error motions. Each capacitance probe will require a Lion Precision probe driver (CLP 290) which includes dual sensitivity control. An analogue to digital converter is also required to connect the output from the probe drivers to a computer interface. Figure 6-9 shows the location of the capacitance probes, relative to the workpiece and the rotating diamond tool.

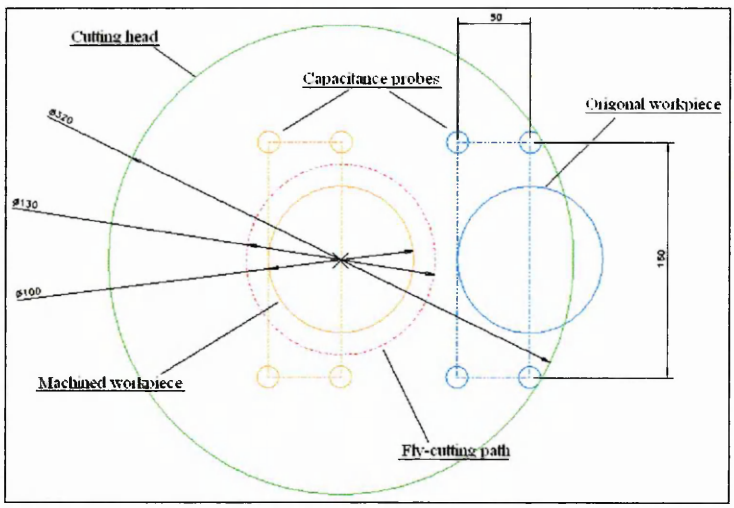

Figure 6-9: Location of capacitance probes

During the setting operation of the fly-cutting system, the axial displacement of the probes must be set and then locked into position. This process is required so that the system may accommodate a variation in the workpiece thickness. Once the relative angle of the capacitance probe is secured, a differential amplifier operating within the computer interface may be used to remove any initial offset value. Compensation for variation in the probe mount angles may be modified within the computer interface, once the surface of a fly-cut component has been evaluated. Figure 6-10 includes a basic design for an adjustable capacitance probe mount. A detailed assembly drawing is shown in Appendix 5.

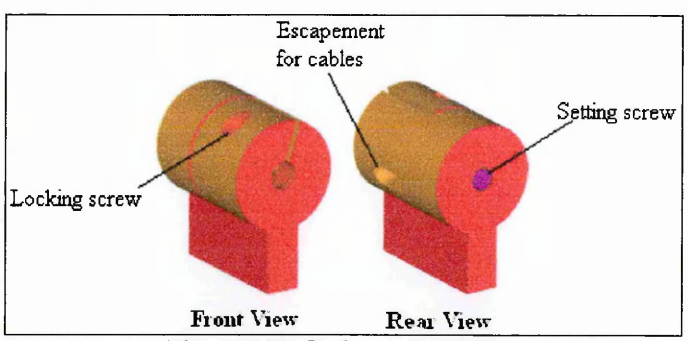

Figure 6-10: Probe mount design

The design in Figure 6-10 includes a rear grub screw for the axial adjustment of the capacitance probe. The probe may then be locked permanently into position, for the duration of the machining cycle.

Implementing Capacitance Probes

During the analysis of the error motions of the aerostatic spindle (documented in section 3.2.5), errors were observed which were attributable to noise from the three phase motor. This noise may be damped by insulating the fly-cutting head from the spindle face place. The grounding capacitance of the fly-cutting head is therefore no longer suitable for a precision measurement. For a precision measurement this grounding capacitance should be one hundred times greater than the sensor capacitance [54] (Figure 6-11).

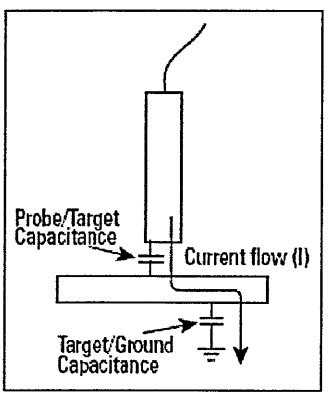

Figure 6-11: Ground capacitance sensor [54]

A technique known as, "A two channel, out of phase measurement" may be employed, as it does not require a grounding capacitance. In this technique, two capacitance probes are synchronised 180° out of phase and the measurements are alternated between the two. The second capacitance sensor only provides the return path for the sensing current [54]. This concept may be seen in Figure 6-12.

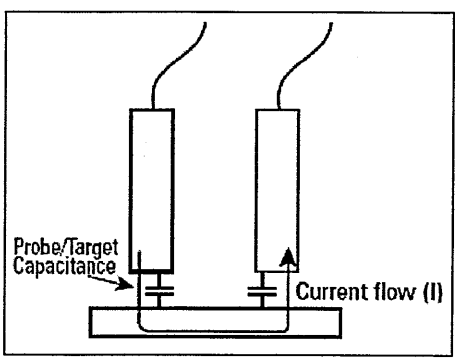

Figure 6-12: Dual capacitance sensor synchronisation [54]

6.3.4 Control Systems

This section introduces the relationship between the displacement of each of the PZT actuators and their influences on the orientation of the workpiece. Suitable actuators, transducers and control techniques have been recommended, along with a system layout. This layout includes the capacitance probes as discussed in the previous section.

Workpiece Orientation

A control system is required to control the relationship between the PZT actuator displacement and the workpiece orientation. The functions within this control system have been expressed in Equation 6-4, according to Figure 6-13 [52].

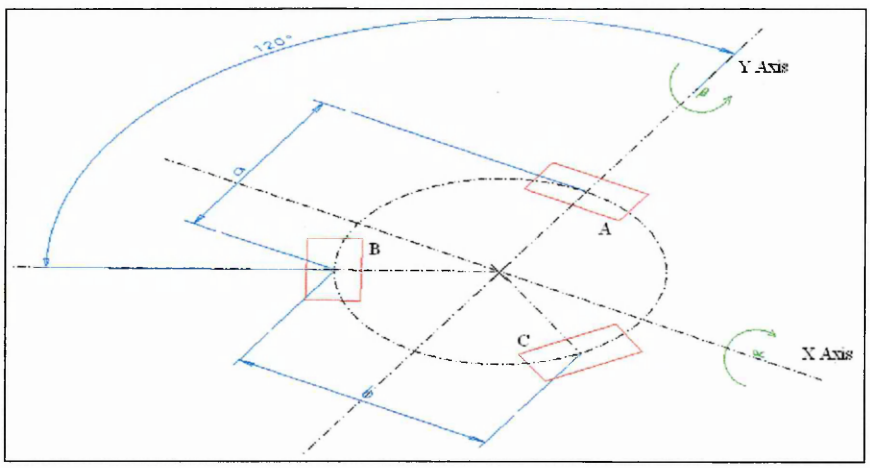

Figure 6-13: 3 Pair flexure control

$$\alpha = \frac{2A-(B+C)}{2a}$$
$$\beta = \frac{(B-C)}{b}$$
$$Z = \frac{(A+B+C)}{3}$$

Equation 6-4: 3 Pair flexure control

Where,

α	: Tip angle (DOF 1)
β	: Tilt angle (DOF 2)
Z	: Axial displacement (DOF 3)
A	: Actuator A displacement
B	: Actuator B displacement
C	: Actuator C displacement
a	: Dimension a
b	: Dimension b

Control System Overview
The control system has been documented in Appendix 6. This appendix contains a control system overview diagram, which includes the key components. By implementing a range of control modules, the error motions of the machine tool have been linked to the orientation of the workpiece.

The low voltage PZT actuators specified for the manipulation of the workpiece holder in section 6.3.1, employ a closed loop control system to improve their displacement accuracy and repeatability. Open loop PZT actuators experience hysteresis and drift errors, which affect their positioning accuracy and repeatability [52]. The closed loop control is achieved by comparing the actual position with the demanded value. The displacement may then be adjusted to equal the two values. A resistive film strain gauge, bonded to the piezo actuator provides the actual displacement value [52]. The demanded value is compared using a proportional integral (PI) controller module (E-509). This module is capable of increasing the stiffness of each of the actuators through control, by varying the operating voltages with load variations.

Each of the PZT actuators requires a low voltage amplifier module (E-503). These modules require a high level of electrical noise filtering, to limit their effects against the resolution of the actuator. A 20 bit analogue to digital converter (E-516.i3) has been specified, to link the displacements of the piezo actuators to a computer interface. The computer interface will link the orientation of the workpiece to the measured error motions of the machine tool. Complex functions may be introduced to the motions of the workpiece holder, to generate complex structured surfaces.

The control modules required for the operation of the PZT actuators are shown in Figure 3-10. This includes the PZT three channel amplifier, the strain gauge sensor module and the analogue to digital converter. These components are housed within an enclosure (E-500), designed to combine their functionality.

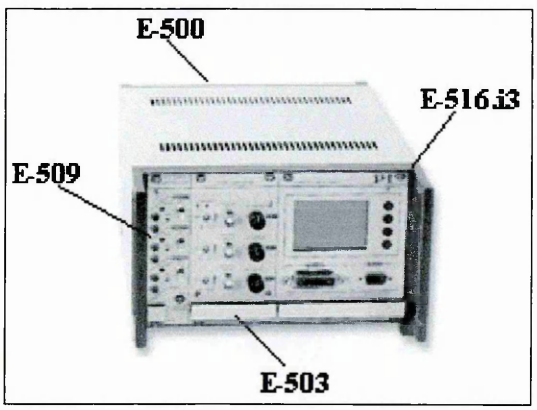

Figure 6-14: Control system overview

7.0 DETAILED DESIGN

The design of the fly cutting head must conform to all of the specifications outlined in section 5.3. The quick release tool holder will serve as an interface between the single point diamond tool and the components of the fly-cutting system. Upon the removal of the tool holder from the cutting face plate, it must be possible to replace the tool holder containing a diamond tool within a repeatable position of +/-5μm.

7.1 Design Methodology

As a result of the large range of technologies available for use in the quick release tool holder a formal design methodology has been produced (Table 7-1). This process has been designed to brainstorm all of the different techniques and produce feasible concepts from these. These concepts have been outlined using a morphological ideas chart and evaluated according to a set of partial functions, using a Pugh's matrix [55].

Design Procedure	
1.	Define partial functions according to technical specification and concept design.
2.	Create a morphological chart from these partial functions.
3.	Apply design ideas to morphological chart.
4.	Identify feasible concept design combinations.
5.	Develop these feasible concepts for further analysis.
6.	Evaluate these concepts using a Pugh's Matrix, to identify the most ideal design components or design concept.
7.	Develop the most ideal concept using knowledge gained from the Pugh's matrix.

Table 7-1: Detailed design procedure

7.1.1 Generation of Design Ideas

A simple brainstorming technique can be used to generate design ideas. These design ideas should not be analysed and disregarded, as each idea may lead to a more advanced iteration.

7.1.2 Morphological Charts

A morphological chart enables a designer to compactly combine all of their design ideas into one location, so they may be sorted into areas defined by the partial functions. A combination of ideas may then be chosen for further development and evaluation.

7.1.3 Pugh's Matrixes

A Pugh's matrix is a design concept evaluation procedure, based on a set of evaluation criteria generated from the technical specifications. The concepts are evaluated against a datum concept, which in this case will be one of the generated concepts. A Pugh's matrix is a very effective method of evaluating developed designs against an original one.

7.2 Definition of Partial Functions

Partial Function 1: The linear position (X, Y, and Z axis) of the diamond tool must be adjustable.

Partial function 2: The diamond tool must be positioned into a repeatable axial position once set within the fly-cutting head.

Partial function 3: The diamond tool must be orientated into a repeatable angular position.

Partial function 4: A quick release locking mechanism is required to secure the diamond tool into the fly-cutting head.

7.3 Morphological Chart

Partial functions		**Design ideas**				
		1	*2*	*3*	*4*	*5*
1	Adjustable Position of diamond tool	Grub screws into holder	Mechanical bush	2 part tool holder	Grub screws into cutting-head	
2	Repeatable axial position	Mechanical block	Kinematic mount	Screw Thread		
3	Repeatable angular position	Key and keyway	Kinematic ball and V-groove	Pin and dowel	Geometric feature	
4	Quick release locking mechanism	Bolt with cup and seat bearing	Flexure spring bush	Hydraulic friction clamp	Vacuum force	System 3R hydraulic tool clamp

Table 7-2: Morphological chart

7.4 Concept Identification

Table 7-3 includes the concepts generated from the morphological chart.

Concept 1		**Concept 2**		**Concept 3**		**Concept 4**	
Partial function	*Design idea*	*Partial function*	*Design idea*	*Partial function*	*Design idea*	*Partial function*	*Design idea*
1	1	1	1	1	2	1	1
2	2	2	2	2	2	2	1
3	2	3	2	3	4	3	1
4	1	4	3	4	2	4	4

Table 7-3: Concept Identification

7.4.1 Design Concept 1

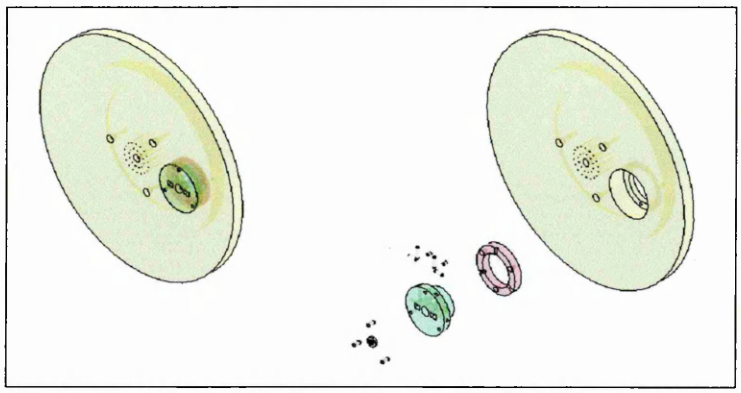

Figure 7-1: Cutting head design concept 1

The diamond tools are located in a holder and secured into position. Up to two tools may be inserted. The tool holder is then kinematically located onto a base which is secured into the balancing disc. The orientation and axial position of the tools may be adjusted, using a three-vee kinematic design. The kinematic balls are secured onto grub screws, and may be adjusted from the front plate of the tool holder. The holder is locked into position using a central securing bolt. The orientation of this bolt is not restricted, as it sits on a mechanical friction cup and seat bearing. This allows the tool holder to tip and tilt, with a 5° displacement. Detailed assembly drawings for all of the design concepts are shown in Appendix 7.

7.4.2 Design Concept 2

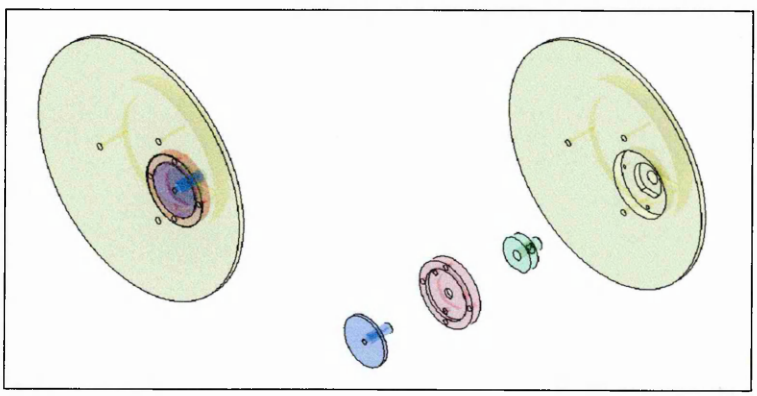

Figure 7-2: Cutting head design concept 2

Concept 2 is based on a hydraulic friction lock (ETP-T), which is used to clamp a tool holder into position. A diamond tool is secured into the tool holder, which locates quasi-kinematically into a face plate. A three-vee kinematic location is machined into the face plate. The tool holder locates into a permanent position using 3, V-shaped notches. The geometric area of these notches is based on the axial and radial stiffness required for the design. The face plate is used to secure the friction lock into its axial position and a feature on the balancing disk secures its angular position. The clamping force is activated through the side of the balancing disk using a 6mm hexagonal tool.

7.4.3 Design Concept 3

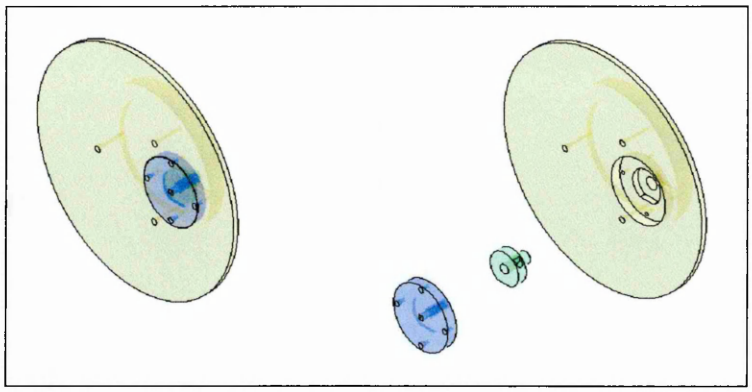

Figure 7-3: Cutting head design concept 3

The third concept employs an identical hydraulic friction lock to the second concept. The front plate and tool holder are designed as one component and the diamond tool is inserted into the cutting head, independent of an external tool holder. The front plate includes a location fit for the diamond tool and a mechanical bush. This mechanical bush is based on a series of flexures, which contract when the friction lock is activated. This secures the diamond tool into position.

7.4.4 Design Concept 4

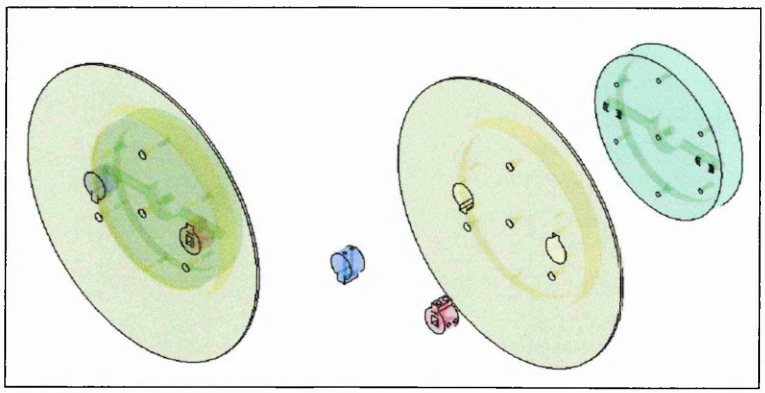

Figure 7-4: Cutting head design concept 4

Unlike concepts 1 to 3, the clamping force in concept 4 is generated by a vacuum. The diamond tool is secured into a removable tool holder. Two tool holders may be inserted into the cutting disk or one blank holder may be used. The holders are aligned into an axial position using a shaped holder and the radial position is secured using a key and keyway design. The outside diameter of the tool holder may be produced very accurately, according to the exact internal diameter of the face place. The keyway may then be machined with the two parts clamped into position. Using a broaching tool a very accurate keyway may be machined. The diamond tool and tool holder will react against the rear vacuum plate. When inserted and a vacuum is applied the holders will position parallel to the front face of the face plate, with a holding force of 1.05N. A small ejection pulse of compressed air from the vacuum generator may be used, to aid the removal of the diamond tool.

7.5 Pugh's Matrix

Evaluation Criteria	Concept number			
	1	*2*	*3*	*4*
High axial stiffness of secured diamond tool	Reference concept	+	+	-
High radial stiffness of secured diamond tool		+	+	+
Effectiveness of quick release tool holder		+	-	+
High position repeatability of tool holder		0	0	0
Ability to accurately position the diamond tool		0	-	0
Low tool to holder mass ratio		-	-	+
Large surface reference for error compensation		0	0	0
Large cut radius		0	0	0
Low imbalanced mass		0	0	+
Low Weight		-	-	+
Low manufacturing costs		+	+	-
$\Sigma +$	0	4	3	5
$\Sigma 0$	0	5	4	4
$\Sigma -$	0	2	4	2
Net Value	0	2	-1	3
Ranking Order	3	2	4	1
Further Development	No	Yes	No	Yes

Table 7-4: Pugh's matrix

The Pugh matrix has highlighted concepts 2 and 4 to be the most ideal. Concept 2 is based on a hydraulic friction lock and has a high clamping force, with a large axial stiffness. The hydraulic friction lock is very heavy and provides an 'over-engineered' solution to the problem. Concept 4 is very dynamically stable and only requires a low amount of mass to be removed from the cutting head. This concept implements a vacuum supply to provide a holding force for the tool. When a 75kPa vacuum force is applied, only a 1.05N holding force is generated to secure each of the holders. The axial stiffness is therefore not sufficient to securely mount the diamond tool within the fly-cutting head. This design also has the largest manufacturing costs, attributable to the complexity of the design and low tolerances required. The relative parts should be manufactured in pairs to decrease these tolerances.

7.6 Fly-Cutting head Design Concept

The final proposed design concept is shown in Figure 7-5. The diamond tools are located in the tool holder shown in Figure 7-6 and may be positioned using setting 4 setting screws. The tool holder should be produced with a high manufacturing tolerance and machined to fit its location within the fly-cutting head. The angular position of the tool holder is set within the fly-cutting head using a key and keyway design. Using a broaching technique, an accurate keyway may be simultaneously machined into the two parts. The final key should be manufactured from silver steel, and bolted into the groove on the tool holder.

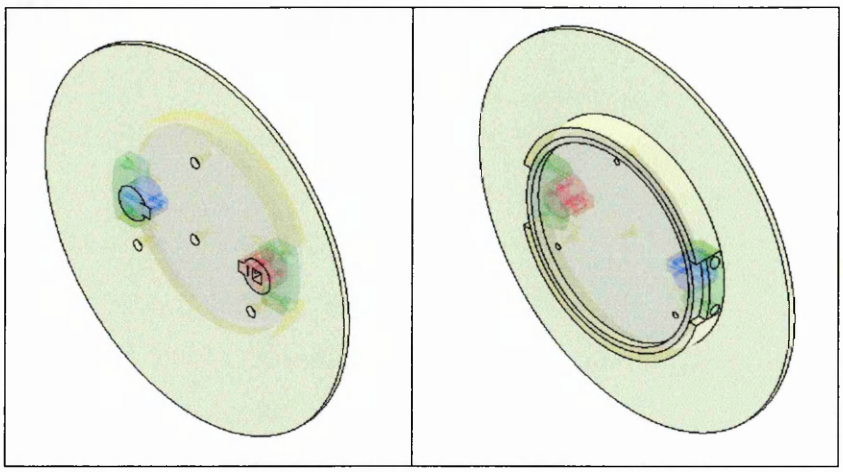

Figure 7-5: Fly-cutting head design concept

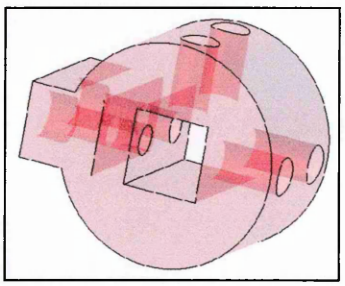

Figure 7-6: Diamond tool holder

The exploded view of the front and rear of the fly-cutting head is shown in Figure 7-7. The tool holder is secured into the fly-cutting head using a semi-kinematic location on the inside of a side locking clamp. The design process has shown these clamps to be the most ideal design, however further research is required on the design of the semi-kinematic location. This location should involve a singular v-groove design to locate the axial position of the tool holder.

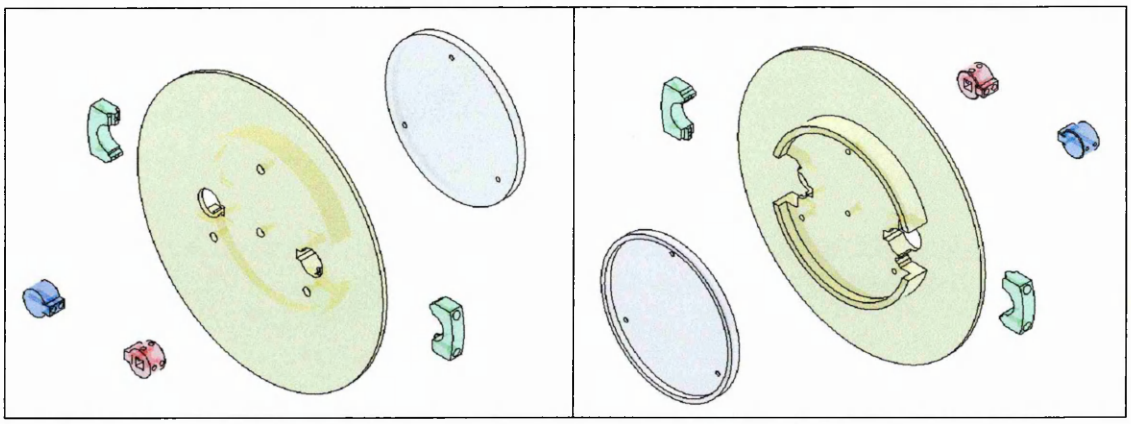

Figure 7-7: Fly-cutting head design concept - exploded views

Consideration should also be given to the manufacturing methods for this part. By tightening the locking bolts within the slide locking clamp, the tool holder will be secured into a repeatable location. An insulation plate has been included in the design. This plate is located between the fly-cutting head and the spindle face plate. The benefits of this part are described in section 6.3.3. A detailed assembly drawing of the fly-cutting head is shown in Appendix 9.

7.7 Design Optimisation

The geometric design of the fly-cutting head may be analysed and then optimised, to improve both its static and dynamic performance. Three dimensional (3D) modelling and analysis packages, such as I-DEAS can be used for both linear and non-linear analysis. Initial estimations of the geometry may be analysed by stiffness calculations based on linear elastic theories or Hertzian contacts [1]. The dynamic analysis will determine the resonant frequencies of the model. At the fundamental frequency, the cutting head will become unstable and will geometrically distort. This distortion will generate errors in the cut surface. The stiffness of the design must be evaluated above the operating frequency of the fly-cutting system (100Hz).

The geometry has been optimised according to the thickness (Dimension A) of the design, as shown in Figure 7-8. The optimisation parameters included minimising the fundamental frequency and total mass.

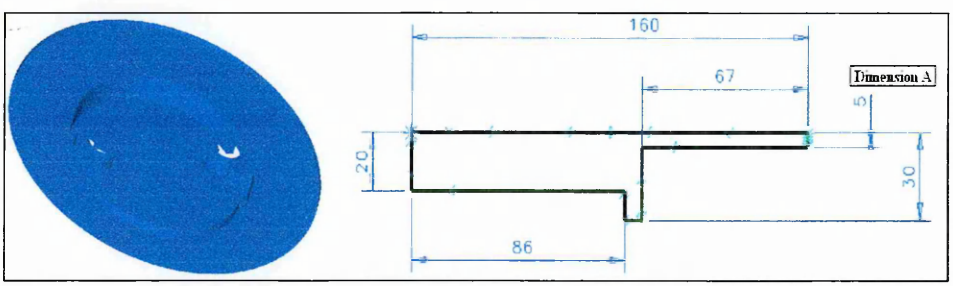

Figure 7-8: Design optimisation geometry

The optimisation results are shown in Table 7-5 and graphically in Appendix 8. These results show how the design modifications affect the fundamental frequency and stiffness values. The stiffness of the fly-cutting head is measured at the external diameter, on the front of the reference surface.

Dimension A *(mm)*	**Mass** *(kg)*	**Volume** *(mm^3)*	**Fundamental Frequency** *(Hz)*	**Stiffness** *(N/μm)*
3	5.26	666781	495	3.51
4	5.7	722136	641	7.87
5	6.14	777487	781	14.66
6	6.57	832835	913	24.27
7	7.02	888178	1040	37.17

Table 7-5: Design optimisation results

Figure – demonstrates how the 1st, 3rd, 5th and 7th modes of the resonant frequency affect the geometry of the component, with a thickness (Dimension A) of 5mm. During the resonant frequencies, these displacements are controlled by the damping coefficient of the structure.

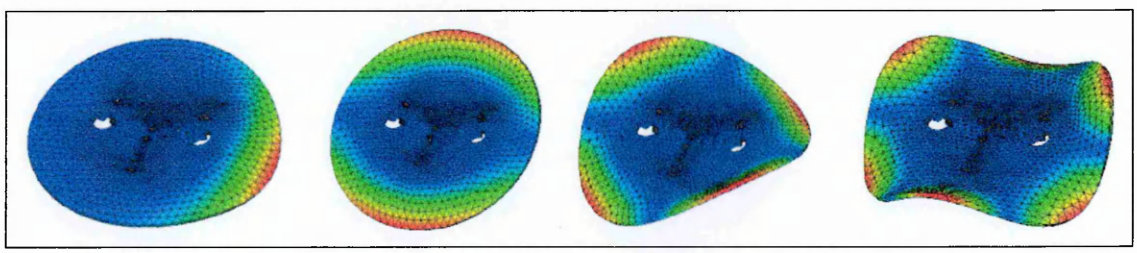

Figure 7-9: Resonant frequency modes, 1, 3, 5 and 7

8.0 DISCUSSION

8.1 System Refurbishment

The refurbishment of the diamond facing lathe included the installation of a new variable frequency induction drive, used to control the rotation of the spindle. This system requires additional safety equipment to be installed, such as an emergency stop switch and safety guarding with interlocks. In its present condition, the facing lathe is considered to be a piece of experimental equipment. Access to the operating region surrounding the machine, should therefore be restricted and sufficient safety equipment supplied to the operators. The analysis procedures documented within this Thesis, conform to these safety regulations.

8.2 Bearing Refurbishment

During the refurbishment procedure of the front thrust aerostatic bearing, it was shown that internal surface damage was the cause of the stationary spindle. A 14μm peak surface scratch was blocking the 10μm air gap between the two surfaces. This scratch may be attributed to a small amount of contamination, between these two surfaces. To prevent any future contamination, compressed air should be continuously supplied to the aerostatic bearing. A combination of this refurbishment process and errors introduced over time, will have affected the performance of the facing lathe. The spindle and slideway error motions have therefore been evaluated, so they may be accounted for in the component design. A stiffness analysis also provides an indication of the performance of the facing lathe.

8.3 Dynamic Performance Analysis

In order to evaluate the error motions of the aerostatic spindle and hydrodynamic slideway, the surface characteristics of a diamond turned sample have been compared to a set of measured results. The error motions of the spindle have been identified, under the guidelines outlined in the ANSI/ASME B89.3.4M standard for specifying and testing axes of rotation. A Lion precision Spindle Analyser was used to measure and record the error motions of the spindle, using a set of pre-positioned capacitance probes. This system monitors the error motions of an unloaded spindle, compared to the error motions visible in the surface topology of the machine sample, which include the cutting force. Single point diamond turning and fly-cutting require low feedrates, high rotational velocities and have very small material removal rates. The small cutting forces experienced during the process (outlined in section 2.6), therefore only slightly influence the error motions of the spindle. The axial and radial deflections, under these cutting forces will be discussed in the analysis of the stiffness results below.

The asynchronous axial error motions of the spindle, affect the surface roughness of a machined part. A two dimensional Wyko Topo interferometer measurement profile of one of the aluminium samples shows there is an asynchronous axial error motion of 25nm, with a peak to valley value roughness (R_t) of 43.5nm. A Taylor Hobson map of the machined surface showed the peak roughness to be 54nm over a large surface area. The arithmetic roughness (R_a) of the machined sample is therefore 5.3nm. During the analysis of the axial error motion of the spindle, the electrical noise of the motor generated a large amount of interference in the results. This problem was solved by

allowing the spindle to free wheel during the collection of these results, however during the measurement period the velocity of the spindle gradually decreased. This effect may be neglected due to the short time duration required for the collection of there results and the low frictional coefficient of the bearing. The results measured by the Lion Precision spindle analyser showed an asynchronous error motion of 53.7nm. When the motor was left on during the result collection, this rose to 303.6nm. An additional grounding connection was attached to the spindle to improve the performance of the capacitance sensors. This analysis process indicated that the face plate should be insulated from the spindle, to remove the electrical noise in the final fly-cutting head design. The cutting forces on the spindle, may account for a slightly lower asynchronous error in the machined samples. This cutting force may have limited some of the vibration modes within the machine tool.

The diamond facing lathe is located within a contaminated laboratory environment, which affects the error motions of the machine tool. The maximum error generated by a worst case scenario floor vibration with a probe mount natural frequency of 392Hz, is 49.6nm (P-V) at a frequency of 296Hz. The axial thermal growth of a spindle rotating at 1500rpm is 8.5μm, over a 4 hour period. The thermal analysis results have also demonstrated the effects of viscous sheering, occurring when the axial thermal growth increases parallel to an increase in the speed of the spindle. The spindle is very sensitive to temperature variations; a 3.25μm displacement was experienced over a 45 minute period, which was shown to be attributable to a 0.2°C temperature increase, in the spindles immediate environment. These results show that machine tool should be located in a temperature controlled environment.

The main set-up error which will have influenced the measured results, is the inaccurate placement of the capacitance probes around a spherical master target. Each probe may be individually positioned and orientated around the spherical target. An improvement would include the design and manufacturer of a target holder, to secure the targets in accurate and repeatable positions and orientations. The maximum tilt and straightness errors of the slideway were recorded using two different component placements. One set-up was based on a diamond tuning process and the other was based on a fly-cutting process. A maximum error of 0.7μm (P-V) was experienced by both equipment setups.

8.4 Stiffness Analysis

The static axial stiffness and dynamic radial stiffness may be compared to the theoretical, experimental and the original specification values, which were documented by Comley in 1990. The theoretical axial stiffness of the spindle is 423.36N/μm, which is close to the original specification of 595N/μm. The actual static axial stiffness is only 33.76N/μm; this decrease may be attributed to the refurbishment of the front thrust bearing. This bearing is responsible for an axial force, loaded against the front of the spindle. The stoning operation and possibly an incorrect tightening torque applied during the refurbishment process, may have affected the bearing's performance. The restrictor holes were manually inspected for contamination, although it is still possible for contamination to exist within the feeding network for these holes. The dynamic radial stiffness is controlled by the internal journal bearing of the aerostatic spindle. The experimental result of 190.80N/μm, is very close to the original specification of

183N/μm. This demonstrates that the journal bearing surrounding the centre of the spindle, has not been affected over time or by the refurbishment process.

8.5 Feasibility Study

The feasibility study of the diamond facing lathe included an evaluation of the error motions and stiffness properties, and how these would affect a fly-cut component. This study was used to produce a set of technical specifications for the concept design. The original acceptable design specification for the roughness of the component has been modified from 50nm (P-V) to 80nm (P-V). This increase is attributable to the maximum measured asynchronous error (50nm) and the optimal cusp depth (18nm). The experimental trial cut, produced a surface roughness of 54nm (P-V) which has been used for the ideal roughness value.

8.6 Concept Design

The fly-cutting system design concept has been separated into two main sections. These are the cutting head and the dynamic workpiece holder. The design concept for the dynamic workpiece holder has been separated into 4 main sections, these include:

- Dynamic orientation of the workpiece
- Non-influential workpiece clamping
- Probe mounting techniques and layout
- Control system overview

8.6.1 Fly-Cutting Head

The fly-cutting head has been designed to minimise the synchronous radial error motions of the spindle, by adopting a circular design. This circular design with a quick release tool holder has been adopted thoughtout a detailed design procedure. This methodology, outlined in section 7.1, has generated and comparatively evaluated a set of design concepts to a list of requirements (partial functions). From the 4 design concepts identified, the final concept implements a semi-kinematic slide locking clamp, to secure the diamond tool holder into position. Accurate keyways control the orientation of the diamond tool, these expensive to manufacturer as the parts have to be produced in pairs and machined as pairs where appropriate. This increases the overall manufacturing time, due to more complex setting procedures. The geometry of this concept has then been optimised, in order to decrease the overall mass. The optimisation graphs may be seen in Appendix 8, where the mass has been decreased down from 7.02kg to 5.26kg. This decrease has lowered the fundamental frequency of the component to 495Hz, which is well above the ideal specification value of 160Hz. The axial stiffness around the circumference of the cutting head is now 3.51N/μm. This value is well below the acceptable value, specified in the technical specifications. Further investigation may be undertaken to increase the axial stiffness and lower the fundamental frequency of the tool holder. This may be accomplished through inserting ribs and fillets into the part's geometry. This technique of modifying a component's geometry will however increase the manufacturing cost of the part.

8.6.2 Workpiece Orientation

The orientation of the workpiece is achieved through the closed loop control of a platform, mounted to a 3 pair flexure design. When a set of known forces is applied, the flexures enable the workpiece to be orientated through two axes of rotation and a single axial axis. The workpiece is capable of a 19μm combined axial displacement and a maximum angular orientation of 24.75arcsec. The resonant frequencies of the flexures should be compared to those belonging to the PZT actuators. This is in order to determine the maximum acceleration frequency of the workpiece, to ensure the flexures do not geometrically distort during their operation. An important future design consideration is what technique should be used to secure the flexures, to the internal and external mounting plates? The author recommends the flexure plate should be produced as a single part and pressed between 2 halves of the mounting plates. The distance between the bolts and their thread depths should then be designed, according to the number of bolts and their individual torques. The compressive force between the two plates should never fall below a critical value, therefore the force envelope belonging to each bolt should overlap.

8.6.3 Workpiece Holder

The workpiece holder has been designed to secure the axial and angular position of a 100mm diameter part. A vacuum has been implemented to secure the axial position and the geometry of the holder limits its angular position. Complex geometries may be machined, by mounting them into a Computer Numerically Controlled (CNC) machined holder. Generally, most advanced parts, including optics will have a solid Computer Aided Design (CAD) model, from which the holder may be automatically designed and machined. The moment of inertia of an accelerating workpiece will have an affect on the fundamental frequency of the flexure design. Further design consideration is therefore required to investigate the effects of the workpiece size and mass, on the fundamental frequency and performance of the system.

8.6.4 Feedback Probes

The location of the capacitance probes, intended to feedback the current error motion of the machine tool has been considered. These locations, enable the control system to monitor the axial position and orientation of the workpiece, with reference to the front surface of the fly-cutting head. These errors may then be converted into three values, describing the tip, tilt and axial location of the workpiece. The individual probe mounts have been designed to modify the axial position of the probe and to secure the probe without displacing its position and orientation. The probes will require an axial adjustment for each geometrically different workpiece. When identical workpieces are being machined, the capacitance probes may be used to set the axial position between operations. During the setting procedure for the first workpiece of a particular geometry, a piece of 100μm plastic shim may be used to set the axial distance between the workpiece and the tip of the diamond tool. A micrometer probe may then be used to monitor the final axial displacement of 100μm and the depth of cut. During the analysis of the axial error motions exhibited by the aerostatic spindle (section 3.2.5), the electrical noise of the motor greatly affected the results of the capacitance probes. This analysis provided an understanding of the implementation of capacitance probes with this particular machine tool. The fly-cutting head has been designed to incorporate an insulation layer between the face plate of the spindle and the main vacuum distributor.

The grounding capacitance of the fly-cutting head will therefore be too low to efficiently implement a single capacitance sensor. A technique known as, "A two channel, out of phase measurement" should be adopted so a more permanent ground, implementing a copper bush does not have to be engineered. This technique synchronises the results between two capacitance probes, operating 180° out of phase. Whilst one probe collects a measurement, the other provides a return path for the sensing current.

8.6.5 Control System

The control system is responsible for linking the input signals from the capacitance probes to the displacement of the PZT actuators. A set of functions have been identified, which relate the 3 output values from the capacitance sensor function, to the inputs required by each of the actuators within the 3 pair flexure design. These values include the tip and tilt orientations, and the axial displacement of the workpiece. The control system and the individual parts have been outlined in Appendix 6. From the Human Interface (HI) on the control system, complex functions may be introduced to the orientation of the workpiece to generate microstructured surfaces.

9.0 CONCLUSIONS AND RECOMMENDATIONS

This thesis has investigated and compared diamond turning and fly-cutting machining techniques, and their design principles. A single point diamond facing lathe has been refurbished upon which the fly-cutting system is to be based. The dynamic error motions and the stiffness properties of this facing lathe have been analysed and documented. These error motions form the basis of a technical specification which governs a design concept, capable of single point diamond fly-cutting a non-ferrous component.

The large non-linear error motions generated by temperature variations in the external environment show that the final design should be placed in a temperature controlled laboratory. The proposed concept will then be capable of single point diamond fly-cutting a surface onto a 100mm diameter component, with an acceptable roughness of 80nm (P-V) and a form accuracy of 200nm (P-V). The axial stiffness analysis of the spindle has shown there is a large variation between, the theoretical and experimental results. Further investigation is required, as the low axial stiffness is not acceptable for a precision machine tool.

The final proposed design contains a fly-cutting head and a dynamic workpiece holder. By implementing a morphological chart, four different ideas have been generated for the fly-cutting head which have been evaluated using a Pugh's matrix. This has been proven to be an effective designing technique. The final concept implements a kinematically located side locking clamp, but further investigation is required to design a semi-kinematic feature to secure the axial position of the tool holder into a repeatable position. The geometry of this design has been optimised, according to a minimum fundamental frequency and a linear stiffness criterion. The final fly-cutting head design has been shown as a detailed engineering assembly drawing. The dynamic workpiece holder has been considered as four individual design concepts. These include the workpiece orientation technique, mounting the workpiece, monitoring the error motions within the machine tool and the overall control system. When considered independently, each of the individual concepts are capable of satisfying the technical specifications. These concepts need to be assembled and analysed accordingly. This analysis should include a loaded and unloaded workpiece holder, with the maximum and minimum orientation accelerations. These factors will influence the moment of inertia, dynamic frequencies and vibrations of the workpiece holder.

The control and mechanical flexibility of the workpiece holder will enable complex micro-structured surfaced to be produced. The fly-cutting system will also allow for future research implementing 2 diamond tools. The design of the fly-cutting head ensures that a maximum of one tool will be in contact with the workpiece at any time. The cutting vibrations between the two tools, will therefore not affect the surface finish.

This thesis has provided the initial steps for producing a feasible, single point diamond fly-cutting system. A second stage of research and development work is required before the concept is at an acceptable level. A final stage of research should include an investigation into complex micro-structured surfaces and their production, with both single and dual diamond tools located within the fly-cutting head.

REFERENCES

1. Design for Precision Engineering: Current Status and Trends
P. Schellekens et al, Eindhoven University of Technology, The Netherlands, CIRP, 1998, Vol. 47/2, p557

2. Smart Machine Tools
J. Corbett, SIMS, Cranfield University, Proc Inst Mech Engrs, 1998, Vol212, Part 1, p203 to 213.

3. Precision Engineering and Nanotechnology, A "State-of-the-art" Overview
P. McKeown, SIMS, Cranfield University, Precision Engineering Short Course Presentation, 10th November 2003

4. Design Principles Short Course Notes
John Corbett, SIMS, Cranfield University, 2003

5. Precision Machine Design
Slocum A. H, Massachusetts Institute of Technology, Prentice Hall, ISBN: 0-13-609918-3, p401

6. Bal-Tec Technical Document
E-Resource: http://www.precisionballs.com/TDSKin-1/index.html

7. Kinematic Couplings for Precision Fixturing
Slocum A.H., Precision Engineering, Vol. 10/2, April, 1988, p85

8. Kinematic Couplings for Precision Fixturing,
Donmez A. et al, Precision Engineering, Vol 10/3, July, 1988, p122

9. MIT Research
E-Resource: http://pergatory.mit.edu/kinematiccouplings/documents/Theses/hale_thesis /Practical_Exact_Constraint.pdf

10. Precision Engineering Short Course Lecture Notes
Ritchard Ray-Miller, SIMS, Cranfield University, 2004

11. The Abbe Principle Revisited: An updated version
Bryan J. B., Precision Engineering, Vol. 1/3, July 1979, p129 to 132

12. Paul Shore – Private Communications
SIMS, Cranfield University, UK

13. Lion Precision Spindle Error Analyser
Instruction Manual, Lion Precision, Minnesota, 2003, Document M014-4800.08, p52

14. International Status of Thermal Error Research
J. Bryan et al, CIRP, Vol39/2, 1990, p645-656

15. Error Budgeting in Technology of Machine Tools
Donaldson, RR, Machine Tool Accuracy, Vol5, 1980

16. Calculation of Thermal Deformation of Machine Tools, in Transient State, with the Effect of Structural Joints Taken into Account
Attia M. H. et al, McGill University, Montreal, CIRP, Vol. 28/1, 1979

17. Characterisation of nanosurface generation in single-point diamond turning
Cheung C.F. et al, Machine Tools and Manufacturer, Vol41, 2001, p851 to 875

18. Bently Pressurised Bearings
E-Resource: http://www.bpb-o.com/articles/printableFiles/00understand_stiff_print.pdf

19. Practical Methods for Vibration Control of Industrial Equipment
Costain A. K. et al, Technical Information Paper, Bretech Engineering Ltd,
E-Resource: http://www.bretech.com/Reference/Practical%20Methods%20for%20Vibration%20Control%20of%20Industrial%20Equipment.pdf

20. Characterisation of nanosurface generation in single-point diamond turning
Cheung C.F. et al, Machine Tools and Manufacturer, Vol. 41, 2001, p851 to 875

21. Private Communications
FC Brown (Bisley), Maintenance Department, Surrey, UK

22. The Fundamentals of Fly Cutters
Richter A, Cutting Tool Engineering, 2003, Vol. 55/3, p20 to 21, 0011-4189

23. Diamond Fly-Cutters
Naville R, Mikron Machine Works Ltd, Bienne (Switzerland), Microtecnic, 1996, Vol. 20/1, p53 to 59

24. Manufacturer of microstructured surfaces using ultraprecision turning, milling and shaping,
Weck M. et al, Fraunhofer-Institute of Production Technology IPT, Aachen,
Proc. First International EUSPEN Conference, Bremen, 1999, p420 to 423

25. Precision Machining Presentation
Prof Brinksmeier, Bremen University, 2005
E-Resource: http://www.viaoptic.de/pdf/vortrag_dr_preuss.pdf

26. 3M Technical Information
E-Resource: http://www.3m.com/intl/it/english/front/full_04.html

27. 3M Technical Information
E-Resource: http://www.mmm.com/intl/de/english/archive/full_02.html

28. Structured, Textured or Engineered Surfaces
Evans C J et al, CIRP, Vol. 48/2, 1999, p541 to 556

29. Precision Machining Lecture Notes
Paul Shore, Cranfield University Short Course (Lecture 12), 2004

30. Factors affecting the form accuracy in diamond turning of optical components
Zhou M. et al, Nanyang Technological University, Singapore, Materials Processing Technology, Vol. 138, 2003, p586 to 589

31. Advancing Cutting Technology
Byrne G. et al, CIRP, Vol. 52/2, 2003, p483

32. An Organised Approach Using Capacitance Sensors
T. Sheridan, Lion Precision, AQT Inc, Minnesota, 1991, p25

33. Kugler Technical Brochure
E-Resource: http://www.kuglerofamerica.com/plf1000_cnc_e.pdf

34. LT Ultra Sales Documentation
Precision Technology GmbH, Aftholderberg, Germany

35. Gildo Wanders - Private Communications
Precitech Ultra Precision, European Business Manager, June 2005,

36. Kugler Technical Brochure
E-Resource: http://www.emagmbh.ch/images/kugler/katalog_eng.pdf

37. Gas Lubricated Bearings
Grassam N.S. et al, Butterworth and Co Ltd, London, 1964, p4

38. Design of Aerostatic Bearings
Powell J.W., Machinery Publishing Co. Ltd., 1970, ISBN: 0 204 85333 5, p16

39. A Description of some results achieved in the application of aerostatic bearings to machine tools
Kammerling K. et al, Gas Bearing Symposium, April 1996, Paper 6, page 10

40. ASPE Course on: The Design of Aerostatic Bearings
Stout K.J., University of Huddersfield, 1999

41. Gas Bearings for high speed rotors
Wildmann M, Gas Bearing Symposium, April 1996, Paper 1, pages 1 to 2,

42. Precision Machine Design
Slocum A. H, Massachusetts Institute of Technology, Prentice Hall,
ISBN: 0-13-609918-3, p700

43. Precision Machine Design
Slocum A. H, Massachusetts Institute of Technology, Prentice Hall,
ISBN: 0-13-609918-3, p81

44. Axes of Rotation, Methods for Specifying and Testing
American National Standard, ANSI/ASME B89.3.4M-1985

45. A Fast Tool Servomechanism for Single Point Diamond Turning
Comley PD, MSc Thesis, Cranfield University, 1990

46. Lion Precision Spindle Error Analyser
Instruction Manual, Lion Precision, Minnesota, 2003, Document M014-4800.08, p79

47. Capacitive Sensor Theory, Operation, and Optimization
Lion Precision, Technical Documentation
E-Resource: http://www.lionprecision.com/tech-library/technotes/cap-0020-sensor-theory.html

48. Tooling Structure: Interface Between Cutting Edge and Machine Tool
Rivin E, CIRP Annuals, Vol. 49/2, 2000, p593

49. Design Strategies for aerostatic spindles
Sarkan P. et al, EUSPEN, Conference Proceedings, 1999, Vol 1, p44.

50. Design of Aerostatic Bearings
Powell J.W., Machinery Publishing Co. Ltd., 1970, ISBN: 0 204 85333 5, p110 to 111

51. Design of Aerostatic Bearings
Powell J.W., Machinery Publishing Co. Ltd., 1970, ISBN: 0 204 85333 5, p17

52. Vorndran S, (EDITOR)
Physic Instruments , MicroPositioning, NanoPositioninf and NanoAutomation, Product Catalogue 2004, CAT 116.NP/US.9/04.4

53. Micro-Tilt Controlled Rotating Face-Plate Stage for Single-Point Diamond Turning
Mizuno H, Ph.D. Thesis, Cranfield University, England, September, 1993, p38

54. Capacitive Sensors – Ungrounded Targets
Lion Precision, Technical Note, LT03-0022, July 2004, p2

55. Development of Superfinishing Technology for Application to Hard Turning Machines,
Gustafsson M, Ph.D. Thesis, 30 Month Review, Cranfield University, SIMS, July 2005

APPENDIX 1: Refurbishment Graph

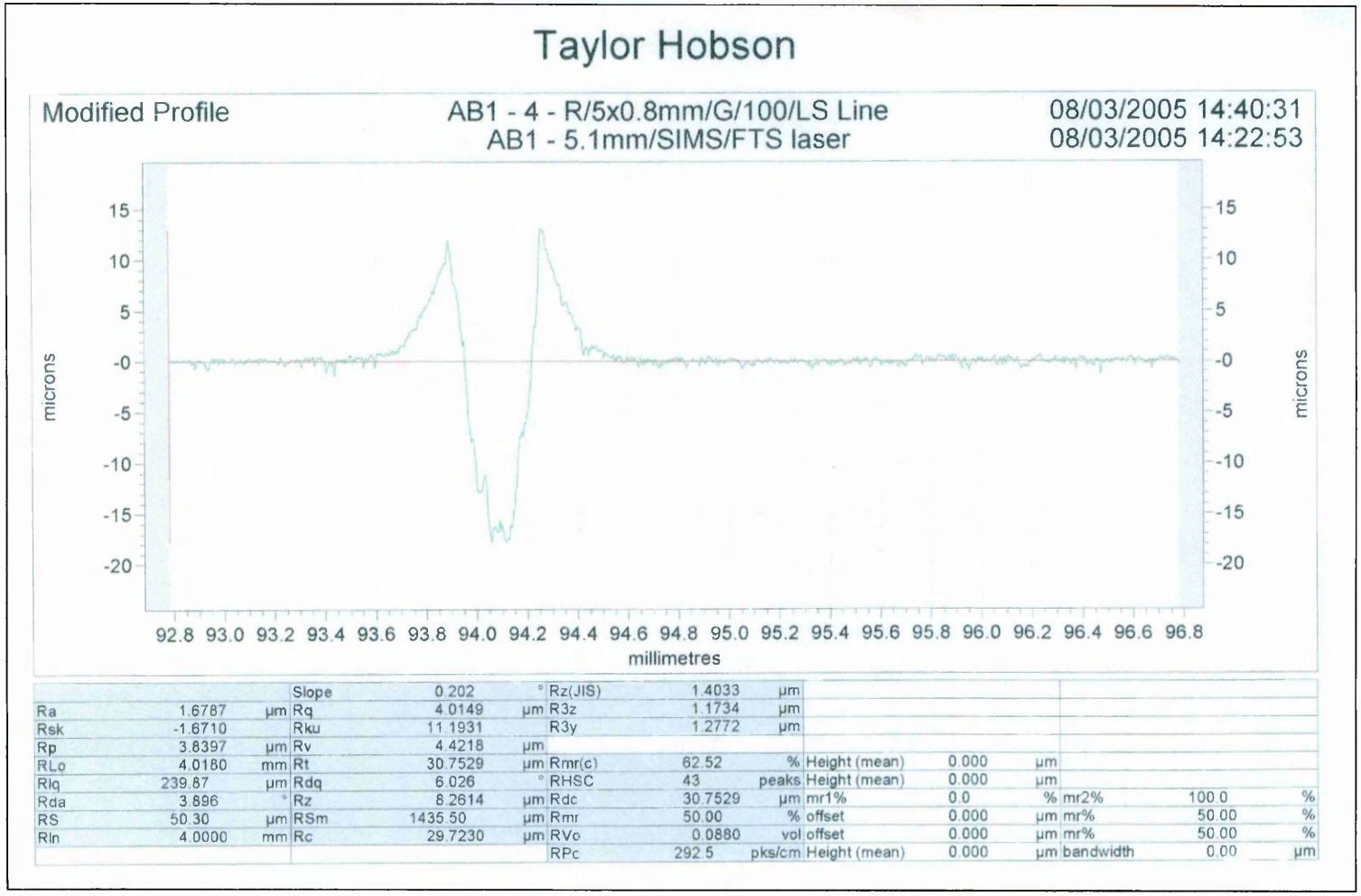

			Slope	0.202	°	Rz(JIS)	1.4033	µm						
Ra	1.6787	µm	Rq	4.0149	µm	R3z	1.1734	µm						
Rsk	-1.6710		Rku	11.1931		R3y	1.2772	µm						
Rp	3.8397	µm	Rv	4.4218	µm									
RLo	4.0180	mm	Rt	30.7529	µm	Rmr(c)	62.52	%	Height (mean)	0.000	µm			
Rlq	239.87	µm	Rdq	6.026	°	RHSC	43	peaks	Height (mean)	0.000	µm			
Rda	3.896	°	Rz	8.2614	µm	Rdc	30.7529	µm	mr1%	0.0	%	mr2%	100.0	%
RS	50.30	µm	RSm	1435.50	µm	Rmr	50.00	%	offset	0.000	µm	mr%	50.00	%
Rln	4.0000	mm	Rc	29.7230	µm	RVo	0.0880	vol	offset	0.000	µm	mr%	50.00	%
						RPc	292.5	pks/cm	Height (mean)	0.000	µm	bandwidth	0.00	µm

Refurbishment Graph

APPENDIX 2: Metrology Graph

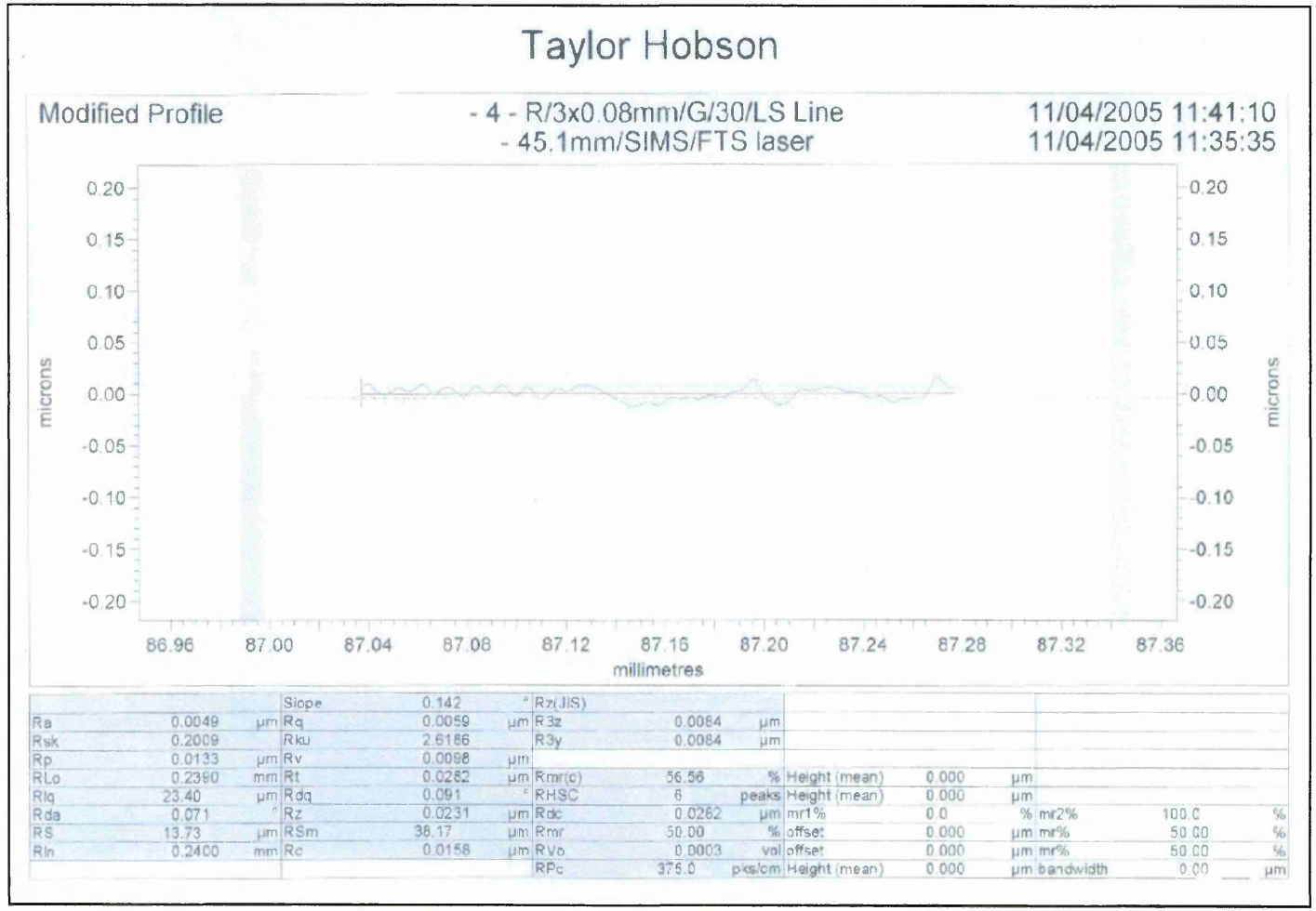

Metrology Graph

APPENDIX 3: Vibrations experienced at machining location

Laboratory Conditions

(Worst case scenario)

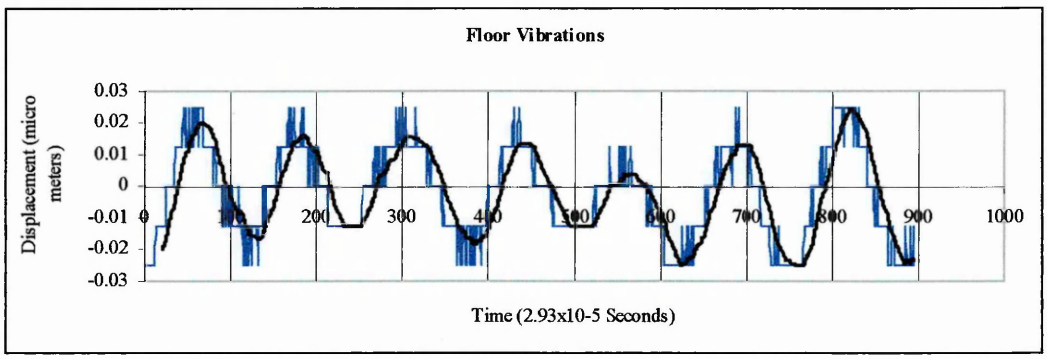

Experienced vibrations

Time Period: 3.3695×10^{-3} sec

Frequency: 296.77Hz

Maximum Amplitude (P-V): 49.6nm

APPENDIX 4: Flexure design, look up table

Length (mm)	Stiffness of 25N/ µm Flexure Width at Thickness						Vertical Deflection of 20µm Flexure Width at Thickness					
	0.5	1	1.5	2	2.5	3	0.5	1	1.5	2	2.5	3
5	121.881	15.23512	4.514109	1.90439	0.975048	0.564264	126.524	15.8155	4.686076	1.976938	1.012192	0.585759
6	210.5758	26.32197	7.799103	3.290247	1.684606	0.974888	220.5086	27.56358	8.166986	3.445447	1.764069	1.020873
7	334.3337	41.79171	12.38273	5.223964	2.67467	1.547841	353.0814	44.13518	13.07709	5.516897	2.824651	1.634636
8	498.9876	**62.37345**	18.48102	7.796681	3.991901	2.310128	531.3294	**66.41617**	19.67887	8.302022	4.250635	2.459858
9	710.3679	88.79599	26.30992	11.0995	5.682943	3.28874	762.505	95.31312	28.24093	11.91414	6.10004	3.530116
10	974.3028	121.7878	36.08529	15.22348	7.794422	4.510661	1054.018	131.7523	39.03772	16.46904	8.432148	4.879715
11	1296.618	162.0773	**48.0229**	20.25966	10.37295	6.002863	1413.431	176.6789	**52.34929**	22.08486	11.30745	6.543661
12	1683.139	210.3924	**62.33848**	26.29905	13.46511	7.79231	1848.447	231.0559	68.46101	28.88199	14.78758	8.557626
13	2139.687	267.4609	79.24767	33.43261	17.1175	9.905958	2366.91	295.8638	87.66335	36.98297	18.93528	10.95792
14	2672.083	334.0104	98.96605	41.7513	21.37667	12.37076	2976.795	372.0993	110.2517	46.51242	23.81436	13.78146
15	3286.148	410.7685	121.7092	**51.34606**	26.28918	15.21365	3686.2	460.775	136.5259	**57.59688**	29.4896	17.06574
16	3987.698	498.4622	147.6925	**62.30778**	31.90158	18.46156	4503.348	562.9185	166.7907	70.36482	36.02679	20.84883
17	4782.551	597.8188	177.1315	74.72735	38.2604	22.14144	5436.575	679.5718	201.3546	84.94648	43.4926	25.16933
18	5676.522	709.5652	210.2415	88.69565	45.41217	26.28019	6494.326	811.7907	240.5306	101.4738	**51.95461**	30.06632
19	6675.426	834.4282	247.238	104.3035	**53.40341**	30.90475	7685.154	960.6443	284.6353	120.0805	**61.48123**	35.57942
20	7785.076	973.1345	288.3362	121.6418	**62.28061**	36.04202	9017.713	1127.214	333.9894	140.9018	72.14171	41.74867

Flexure Design Table

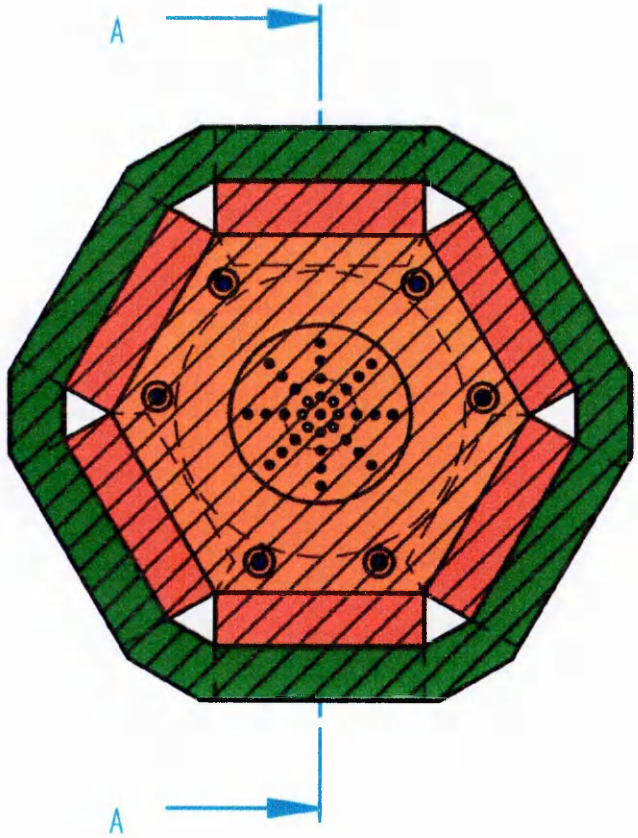

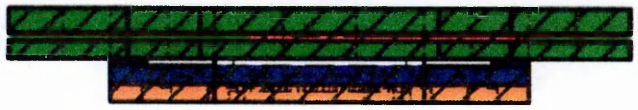

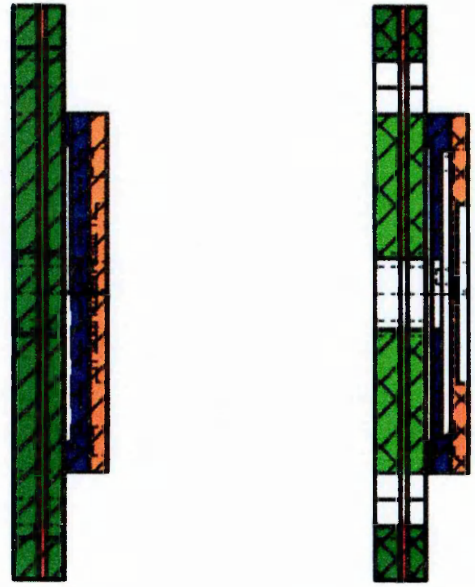

SECTION A-A

	NAME	DATE
DRAWN	J. JARRETT	30/09/2005

THIRD ANGLE

UNLESS OTHERWISE SPECIFIED
DIMENSIONS ARE IN MILLIMETERS
ANGLES ±0.1°

APPENDIX 5

Cranfield UNIVERSITY

TITLE: Workpiece Mounting – Design Concept

SIZE		REV
A4		

MATERIAL: MILD STEEL	FINISH:

SCALE: 1 : 2	WEIGHT: <10KG	SHEET: 1 OF 1

APPENDIX 6: Control System Layout

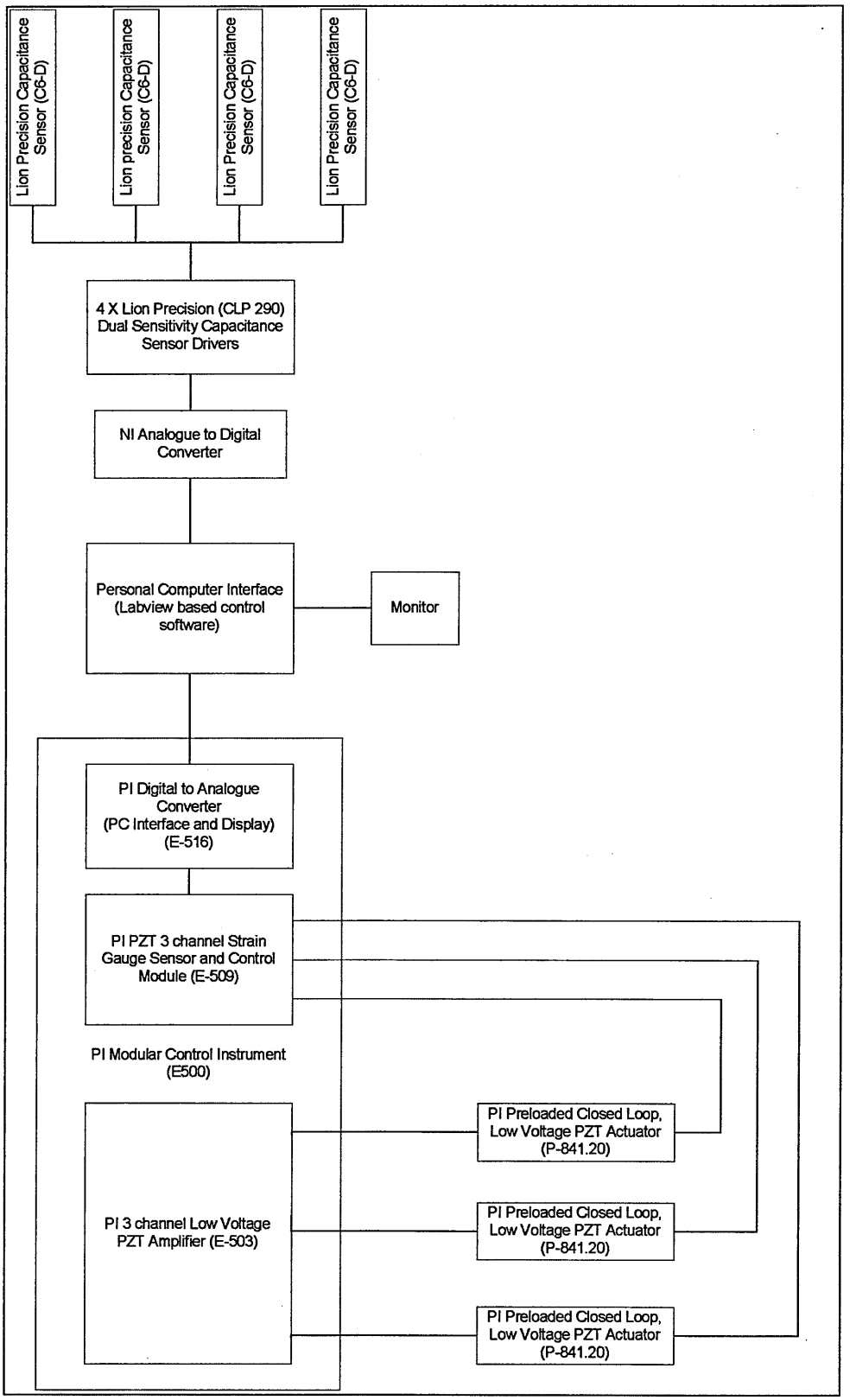

Control system layout

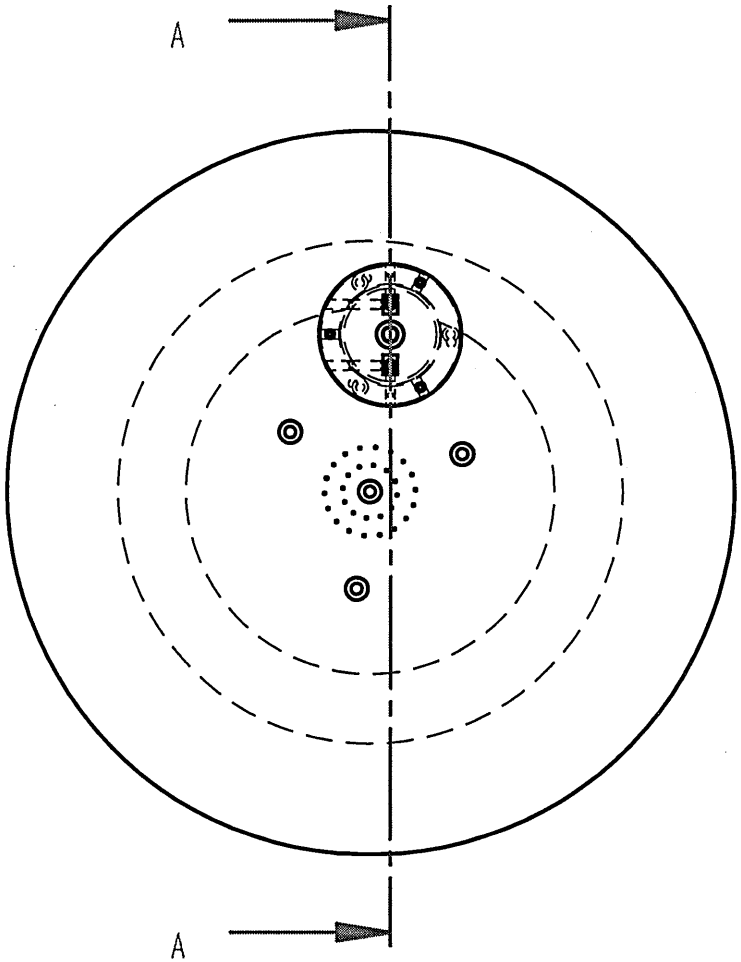

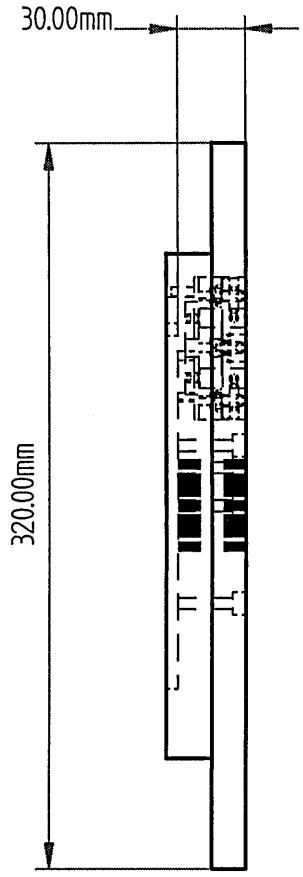

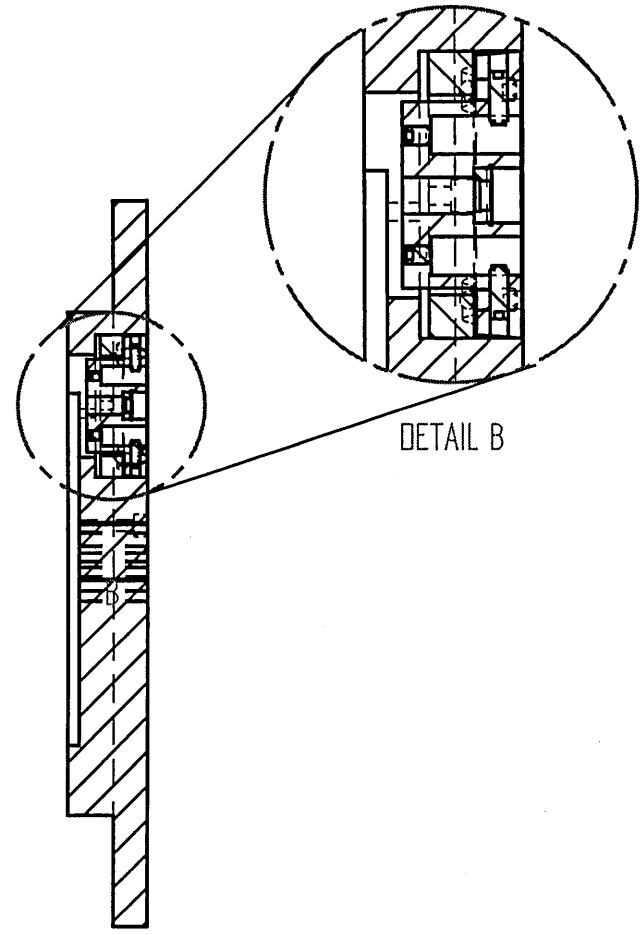

SECTION A-A

	NAME	DATE
DRAWN	J. JARRETT	30/09/2005

THIRD ANGLE

UNLESS OTHERWISE SPECIFIED
DIMENSIONS ARE IN MILLIMETERS
ANGLES ±0.1°

APPENDIX 7

Cranfield UNIVERSITY

TITLE
FLY-CUTTING HEAD ASSEMBLY

SIZE		REV
A4	CONCEPT 1	

MATERIAL: MILD STEEL	FINISH:

SCALE: 1 : 4	WEIGHT: <10KG	SHEET: 1 OF 4

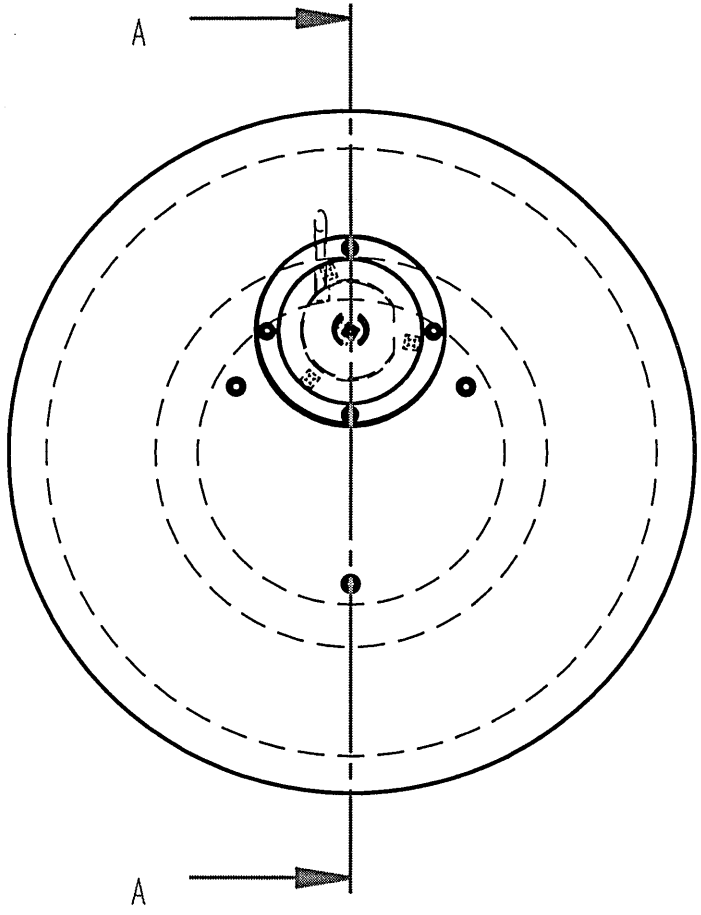

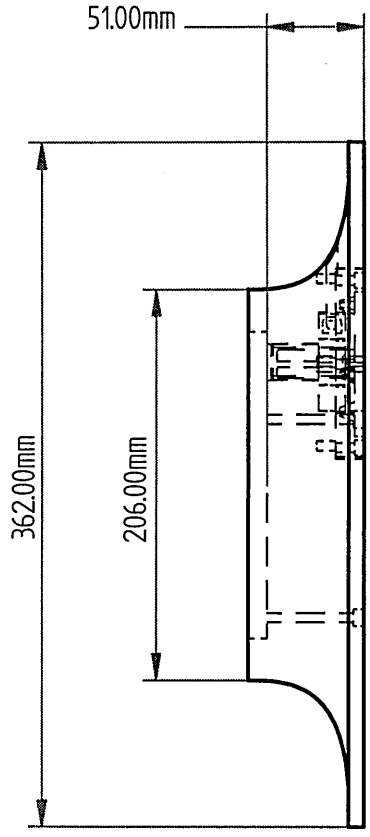

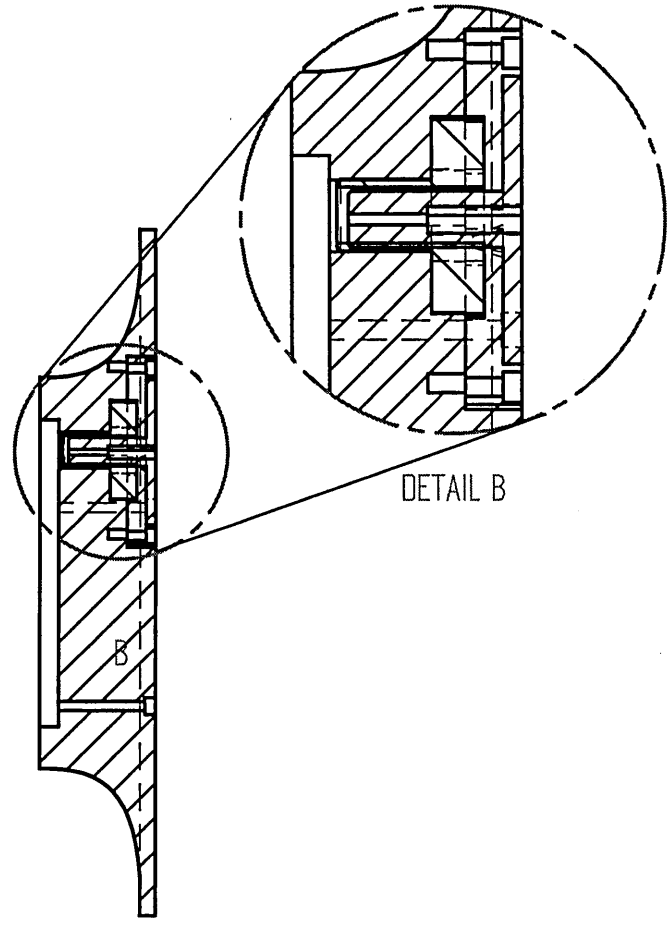

SECTION A–A

	NAME	DATE
DRAWN	J. JARRETT	30/09/2005

THIRD ANGLE

UNLESS OTHERWISE SPECIFIED
DIMENSIONS ARE IN MILLIMETERS
ANGLES ±0.1°

APPENDIX 7

Cranfield UNIVERSITY

TITLE: FLY-CUTTING HEAD ASSEMBLY

SIZE		REV
A4	CONCEPT 2	

MATERIAL: MILD STEEL	FINISH:

SCALE: 1 : 4	WEIGHT: <10KG	SHEET: 2 OF 4

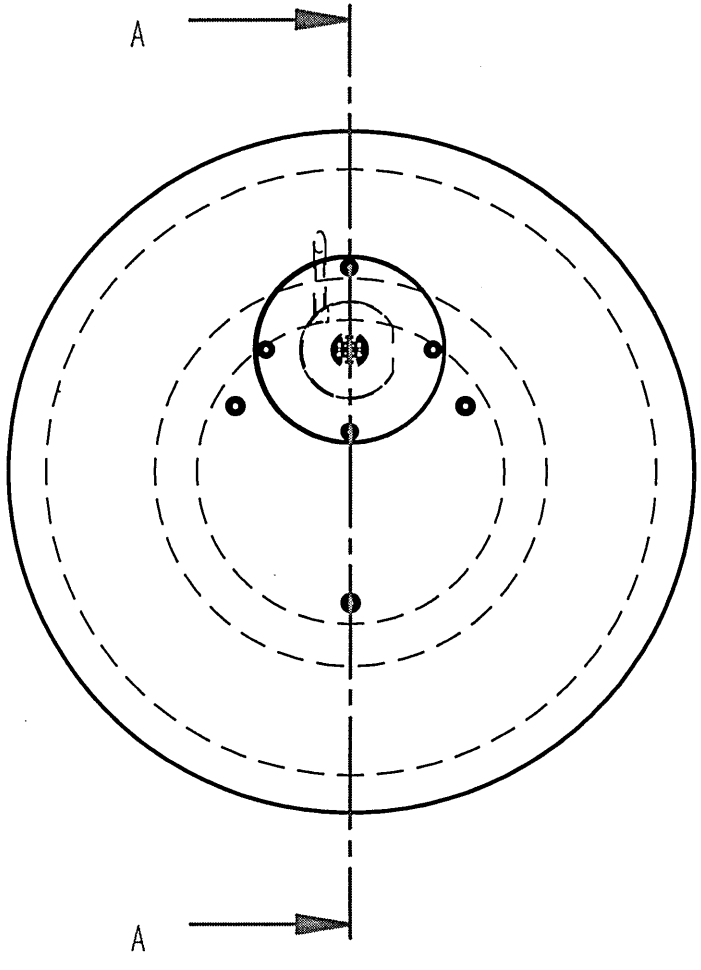

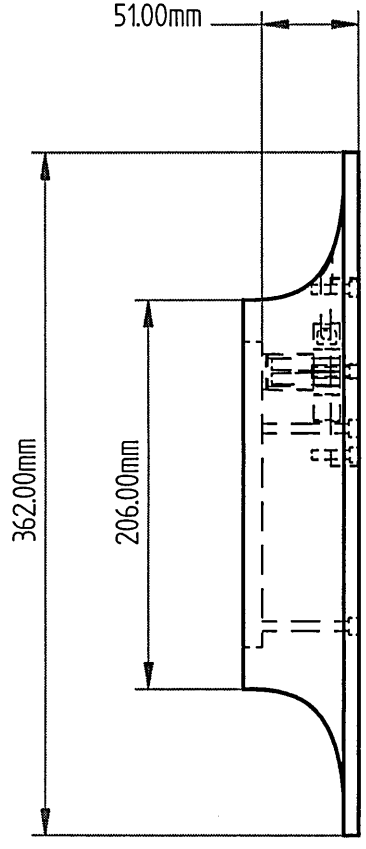

SECTION A-A

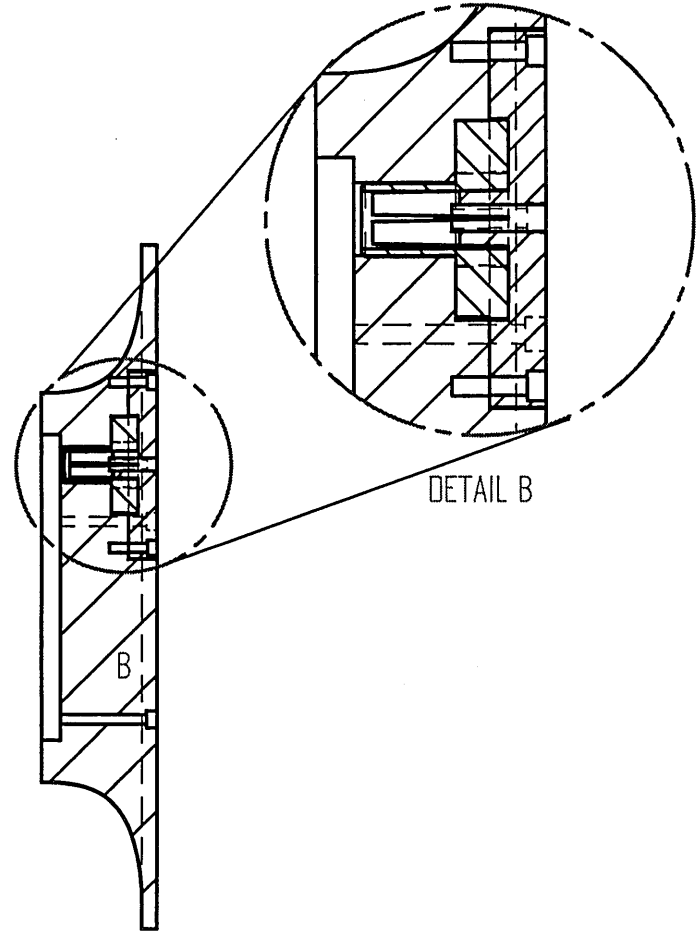

	NAME	DATE
DRAWN	J. JARRETT	30/09/2005

THIRD ANGLE

UNLESS OTHERWISE SPECIFIED
DIMENSIONS ARE IN MILLIMETERS
ANGLES ±0.1°

APPENDIX 7

Cranfield UNIVERSITY

TITLE: FLY-CUTTING HEAD ASSEMBLY

SIZE		REV
A4	CONCEPT 3	

MATERIAL: MILD STEEL	FINISH:

SCALE: 1 : 4	WEIGHT: <10KG	SHEET: 3 OF 4

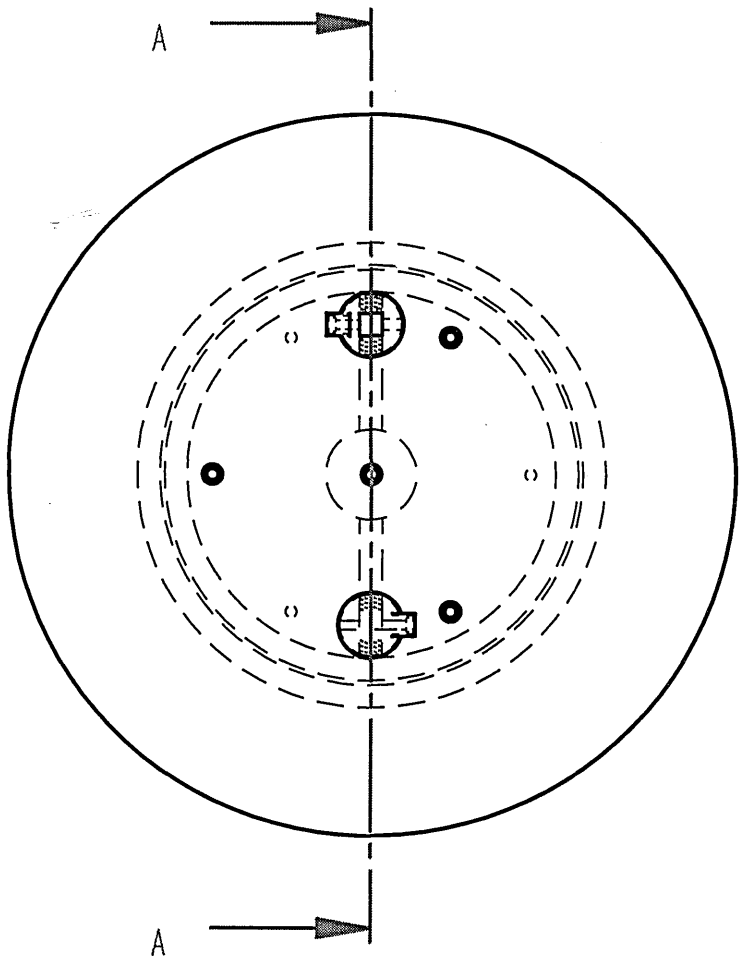

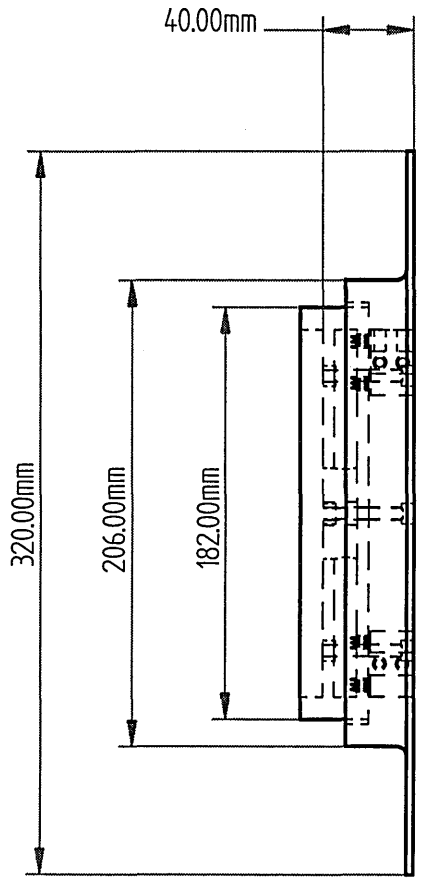

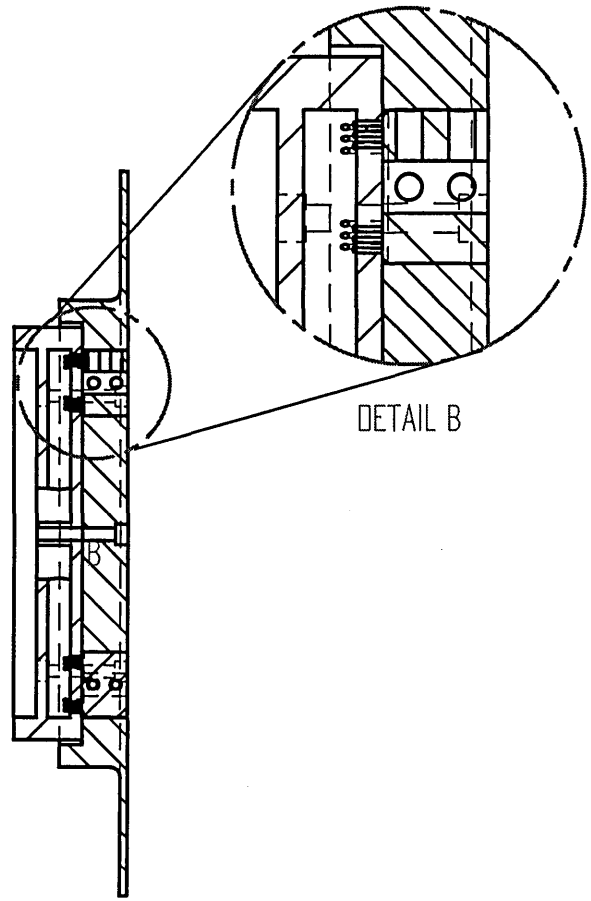

SECTION A–A

	NAME	DATE
DRAWN	J. JARRETT	30/09/2005

THIRD ANGLE

UNLESS OTHERWISE SPECIFIED
DIMENSIONS ARE IN MILLIMETERS
ANGLES ±0.1°

APPENDIX 7

Cranfield UNIVERSITY

TITLE: FLY-CUTTING HEAD ASSEMBLY

SIZE		REV
A4	CONCEPT 4	

MATERIAL: MILD STEEL	FINISH:

SCALE: 1 : 4	WEIGHT: <10KG	SHEET: 4 OF 4

APPENDIX 8: Fly-cutting head design optimisation

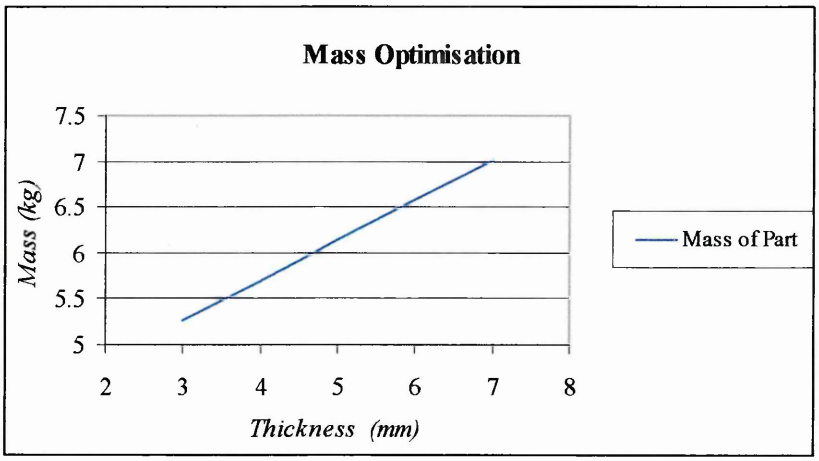

Mass Optimisation

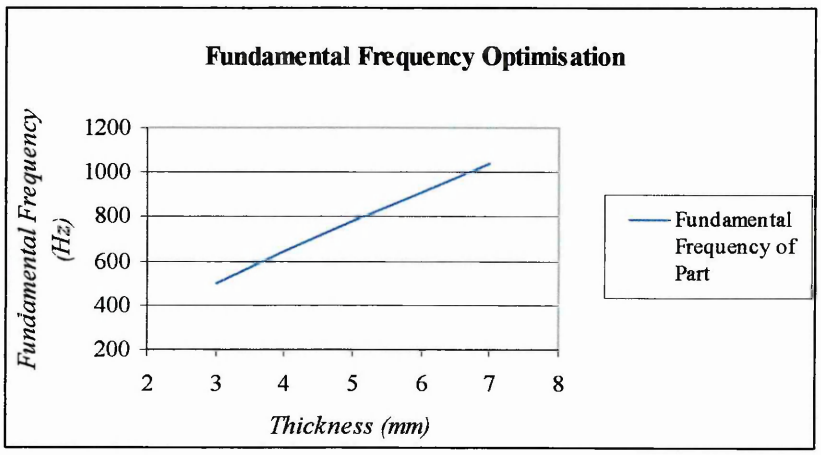

Fundamental Frequency Optimisation

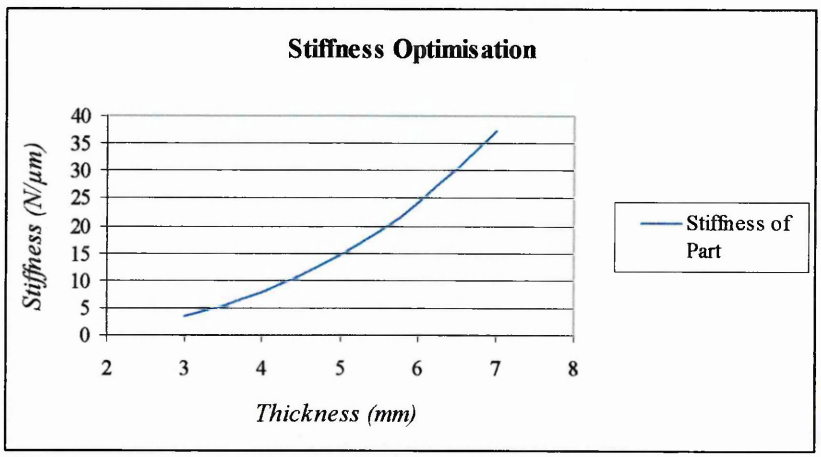

Stiffness Optimisation

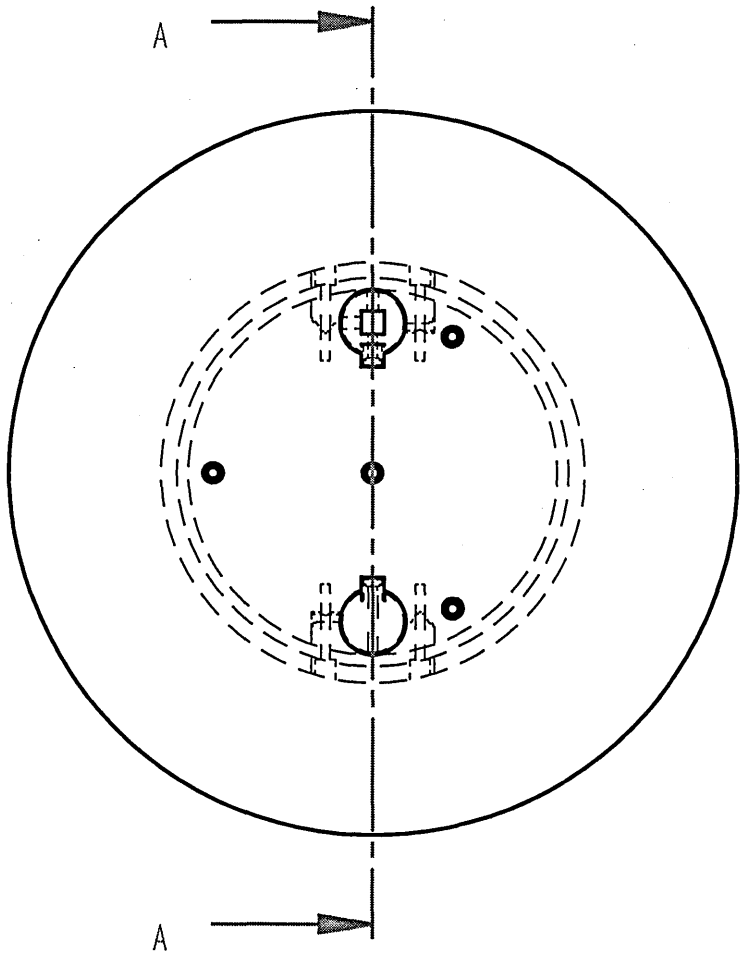

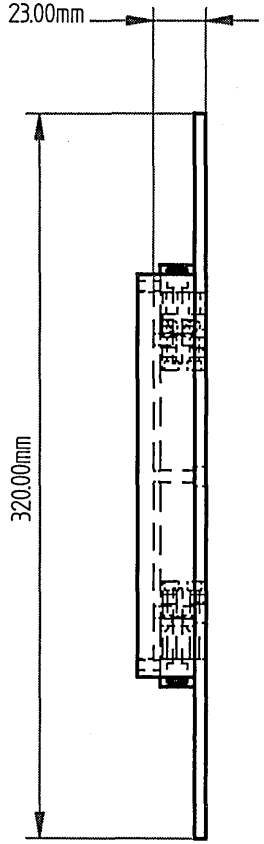

SECTION A-A

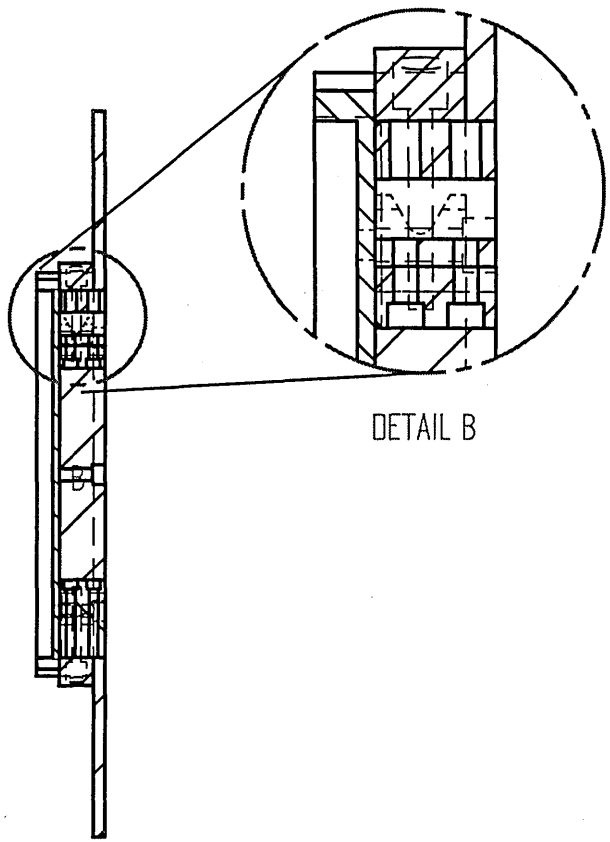

DETAIL B

	NAME	DATE
DRAWN	J. JARRETT	30/09/2005

THIRD ANGLE

UNLESS OTHERWISE SPECIFIED
DIMENSIONS ARE IN MILLIMETERS
ANGLES ±0.1°

APPENDIX 9

Cranfield UNIVERSITY

TITLE: FLY-CUTTING HEAD ASSEMBLY

SIZE		REV
A4	FINAL DESIGN	

MATERIAL: MILD STEEL	FINISH:

SCALE: 0.3:1	WEIGHT: <10KG	SHEET: 1 OF 2

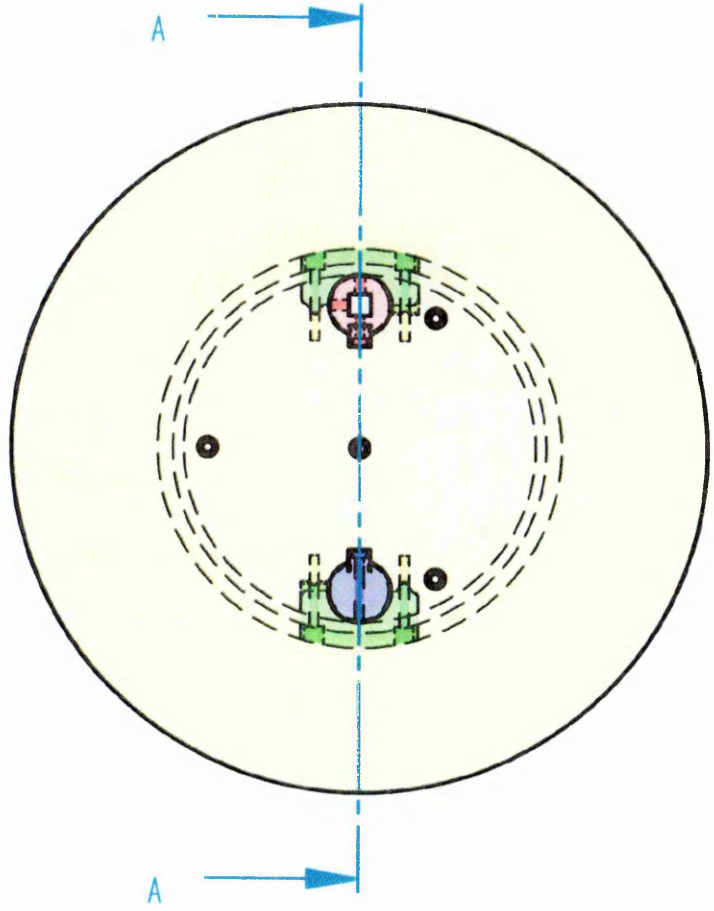

SECTION A-A

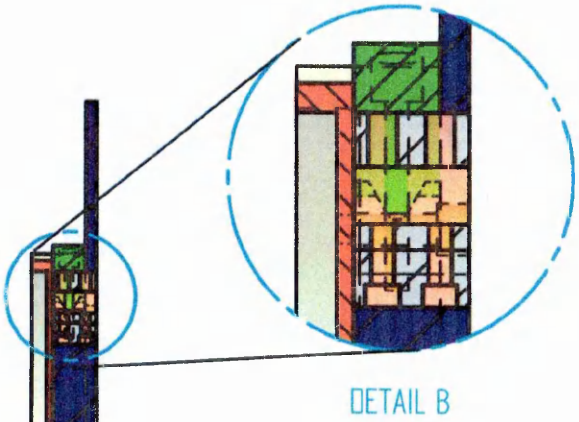

DETAIL B

	NAME	DATE
DRAWN	J. JARRETT	30/09/2005

THIRD ANGLE

UNLESS OTHERWISE SPECIFIED
DIMENSIONS ARE IN MILLIMETERS
ANGLES ±0.1°

APPENDIX 9

Cranfield UNIVERSITY

TITLE: FLY-CUTTING HEAD ASSEMBLY

SIZE		REV
A4	FINAL DESIGN	

MATERIAL: MILD STEEL	FINISH:

SCALE: 0.3:1	WEIGHT: <10KG	SHEET: 2 OF 2